

TOWSON UNIVERSITY
OFFICE OF GRADUATE STUDIES

ASSESSING THE RAMIFICATIONS OF CLIMATE CHANGE FOR THE PURPOSE
OF MODELING STREAMFLOW WITHIN THE UPPER MERCED BASIN IN
CALIFORNIA: 1984-2099

by

Megan B. Cole

A thesis
Presented to the faculty of
Towson University
in partial fulfillment
of the requirements for the degree
Master of Science
Department of Environmental Science
Towson University, Towson, Maryland 21252
(December, 2017)

**TOWSON UNIVERSITY
OFFICE OF GRADUATE STUDIES**

THESIS APPROVAL PAGE

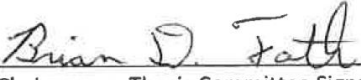
This is to certify that the thesis prepared by Megan Cole

Assessing the Ramifications of Climate Change for the Purpose of Modeling
entitled Streamflow within the Upper Merced Basin, California Using the Soil and Water Assessment


Tool (SWAT), 1984-2099

Tool (SWAT), 1984-2099

has been approved by the thesis committee as satisfactorily completing the thesis requirements for the degree Master of Science in Environmental Science


	Brian Fath	10/11/2017
Chairperson, Thesis Committee Signature	Type Name	Date

Digitally signed by Michael S Haire DN: cn=Michael S Haire, o=ou, email=mhairs@towson.edu, c=US Date: 2017.12.20 07:46:01 -0500	Michael Haire	10/11/2017
Committee Member Signature	Type Name	Date

	Joel Moore	10/11/2017
Committee Member Signature	Type Name	Date

Committee Member Signature	Type Name	Date
----------------------------	-----------	------

Committee Member Signature	Type Name	Date
----------------------------	-----------	------

	Janet V. DeLany, DEd	11/3/18
Dean of Graduate Studies		Date

ABSTRACT

Hydrological responses within the Upper Merced Basin of California to future climate variations were assessed over a continuous 60-yr period. Using a calibrated SWAT (Soil and Water Assessment Tool) basin model, future monthly peak flow and streamflow discharge sensitivity was tested under climate schemes from 2040-2099. Two general circulation models (GCMs) utilized in this study, the Met Office Hadley Centre Model 2 -- Carbon Cycle (HadGEM2-CC) and The National Center for Atmospheric Research (CCSM4), were inputted into the Upper Merced SWAT model under IPCC forcing scenarios RCP 6.5 and 8.0. Probabilities of discharge peaks were determined using the respective climate model's temperature, precipitation, and solar radiation.

Results indicate that times of projected peak flow may occur one to three months earlier than the studied historical time period (1984-2013). Under the historical observed time period of 1984-2007, average Upper Merced peak flow occurred most often in May (22%) and April (20%) (Figure 6.4). Under future climate scenarios tested from 2040-2099, streamflow peak flow shifted to earlier in the winter/spring seasons. HadGem2-CC RCP6.0 scenario shows peak flow most likely occurring in January (33.8%) and February (35.6%). During the same time period under CCSM4, peak flow is shown to occur during December (33.8%) and February (23.7%). HadGem2-CC RCP 8.5 peak flow stretches across January (27.1%), December (22%), and February (22%), while CCSM4 RCP 8.5 similarly shows peak flow shared between January (28.8%), February (25.4%), and December (27.1%). Modeled future streamflows exhibit high relative sensitivities to

temperature and precipitation change due to warming conditions. These findings in collaboration with Upper Merced basin characteristics of high elevation, low groundwater influence, and late season snowmelt, indicate high hydrological sensitivity to snowpack reduction. Results underscore the importance of a flexible management style for water resources dependent on snowpack. Increased and thorough climate monitoring is necessary to assess climate impacts within vulnerable high-elevation mountainous regions.

TABLE OF CONTENTS

LIST OF FIGURES	ix
LIST OF TABLES.....	xii

Chapter 1. Introduction

1.1 CALIFORNIA CLIMATE EXTREMES	1
1.2 STUDY OBJECTIVE.....	2
1.3 WATER MANAGEMENT AND ACCOUNTING	3
1.4 WATER BALANCE APPROACH.....	5
1.5 SCENARIOS OF CO ₂ CONCENTRATION, PRECIPITATION, AND TEMPERATURE CHANGES.....	6

Chapter 2. Study Area Characteristics

2.1 SAN JOAQUIN VALLEY	9
2.2 SITE SELECTION: UPPER MERCED BASIN.....	10
2.2.1 Climate.....	11
2.2.2 Topography, geology, and soils.....	12
2.2.3 Watershed surface-water hydrology.....	14
2.3 STUDY AREA WATER RESOURCES	16
2.3.1 Water availability.....	16
2.3.2 Water use.....	17
2.3.3 Water quantity concerns.....	19

Chapter 3. Literature Review

3.1 CALIFORNIA: OBSERVED AND FUTURE CLIMATE.....	23
3.1.1 Temperature change.....	24
3.1.2 Runoff timing.....	25
3.1.2 Snowpack accumulation.....	26
3.2 METHODOLOGY OF ASSESSING CLIMATE CHANGE IMPACTS ON CALIFORNIA STREAMFLOW.....	27
3.2.1 Establishing changes in temperature and precipitation	28
3.2.2 Determining changes in natural runoff	30
3.3 GCMs: PREDICTED TRENDS IN ENVIRONMENTAL INDICATORS.....	31
3.3.1 Temperature and precipitation.....	31
3.3.2 Loss of snowpack.....	32
3.4 GCMs: PREDICTED TRENDS IN RUNOFF AND NATURAL STREAMFLOW.....	33

Chapter 4. Background on Utilized Modeling Program and Climate Modeling Data

4.1 INTRODUCTION	36
4.2 SOIL AND WATER ASSESSMENT TOOL (SWAT)	37
4.3 THEORETICAL BACKGROUND OF SWAT.....	38
4.3.1 Water yield.....	39
4.3.2 Surface runoff	40
4.3.3 Retention parameter	40

4.3.4 Evapotranspiration 41

4.3.5 Sediment yield 42

4.4 SENSITIVITY ANALYSIS: LH-OAT 42

4.5 CALIBRATION AND VALIDATION METHODS: SWAT-CUP..... 44

Chapter 5. METHODOLOGY

5.1 INTRODUCTION 48

5.2 SWAT MODELING..... 50

 5.2.1 Water delineation 50

 5.2.2 HRU analysis 52

5.3 DATA INPUTS..... 53

 5.3.1 Land cover data 53

 5.3.2 Topography and soil data 54

 5.3.3 Climate data 55

 5.3.4 Snow data 56

5.4 SWAT-CUP CALIBRATION AND VALIDATION..... 57

 5.4.1 Parameter fitting..... 58

 5.4.2 Observation files 65

5.5 CLIMATE SCENARIO MODELING..... 65

Chapter 6. RESULTS

6.1 SENSITIVITY ANALYSIS 67

6.2 CALIBRATION AND VALIDATION..... 68

6.2.1 Final model parameter ranges	71
6.2.2 Observed, uncalibrated, and calibrated streamflow comparison	74
6.3 HISTORICAL DATA PEAK STREAMFLOW.....	76
6.4 CLIMATE PROJECTION PEAK STREAMFLOW	77
6.5 PROJECTED MONTHLY STREAMFLOW	82
Chapter 7. DISCUSSION	
7.1 VALIDATION	86
7.2 OBSERVED PEAK STREAMFLOW.....	86
7.3 FUTURE CLIMATE SCENARIOS.....	87
7.4 PROJECTED ANNUAL PEAK FLOWS	89
7.5 LIMITATIONS.....	89
7.5.1 SWAT and SWAT-CUP video tutorials.....	92
7.6 SUGGESTIONS	94
7.7 SWAT-USER AND SWAT CUP GROUPS	95
7.8 CONCLUDING THOUGHTS	96
REFERENCES	98
CURRICULUM VITAE	119

LIST OF FIGURES

Chapter 2. Study Area Characteristics

Figure 2.1. Hydrological map of the Upper Merced Basin in California. 11

Figure 2.2. Hydrological map of the Northern San Joaquin watershed. 15

Figure 2.3. Regional map of the San Joaquin Valley. 19

Chapter 3: Literature Review

Figure 3.1. Bar graph showing the percentage of precipitation falling as rain over 33 main water supply watersheds in California during the period of October 1948 to September 2012..... 25

Figure 3.2. Conceptual model illustrating two approaches, hypothetical scenarios and general circulation models (GCMs), for determining changes in the hydrological cycle in accordance with climate change impacts..... 28

Chapter 4: Background on Utilized Modeling Program and Climate Scenario Data

Figure 4.1. Schematic diagram showing water movement pathways within the Soil and Water Assessment (SWAT) modeling program..... 44

Chapter 5: Methodology

Figure 5.1. ArcSWAT framework for climate change assessment on future streamflow.....49

Figure 5.2. Setup window for model run in the Soil and Water Assessment (SWAT) modeling program.....	50
Figure 5.3. Upper Merced basin stream network and hydrological unit layer projected in ArcMap through the Soil and Water Assessment (SWAT) modeling program.....	51
Figure 5.4. Upper Merced basin DEM layer projected in ArcMap through the Soil and Water Assessment (SWAT) modeling program.....	51
Figure 5.5. Upper Merced basin water delineation box within the Soil and Water Assessment (SWAT) modeling program.....	52
Figure 5.6. Upper Merced basin hydrological response unit (HRU) definition box within the Soil and Water Assessment (SWAT) modeling program.....	53
Figure 5.7. Upper Merced basin land use layer projected in ArcMap through the Soil and Water Assessment (SWAT) modeling program.....	54
Figure 5.8. Upper Merced basin soil layer projected in ArcMap through the Soil and Water Assessment (SWAT) modeling program.....	55
Figure 5.9. Weather data definition prompt box within the Soil and Water Assessment (SWAT) modeling program.....	56
Figure 5.10. SWAT-CUP elevation parameter calibration: PLAPS, TLAPS.....	62
Figure 5.11. SWAT-CUP parameter calibration for .sno parameters: SFTMP, SMTMP, SMFMX, TIMP, SMFMN, SNO50COV, SNOCOVMX.....	62
Figure 5.12. SWAT-CUP parameter calibration for .gw, .hru, .mgt parameters.....	63

Chapter 6: Results

Figure 6.1. SWAT-CUP validation..... 71

Figure 6.2. Uncalibrated, calibrated, and observed streamflow: 1984-1999..... 75

Figure 6.3. Uncalibrated with elevation parameters, calibrated, and observed streamflow:
1984-1999..... 75

Figure 6.4. Observed annual streamflow (cms) at USGS Pohono Bridge..... 76

Figure 6.5. HadGem2-CC 6.0 annual peak flow from 2040-2069 (cms)..... 78

Figure 6.6. HadGem2-CC 6.0 annual peak flow from 2070-2099 (cms)..... 78

Figure 6.7. CCSM4 6.0 annual peak flow from 2040-2069 (cms)..... 79

Figure 6.8. CCSM4 6.0 annual peak flow from 2070-2099 (cms)..... 79

Figure 6.9. HadGem2-CC 8.5 annual peak flow from 2040-2069 (cms)..... 80

Figure 6.10. HadGem2-CC 8.5 annual peak flow from 2060-2099 (cms)..... 80

Figure 6.11. CCSM4 8.5 annual peak flow from 2040-2069 (cms)..... 81

Figure 6.12. CCSM4 8.5 annual peak flow from 2070-2099 (cms)..... 81

Figure 6.13. Average projected monthly streamflow from May 2048-2050..... 82

Figure 6.14. Average projected monthly streamflow from May 2068-2070..... 83

Figure 6.15. Average projected monthly streamflow from May 2078-2080..... 84

LIST OF TABLES

Chapter 1. Introduction

Table 1.1. Global mean surface temperature change (°C) for periods 2046-2065 and 2081-2100 7

Table 1.2. Global cumulative CO₂ emissions for 2012-2100, shown with RCP atmospheric concentrations 8

Chapter 5. Methodology

Table 5.1. ArcSWAT framework for climate change assessment on future streamflow..... 66

Chapter 6: Results

Table 6.1. Upper Merced SWAT model sensitivity results obtained through Latin-Hypercube sampling 67

Table 6.2. General performance ratings for NSE and PBIAS statistics under a monthly time step..... 69

Table 6.3. General NSE and PBIAS ratings under daily and monthly timestep..... 69

Table 6.4. Model statistics RSR, PBIAS, and NSE of streamflow during initial, calibration, and validation runs..... 70

Table 6.5. Parameters chosen for the SWAT-Cup project in order to calibrate and validate the corresponding SWAT model..... 73

CHAPTER 1

INTRODUCTION

1.1 CALIFORNIA CLIMATE EXTREMES

California's five-year drought has abruptly ended in spectacular fashion. Flash storms are pouring into choked reservoirs, continued above-average precipitation has restored the iconic agricultural fields of the Central Valley, and Sierra Nevada snowpack is piled high enough for an unusually long mid-June ski season. As of January 2017, California has 189 percent of average snowpack accumulation, in excess of 200 percent average precipitation, and 112 percent of long-term average reservoir storage (Hanak et al. 2017). This respite from prolonged arid conditions has brought comfort to the state. Two years prior, amidst drought, California reservoir storage sunk to 8 million acre-ft below the long-term average (Hanak et al. 2017).

Subject to a dry desert climate, Californian society is built upon a series of waterways contingent on historical weather patterns. Dams, concrete channels, and diversions, enable the region's success by way of funneling precipitation to where it is needed. With such demand for consistent water supply in both volume and location, observed extremes in weather patterns threaten the ability of water infrastructure to provide for the state. Governor Jerry Brown had issued a state-wide drought emergency as a response to water deficits affecting municipal, agricultural, and industrial communities, but conditions have quickly changed with 2017 flooding ripping apart key spillways endangering nearby localities. Water issues have rapidly flip-flopped from too-little to too-

much surface water discharge as intense precipitation continues to overload state infrastructure in select municipalities.

Despite the most recent drought coming to a close, Governor Jerry Brown highlighted the necessity of water management preparation as he lifted California's drought emergency in April 2017. Warning that conservation must "be a way of life", Governor Brown advocated for increased management and planning during times of both water scarcity and abundance (Dwyer 2017). Alarms raised by the larger water management community echo the Governor's sentiments. Future temperature increases will break established precipitation trends, causing heightened variability in climate conditions. Current predictions of climate conditions foresee prolonged and emboldened periods of both acute drought and severe floods, throwing California into a persistent crisis of either deficit or drowning. To this point, Governor Brown further stated in his address that "the [2012–2017] drought emergency is over, but the next drought [might] be around the corner" (Dwyer 2017).

1.2 STUDY OBJECTIVE

The major goal of this research is to improve information on current and future water demand for the Upper Merced subbasin. To evaluate the consequences of climate change, a water balance model for the Upper Merced basin under current conditions and future climate conditions are evaluated. The intention of this analysis is to collect and integrate data within the water accounting system for the Upper Merced basin so that these findings might assist in the greater scientific endeavor of mapping water balance for the basin and its greater watershed, the San Joaquin Basin. According to a report by the Public

Policy Institute of California (2016), the recent drought has “spotlighted serious gaps and fragmentation in California’s water accounting system,” as state water infrastructure is physically interconnected, but institutionally splintered. As a whole, California’s water balance sheet is nearly blank. Aside from a few elemental assessments focused on appraising water fees in towns such Santa Clara Valley and Orange County, the majority of Californian basins are in need of any water accounting research. Review of California’s Department of Water Resources (DWR) and the U.S. Bureau of Reclamation (USBR) (2016) annual estimates for water use and availability, shows significant breaks with missing or inadequate data (Escriva-Bou et al. 2016). In support of developing a common accounting framework for the state, changes in groundwater storage are estimated to determine the water balance for the Upper Merced Subbasin (HU# 18040008) using a well-known and often-published modeling program, Soil and Water Assessment Tool (SWAT). Measurements of local inflows, “consumptive” water use, water imports, outflows, and groundwater/surface storage will be calculated. Furthermore, forecasted flows are subsequently determined from this historical data under two climate change scenarios (RCP 6.5 and RCP 8).

1.3 WATER MANAGEMENT AND ACCOUNTING

Despite engineering “one of the most complex water systems in the world”, investment in basin accounting research is instituted more completely in Australia, Spain, and 11 other western states (Arizona, Colorado, Idaho, Kansas, Nebraska, Nevada, New Mexico, Oregon, Texas, Utah and Washington) than it is in California (Escriva-Bou et al. 2016). The aforementioned western states have developed economies dependent on the

environment, yet share in California's resource management difficulties on account of similar arid but variable climates. Advanced water research knowledge enables states to enact practices suitable for alleviating water stress for their region through economizing the supply. With an understanding of water assets, conservation is the moral of western management frameworks. State water information allows for a strategic and suitable allotment of supply for sustainable groundwater management, surface water during shortages, and surrounding environment, for the respective region.

Internal pressures of population and industry on water supply are exacerbated by extreme climate swings, rendering the state's infrastructure inoperable without constant monitoring and management application. In order to map the reality of present and projected water supply while quickening our ability to manage for these differences, regional water balances for both the historical past and future should be performed. By calculating estimates for water use and availability on a regional to local level, the purveyor is able to delineate inflows, outflows, and exports, within the total net water supply. Further, local and imported inflows, changes in groundwater storage (overdraft or recharge), and precipitation levels, can be teased out from the sum of net water stored within reservoirs and aquifers. Areas dependent on conveyances for supply especially benefit from the above assessments. During times of exceptional drought or flooding, compensation is made through routine interventions such as pumping for groundwater or supplying reservoir overdraft or recharge for industry.

Here, this study, performs current and estimated water balances for the Upper Merced subbasin, HU #18040008; a subbasin part of the greater San Joaquin Basin and positioned to the left of the California Delta, HU #18040003.

1.4 WATER BALANCE APPROACH

A water balance equation is used to describe the flow of water in and out of a system at any period of time. The approach considers inflows and outflows from basins, sub-basins, service and use at all levels (Kopnina and Shoreman-Ouimet 2015). The water balance method can then evaluate the various ways in which water can be expended. It is defined by the general hydrological equation, which is essentially the law of conservation of mass applied to the hydrologic cycle meaning that water balance equations evaluate all inflow, outflow, and change in water storage. The main goal of a water balance approach to irrigation scheduling is to determine soil water deficit by accounting for all water additions and subtractions from the soil root zone. The most commonly used crop-water balance model is given as:

(1)

$$P - R - E - T_w - T_c - S - D + I = 0$$

Where P is precipitation, R is runoff, E is evaporation, T_c & T_w are weed and crop transpiration, S is change in soil water storage, D is deep drainage, and I is irrigation. (Lal 1991).

The crop water requirement or crop evapotranspiration (ET_c) must be met in order to produce significant yields. To calculate water use efficiency, assimilation (carbon fixation) is divided by transpiration. With increased temperatures and solar radiation, leaf temperature increases with increases in transpiration, while higher CO₂ results in partial

stomatal closure and decrease in transpiration. As global warming continues, harmful GHGs such as CO₂ will increase (Lal 1991). The Penman-Monteith equation calculates evapotranspiration of a crop as a function of solar radiation, humidity, temperature, and wind in SWAT.

Understanding how increased temperature and CO₂ affect plants is crucial to the understanding of how to manipulate a water balance table program for future hypothetical climate change scenarios. As temperature and CO₂ increase, solar radiation becomes more important for the plant, vapor deficit pressure and wind are less important, and the change in latent energy depends on the solar radiation change (Lal 1991).

1.5 SCENARIOS OF CO₂ CONCENTRATION, PRECIPITATION, AND TEMPERATURE CHANGES

RCP scenarios are derived from spatially resolved data sets of land use change and sector-based emissions of atmospheric pollutants. The scenarios are characterized by their approximate radiative forcing in year 2100 relative to year 1750: RCP2.6 at 2.6 W m⁻², RCP4.5 at 4.5 W m⁻², RCP6.0 at 6.0 W m⁻², and RCP8.5 at 8.5 W m⁻². To represent a range of climate change policy implementation schemes, one stabilization scenarios (RCP6), and high GHG emissions scenario (RCP8.5) were simulated. According the Intergovernmental Panel on Climate Change's Fifth Assessment Report, radioactive forcing does not peak by 2100 for RCP6.0 and RCP8.5. Table 1.1. lists four RCP scenarios from the most recent IPCC report with their respective global mean surface change (°C) and global mean sea-level rise (m).

CMIP5 predictions are designed in relation to a common baseline period (1986-2005) with climate change expressed as fluctuations with respect to recent history, not from a period before anthropogenic influence. Having said that, there is evidence of consequences of climate change occurring in or before 1985-2005 (IPCC 2014). The CMIP5 simulations were executed with CO₂, CH₄ and N₂O concentrations, increasing overall combined CO₂ levels to 800 ppm (RCP6.0), and 1313 ppm (RCP8.5) (Table 1.1; Table 1.2). Scenarios without mitigation policies targeting emissions are “baseline scenarios” and are represented in the range between RCP6.0 and RCP8.5. In general, RCP8.5 can be compared to the SRES A2/A1F1 scenario and RCP6.0 to the SRES B2 scenario of previous IPCC reports. CO₂ or CH₄ atmospheric emissions from thawing permafrost carbon stocks is assessed with low confidence to be in the range of 50 to 250 GtC for RCP8.5.

Scenario	Global Mean Surface Temperature Change (°C)			
	2046-2065		2081-2100	
	Mean	Likely Range	Mean	Likely Range
RCP2.6	1	0.4–1.6	1	0.3–1.7
RCP4.5	1.4	0.9–2.0	1.8	1.1–2.6
RCP6.0	1.3	0.8–1.8	2.2	1.4–3.1
RCP8.5	2	1.4–2.6	3.7	2.6–4.8

Table 1.1. Global mean surface temperature change (°C) for periods 2046-2065 and 2081-2100. Calculated projections are 5 % to 95% ranges and evaluated to be likely ranges after accounting for additional uncertainties or different levels of confidence in models. Table adapted from the Intergovernmental Panel on Climate Change’s Fifth Assessment Report.

Scenario	Cumulative CO ₂ Emissions 2012 to 2100			
	GtC		GtCO _{2e}	
	Mean	Range	Mean	Range
RCP2.6	270	140–410	990	510–1505
RCP4.5	780	595–1005	2860	2180–3690
RCP6.0	1060	840–1250	3885	3080–4585
RCP8.5	1685	1415–1910	6180	5185–7005

Table 1.2. Global cumulative CO₂ emissions for 2012-2100, shown with RCP atmospheric concentrations. 1 Gigatonne of carbon = 1 GtC = 10¹⁵ grams of carbon. Table adapted from the Intergovernmental Panel on Climate Change's Fifth Assessment Report.

CHAPTER 2

STUDY AREA CHARACTERISTICS

2.1 SAN JOAQUIN VALLEY

Climate variability and extreme weather are consequences of global climate change, which can cause unstable water dependent ecosystems to become vulnerable. An estimated 19% of California's total energy usage is allocated for the collection, transportation, and treatment of water (CRC Report R43200). Increased temperatures, extreme droughts, and sea level rise are likely to have an absolute effect on California's hydrological cycle. Concerns of major fluctuations in the hydrological cycle causing increases in water demand while degrading water quality and stressing the agricultural industry, have spurred the need for a greater understanding of climate change repercussions on California's water supply.

The impacts of climate change are expected to exacerbate existing demands on California's water resources. The Western United States' climate is highly variable in both space and time, causing known hydrological patterns to become vulnerable under consequences of climate change. A shifting network of heat, moisture, and energy between the atmosphere and ocean determine conditions of precipitation over the region. Whether this moisture falls as snow or rain is contingent on the region's topography. Historically, the lion share of Western precipitation has been experienced as snow, compounding on the Sierra Nevada awaiting trickle-down in the spring. Mountain snowpack provide water storage by reserving supply during winter months to avoid flood risk, and expelling water

into valleys and rivers for irrigation during spring and early summer months. Surrounding the snowcapped mountains, arid rain-shadow landscapes sit leeward across from irrigated windside areas fed mainly by rivers. Circumstances of river flow are dependent on snowpack accumulation and its subsequent meltwater. Nearly all major rivers flowing through the Western United States are fed from snowpack mountain watersheds, and so a reduction in snowcap mass greatly affects water resources for irrigation and human use. Anticipating such changes is vital for regions with limited water resources such as the Upper Merced Basin (HU #18040008), a subbasin within the greater San Joaquin Valley (SJV).

2.2 SITE SELECTION: Upper Merced Basin

The San Joaquin Valley (SJV) is a gently sloping alluvial plane about 400 km long and 40 to 90 km wide, sitting at Latitude 36°30' N to 38°50'N and Longitude 119°45'W to 121°30'W (Ritter 2005). Split into two regions, the SJV comprises of the southern two-thirds in the Central Valley of California and the northern one-third in the Sacramento Valley (Phillips et al. 2007). Both valleys' namesakes are derived from the major rivers that they drain into. The San Joaquin River flows from the Sierra Nevada down onto the valley floor, where it runs along a northern path toward the Sacramento- San Joaquin Delta. The valley floor acts as a deep bowl, capturing marine and continental sediment up to 10 km thick and receiving an average of 5 to 16 inches of rainfall annually (Gronberg et al. 1998). The San Joaquin River drains an area of 35,983 km², from the northern part of the SJV through the San Francisco Bay. The Upper Merced subbasin is located in Central California, with an area size of 5,253 km². The Merced River flows through the small

basin and runs off into the San Joaquin River as a tributary (Stillwater Sciences 2008).

Figure 2.1 provides a detailed map of the study basin, focusing on location and land use.

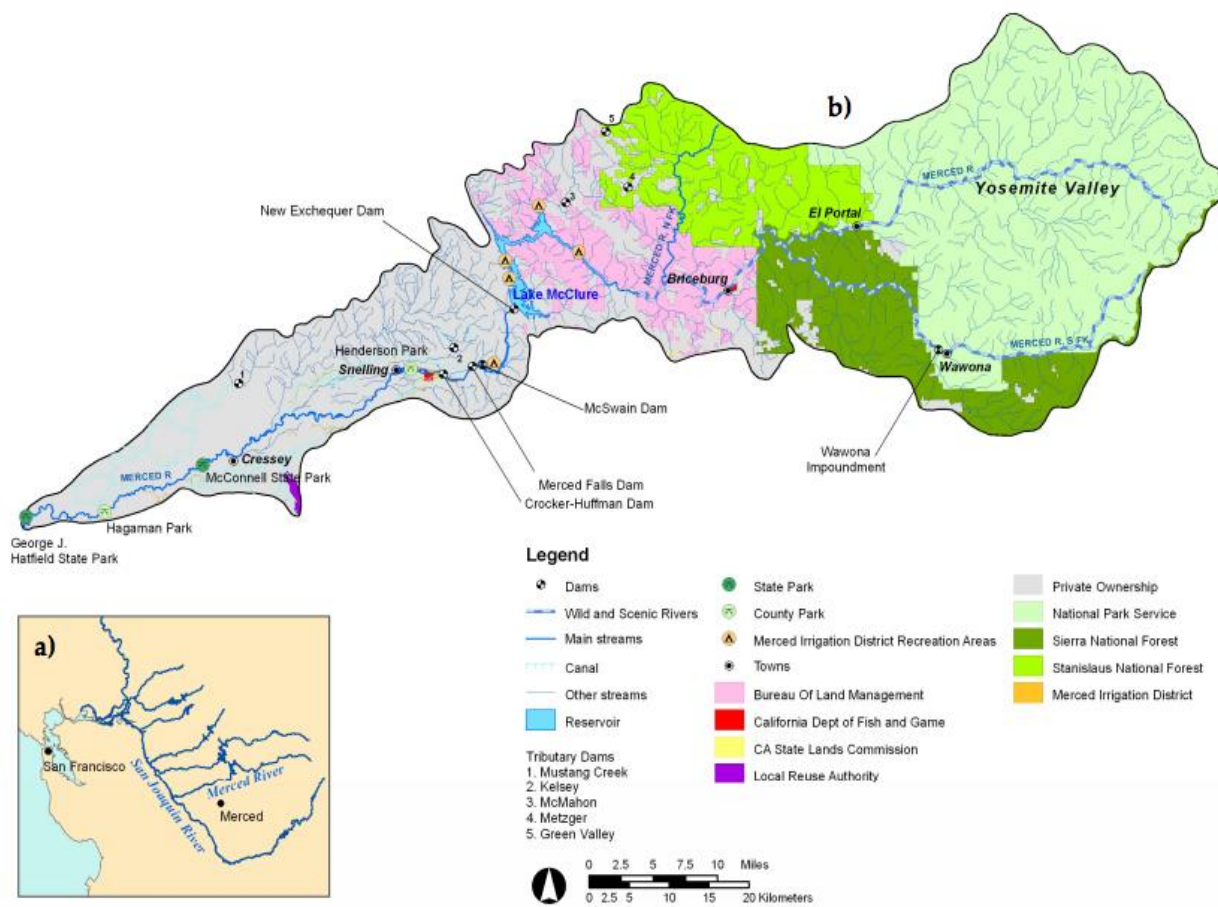


Figure 2.1. Upper Merced basin located in the San Joaquin Valley watershed. (Stillwater Sciences 2008). The Merced River is visible as a tributary of the San Joaquin River, flowing north into the Delta.

2.2.1 Climate

The climate of the San Joaquin Valley varies spatially and is most often characterized as Mediterranean with a dry summer season and a cool, wet winter season. Temperate, semi-arid conditions enable a year-round growing season (Phillips et al. 2007). During the summer (June, July, and August) average temperatures range from 22.9°C to 27.4°C. In the winter (December, January, and February) average temperatures fall

between 7.3°C to 11.2°C. Average rainfall is approximately 200–300 mm with most rainfall occurring during the months between November–April and to a lesser extent, May–October (NOAA 2015). Weather stations located in the SWAT model domain were selected to help describe the study area’s climate. Weather station data include daily data precipitation, maximum and minimum temperature, relative humidity, and wind speed.

Temperature increases as rainfall decreases while examining the area from north to south. About 85 percent of annual precipitation occurs during the winter and spring season month (November–April). Whereas the summer months, June, July, and August, are the most arid, with negligible rainfall from May to October (Ficklin et al. 2009). Precipitation most often evapotranspires before it is able to recharge the subsurface, falling as either rain or trickling into the basin as snowmelt. Average precipitation estimates using SWAT are variable but snowmelt account for an average 85% of annual discharge in the Merced River (Wang and Melesse 2006).

2.2.2 Topography, geology, and soils

The land surface in the study slopes westward from the Sierra Nevada Mountains and Coast Ranges to the San Joaquin River. Overall, the Central Valley is flat stands at a low altitude, with gradients ranging from less than 1 m/km by the San Joaquin River to more than 5 m/km by the foothills, neighboring rivers and streams, and the surrounding local area (Phillips et al. 2007). According to Bolger (2009), slope calculations using HydroGeoSphere (HGS) calculated elevation gradients within a similar model domain range from 0 to 144.4% (about 0 m/km to 144,356 m/km). Average elevation of the Upper Merced subbasin is 1,392 m, with an elevation range of 18 m to 3,979 m. The Upper

Merced subbasin is predominately evergreen forest (41%), range-bush (28%), and range-grasses (16%) (NLCD 2006).

The San Joaquin Valley is a sediment-filled forearc basin, which is bound to the western California Coast Ranges, and to the eastern Sierra Nevada Mountains. The asymmetrical basin is relatively new to the Americas, having first come into being 65 million years ago during the Mesozoic era. When the SJV was formed, it was an inland sea wedged between two mountain ranges. As the volcanic cover of the Sierras corroded and the Coast Ranges eroded, sediment fell into the Valley below transforming the inland sea into the continental basin of today. Over time, sediment amassing from high elevations, eroding granite, and streamflow, established an adjacent low and flat Central Valley below the southern Sierra Nevada Range. The resultant structure is called a down-warping geosyncline, or a large scale syncline fold (Sneed 2001). Marine sediments and continental deposits forced the rivers to flow around pockets of growing sediment, effectively transforming the fluvial system in geological time. Deposited sediment and organisms accumulated on the basin floor, resulting in the region's iconic nutrient-rich soil.

Most of California is dominated by Mesozoic and Cenozoic Era rocks and so principal rocks observed in the region are Mesozoic plutonic and metamorphic rocks. Along the eastern part of the valley, pre-Tertiary crystalline and metamorphic rocks run underneath the sediment. To the west, pre-Tertiary mafic and ultramafic complex line the trough. The Sierra Nevada is comprised of granite, plutonic, metasedimentary, and metavolcanic rocks (Bertoldi et al. 1991). Negligible water quantities rest within these rocks, held by small scale fractures and joints.

2.2.3 Watershed surface-water hydrology

The San Joaquin Valley River watershed encompasses the following four hydrologic units: the middle San Joaquin and lower Chowchilla watersheds, the middle San Joaquin, lower Merced, and lower Stanislaus River watersheds, the upper Chowchilla and upper Fresno River watersheds, and the Panoche and San Luis Reservoir watersheds (VanRheenen et al. 2004). Running parallel with the Pacific Coast, the watershed covers 280 by 115 miles of seventeen California counties, reaching from north of Lodi County to south of Bakersfield County. The highest headwaters are over 12,000 ft, but flows to 580 ft at the foothills of the southern Tehachapi Mountains near the Mojave Desert. To the north, ridges separate the San Joaquin River Basin from the Sacramento River, and drainages of the Pajaro River, Salinas River, and Carrizo Plain border the basin to the west (Figure 2.2).

Snowmelt trickling from the surrounding mountains drains eastward into the valley, eventually joining the San Joaquin River to the Sacramento-San Joaquin Delta, further flowing through the Suisun Bay and San Francisco Bay, and eventually meets the Pacific Ocean. The Sierra Nevada is the main source of runoff, with the Coast Ranges experiencing less rainfall and therefore less able to sustain streamflow (Hanak and Stryjewski 2002). There are seven major tributaries which drain directly into the San Joaquin River, all flowing west from the Sierra Nevada: Mokelumne, Calaveras, Stanislaus, Tuolumne, Merced, Chowchilla, and Fresno Rivers. The observed discharge of the San Joaquin River from a period 1930 to 1983 ranged from 241 cubic feet per second (cfs) to 99,900 cfs; the average discharge was 4,783 cfs (USGS). The Tuolumne River has

the longest and highest discharge, followed by the Merced River. Discharge of the Kings River also enters the Basin through a tributary (VanRheenen et al. 2004).

The San Joaquin River and accompanying tributaries have been severely regulated for agricultural, municipal, and industrial use. Erected dams along the SJV have helped create reservoirs mainly for irrigation uses and power supply, but have transformed the area's native ecology drastically. Before human intervention, tule marshes, riparian corridors, and other wetlands ran along the banks of the SJV (CERES 2005). Leftover wetlands are less than 8% of the wetland acreage before the 19th century. Of these remnant wetlands, most are public lands managed at the state and federal levels, and privately owned duck clubs (CERES 2005). Unfortunately, a hundred years of flow capture and diversion practices have dried adjacent wetlands and lessened overall SJV biodiversity.

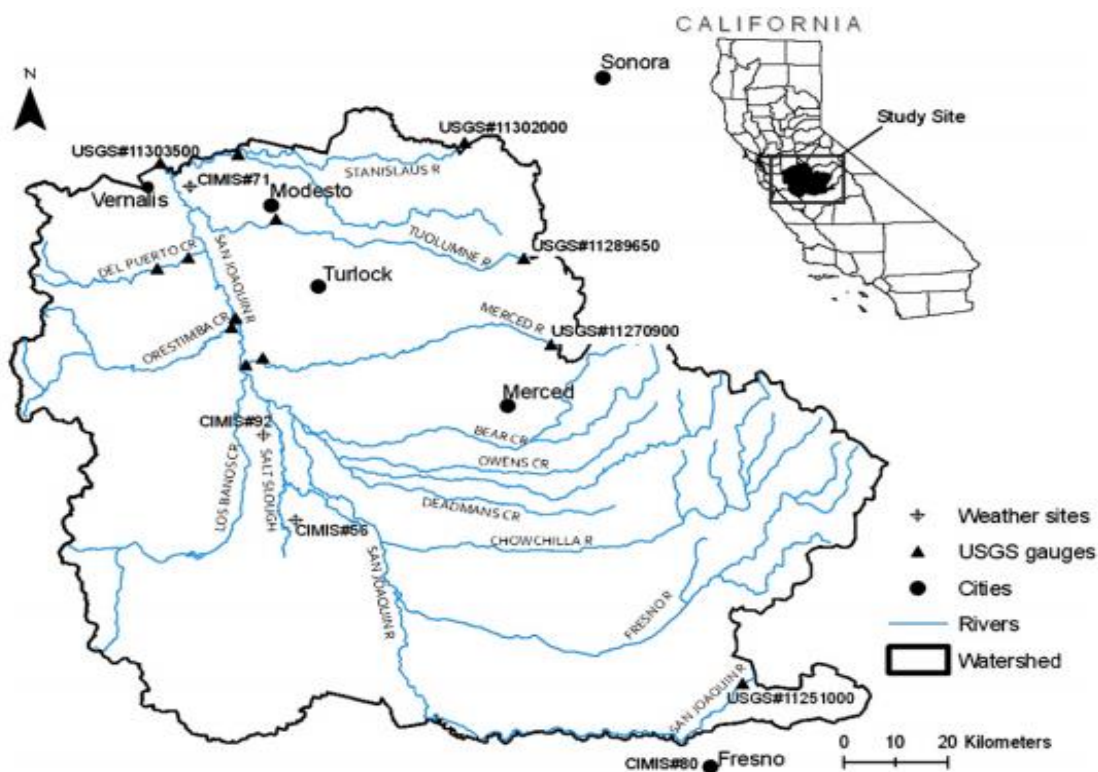


Figure 2.2. Depiction of Northern San Joaquin watershed. Adapted from D.L. Ficklin et al. 2009.

2.3 STUDY AREA WATER REOURCES

2.3.1 Water Availability

Much of the water provided to residents and farmers of the San Joaquin Valley has been through federal and state water supply infrastructure. Federal investment in infrastructure under the Reclamation Act of 1902 enabled the Central Valley Project (CVP) and the State Water Project authority to provide water to farmers within the San Joaquin Valley. Water deliveries range from six to seven million acre-feet annually, with 1.5 acre-feet diverted from the San Joaquin River via the Friant-Kern and Madera Canals. Of the San Joaquin Valley's total developed water supply in 2000, approximately 44% is derived from surface sources, 23% is imported surface supplies through the CVP and the State Water Project, and 33% is pumped from groundwater sources (Hanak and Stryjewski 2002).

Groundwater supply develops in unconfined or partially-confined, shallow aquifers across the valley. According to Sneed (2001), three unique groundwater bodies are found across the western, central, and southeastern parts of the valley: unconfined and semi-confined fresh water bodies in alluvial deposits overlaying the Corcoran Clay unit, fresh water in alluvial and lacustrine deposits confined underneath the Corcoran Clay unit, and a zone of saline water trapped in marine sediments beneath fresh water bodies throughout the region. Before development in the early 20st century, groundwater in alluvial sediments were replenished via infiltration through stream channels near the valley. Eastern-valley streams carrying runoff from the Sierra Nevada snowpack supported the lion's share of recharge for valley aquifers. Additional water recharge is provided through rainfall and

lake or stream seepage, but in small amounts due to California arid climate. Barring human intervention, groundwater discharge provided a balance between natural replenishment and natural depletion by way of evapotranspiration and streamflow (Sneed, 2001).

The San Joaquin River has been drastically altered for human use. Due to lack of groundwater record keeping, concrete measurements of groundwater divestment is not available. Estimations of the groundwater deficit may have totaled nearly 800,000 acre-feet per year during the 1960s, before the impacts of climate change augmented California's water shortage (Hanak and Stryjewski 2002).

2.3.2 Water Use

The valley is predominately farmland with pockets of urban development. Eighty percent is utilized for agricultural use, six percent of the region is urban cover, and the remaining lands are covered in natural vegetation near the foothills and riparian area (CDWA 2007). Agriculture is the primary land use, with seven of the top ten farming counties in the state residing in the valley, with over 30.6 billion in crop receipts (CDWA 2007). The watershed provides for the most agriculturally active counties such as Stanislaus, Merced, Madera, and a portion of San Joaquin and Fresno counties, seen in Figure 2.3. Farmland varies between counties, but constitutes 45% to 90% of land area in all San Joaquin Valley counties. In total, irrigated land constitutes 30% of the watershed, while forest and park land encompass 26.8% of total land area.

Agriculture in the San Joaquin Valley is largely dependent on irrigation due to arid conditions. Farmers in the area use both groundwater and surface-water to irrigate

croplands. In order to meet their irrigation needs, water is developed and delivered by a number of government organizations, such as the Central Valley Project and the State Project, which both sell long-term water contracts to irrigation districts like Modesto and South San Joaquin. Irrigation districts then transfer water to farmers through irrigation canals and aqueducts. Historically, surface-water irrigation supplies derive from reservoirs at the Sierra Nevada foothills and snowmelt during late-winter and spring seasons. Private agricultural user and irrigation districts often pump groundwater for irrigation when surface-water levels are low or when the water table rises too significantly and threatens to drown crop fields (Phillips et al. 2007). Groundwater pumping remains unregulated (Ficklin et al. 2009), but has been estimated to have been approximately 32 percent of total agricultural water use in 2000 (Phillips et al. 2007).

By the same token, urban water demand is filled by both surface-water and groundwater supply. Based off the work of Burow and others (2004), about 55 percent of urban water demand was met by groundwater in 2000. Modesto, the largest city in the valley, utilized groundwater exclusively for municipal water supply. A surface-water treatment plant was built post 1995, providing for half of the industrial and private water demands (Phillips et al. 2007). Based on local drillers' records, about 60 percent of groundwater wells in the valley are for domestic use, 27 percent for irrigation, 4 percent for public supply, and 7 percent for other uses such as industrial use (Phillips et al. 2007).



Figure 2.3. San Joaquin Valley region map with the eight counties studied labeled. Image originating from the “San Joaquin Valley Greenprint State of the Valley Report” published by Fresno Council of Governments, and written by Thorne, J.H., Roth, N.E., Boynton, R.M., Woodard, N. (2014).

2.3.3 Water Quantity Concerns

The consequences of climate change have been observed in temperature, precipitation, and runoff data. By comparing these observed parameters in change from “naturally” and “anthropogenically” forced global change models, Barnett et al (2008) demonstrated developing temperature, precipitation, and runoff trends in the Western United States beyond natural variability and attributed about 60% of 1949–1999 trends to anthropogenic catalysts such as increased GHG’s and sulfate aerosols. Therefore, over half

of California's variation in hydrological patterns has been found to be products of anthropogenic activity.

Temperature change is the main driver for disruptions in the hydrological cycle. When mean atmospheric temperature increases, the vapor pressure difference between ocean surfaces and the atmosphere widens, creating a positive feed-back loop perpetuating more water evaporation. As reported by the National Centers for Environmental Information, California has sustained a gradual increase of 1.1–2° F in temperature over the past century. Minimum and maximum annual temperatures have increased, but minimum temperatures (+1.6 to 2.5° F) have warmed more than maximum temperatures (+0.4 to 1.6° F) (NOAA 2015). Warmer temperatures push the snow line higher and lessen snowpack, abating California's most significant water storage reservoirs. According to the California Department of Water Resources, a trend towards more rain than snow in total precipitation volume has evidenced in recent decades.

Variation in runoff timing has materialized from greater temperatures and rainfall, shifting runoff to earlier in the spring season. Numerous studies of changes to California streamflow patterns have confirmed such behavior, supporting evidence that seasonal fraction of runoff flowing through the spring season has decreased throughout the twentieth century (Roos 1991; Aguado et al. 1992; Dettinger and Cayan 1995; Freeman 2002; Stewart et al. 2005). Precipitation patterns have increased winter runoff and decreased spring runoff, which is in contrast with the design of California's water infrastructure. Flood protection and water supply infrastructure have been developed for historical conditions, built to catch slow spring runoff and deliver it to users during the more arid summer and winter months. Although shifting runoff timing is not a certain

manifestation of climate change, a larger volume of runoff is flowing downstream earlier in the season (Aguado et al. 1992; Dettinger and Cayan 1995; Stewart et al. 2005). Without adaptations to existing water infrastructure, earlier runoff reduces the state's ability to refill reservoirs during and after the flood season has occurred.

The Sierra Nevada snowpack has exhibited corroding trends in recent years due to annual precipitation falling as rain and greater temperatures reaching high altitudes causing snowmelt. Historically, the montane landscape has been a reliable snow zone, capturing reservoirs of fresh water as snow from late March until early summer. In recent years, studies have warned of a decreasing trend in snowmelt-fed basins correlating with temperature increases throughout the Western United States (Regonda et al. 2005; Mote et al. 2005). Snowpack is measured in “snow water equivalent” (SWE), or how much water would result if the snow were to melt. On April 1, 2015, the Sierra Nevada measured a record-breaking 10 percent of normal “snow water equivalent” (SWE) for the season during the second warmest year in California, recording an average temperature of 1.5° F higher than 2014. Following the lowest SWE levels ever documented, 2016 SWE levels in Northern California measured 90 percent of normal SWE on April 1 (Swain et al. 2016). El Niño conditions bolstered this year's mountain snowpack – drenching Northern California in a series of March storms. Despite a wet winter in Northern California, Southern California continued to endure extremely dry conditions. Normally El Niño winters flood both North and South California, but a high pressure “ridiculously resilient ridge” over the Pacific Ocean buffered storms from the South (Swain et al. 2016). Lien-Mager (2016), a spokeswoman for the Association of California Water Agencies, reflected on the deepening of snowmelt depletion after the April 2016 reading, “[this] flips our system on

its end. It is designed to capture gradual runoff from snowmelt. If we're moving away from that kind of pattern, then we may be getting too much runoff at a certain time, and we won't necessarily be able to capture it all," (Upton 2016). Overall, the main observed effects warmer temperatures have on snowpack have included shifts in ratio of rain to snow, delays and reductions in snow season, and expedited spring snowmelt.

CHAPTER 3

Literature Review

3.1 CALIFORNIA: OBSERVED AND FUTURE CLIMATE

The impacts of climate change are expected to exacerbate existing demands on California's water resources. The West's climate is highly variable in both space and time, causing known hydrological patterns to become vulnerable under consequences of climate change. A shifting network of heat, moisture, and energy between the atmosphere and ocean determine conditions of precipitation over the region. Whether this moisture falls as snow or rain is contingent on the region's topography.

Historically, the majority of Western precipitation has been experienced as snow, capping the Sierra Nevada Mountains while awaiting trickle-down in the spring. Sierra Nevada snowpack provide water storage by reserving supply during winter months to avoid flood risk, and expelling water into valleys and rivers for irrigation during spring and early summer months. Surrounding the snowcapped mountains, arid rain-shadow landscapes sit leeward across from irrigated windside areas fed mainly by rivers. Circumstances of river flow are dependent on snowpack accumulation and its subsequent meltwater. Nearly all major rivers flowing through the Western United States are fed from snowpack mountain watersheds, and so a reduction in snowcap mass greatly affects water resources for irrigation and human use.

The consequences of climate change have been observed in temperature, precipitation, and runoff data. Concerns of major fluctuations in the hydrological cycle

causing increases in water demand have spurred the need for a greater understanding of climate change repercussions on California's water supply. To estimate future burdens of climate change borne by California's water resources, researchers determine projected changes in climatic variables and evaluate the resulting divergence in streamflow from observed historical patterns via global climate change models (GCMs). By comparing these observed parameters in change from "naturally" and "anthropogenically" forced global change models (GCMs), GCMs have demonstrated developing temperature, precipitation, and runoff trends in the Western United States beyond natural variability. Although GCMs have projected an increase in temperature for California of between 2.5 °C to 9°C consistently by 2100, there is much greater variability in precipitation projections (Dettinger 2005). In order to reach more sound conclusions on precipitation and resulting runoff and streamflow patterns, research has been conducted using a multitude of GCMs and emissions scenarios. Therefore, the scientific community has not reached a general agreement on precipitation or streamflow projections for California.

3.1.1 Temperature change

Temperature change is the main driver for disruptions in the hydrological cycle. When mean atmospheric temperature increases, the vapor pressure difference between ocean surfaces and the atmosphere widens, creating a positive feed-back loop perpetuating more water evaporation. As reported by the National Centers for Environmental Information, California has sustained a gradual increase of 1.1–2° F in temperature over the past century. Minimum and maximum annual temperatures have increased, but minimum temperatures (+1.6 to 2.5° F) have warmed more than maximum temperatures

(+0.4 to 1.6°F) (NOAA 2015). Warmer temperatures push the snow line higher and lessen snowpack, abating California's most significant water storage reservoirs. According to the California Department of Water Resources, there is evidence of a trend towards more rain than snow in total precipitation volume has evidenced in recent decades. As seen in Figure 3.1, percentage of precipitation falling as rain is more common in later years of record.

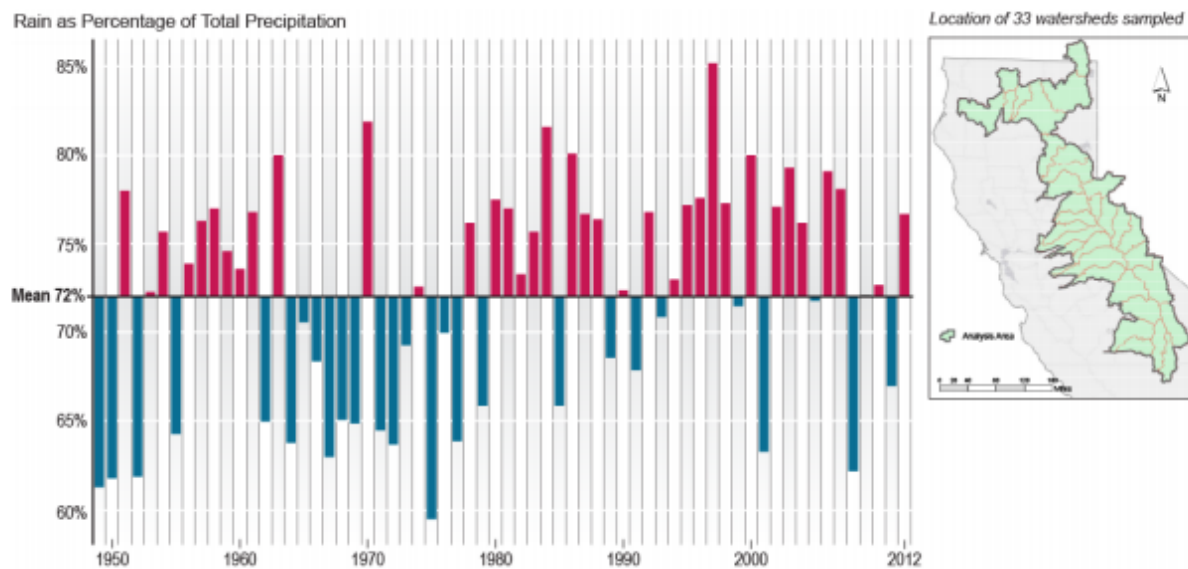


Figure 3.1. Percentage of precipitation falling as rain over 33 main water supply watersheds in California during the period of October 1948 to September 2012. Data are analyzed using Western Region historic precipitation and freezing level re-analysis and published by the California Department of Water Resources. Observed watersheds experience a mean of 72 percent of precipitation as rain overall; red bars indicate a higher percentage of rain than the mean for a given year, blue bars demonstrate a lower percentage of rain than the mean for a given year. Figure from the “California Water Plan” 2013 update, published by the Division of Integrated Regional Water Management within the Department of Water Resource. Retrieved from http://www.water.ca.gov/waterplan/docs/cwpu2013/Final/Vol2_SanJoaquinRiverRR.pdf.

3.1.2 Runoff timing

Variation in runoff timing has materialized from greater temperatures and rainfall, shifting runoff to earlier in the spring season. Numerous studies of changes to California streamflow patterns have confirmed such behavior, supporting evidence that seasonal fraction of runoff flowing through the spring season has decreased throughout the

twentieth century (Roos 1991; Aguado et al. 1992; Dettinger and Cayan 1995; Freeman 2002; Stewart et al. 2005). Precipitation patterns have increased winter runoff and decreased spring runoff, which is in contrast with the design of California's water infrastructure. Flood protection and water supply infrastructure have been developed for historical conditions, built to catch slow spring runoff and deliver it to users during the more arid summer and winter months. Although shifting runoff timing is not a certain manifestation of climate change, a larger volume of runoff is flowing downstream earlier in the season (Aguado et al. 1992; Dettinger and Cayan 1995; Stewart et al. 2005). Without adaptations to existing water infrastructure, earlier runoff reduces the state's ability to refill reservoirs during and after the flood season has occurred.

3.1.3 Snowpack accumulation

The Sierra Nevada snowpack has exhibited melting trends in recent years due to annual precipitation falling as rain and greater temperatures reaching high altitudes causing snowmelt. Historically, the montane landscape has been a reliable snow zone, capturing reservoirs of fresh water as snow from late March until early summer. In recent years, studies have warned of a decreasing trend in snowmelt-fed basins correlating with temperature increases throughout the Western United States (Regonda et al. 2005). Snowpack is measured in "snow water equivalent" (SWE), or how much water would result if the snow were to melt. On April 1, 2015, the Sierra Nevada measured a record-breaking 10 percent of normal "snow water equivalent" (SWE) for the season during the second warmest year in California, recording an average temperature of 1.5° F higher than 2014 (Swain et al. 2016). Following the lowest SWE levels ever documented, 2016 SWE

levels in Northern California measured 90 percent of normal SWE on April 1 (Swain et al. 2016). El Niño conditions bolstered 2016 early mountain snowpack – drenching Northern California in a series of March storms. Despite a wet winter in Northern California, Southern California continued to endure extremely dry conditions. Normally El Niño winters flood both North and South California, but a high pressure “ridiculously resilient ridge” over the Pacific Ocean buffered storms from the South (Swain et al. 2016). Overall, the main observed effects warmer temperatures have on snowpack have included shifts in ratio of rain to snow, delays and reductions in snow season, and expedited spring snowmelt.

3.2 METHODOLOGY OF ASSESSING CLIMATE CHANGE IMPACTS ON CALIFORNIA STREAMFLOW

To assess future consequences of climate change on hydrological systems, research is conducted using two methods: (1) an evaluation of hypothetical scenarios involving increases in temperature and/or CO₂ and; (2) an assessment of projected climatic fluctuations via general circulation model (GCM) outputs. Either methodology estimates shifts in climatological variables (for example temperature, precipitation, and evapotranspiration), which can be used to assess the burden that greater climate change places on hydrological components such as streamflow. Figure 3.2 provided by Vicuna and Dracup (2005), illustrates the above methodologies used to determine hydrologic implications of climate change from initial CO₂ emission scenario information.

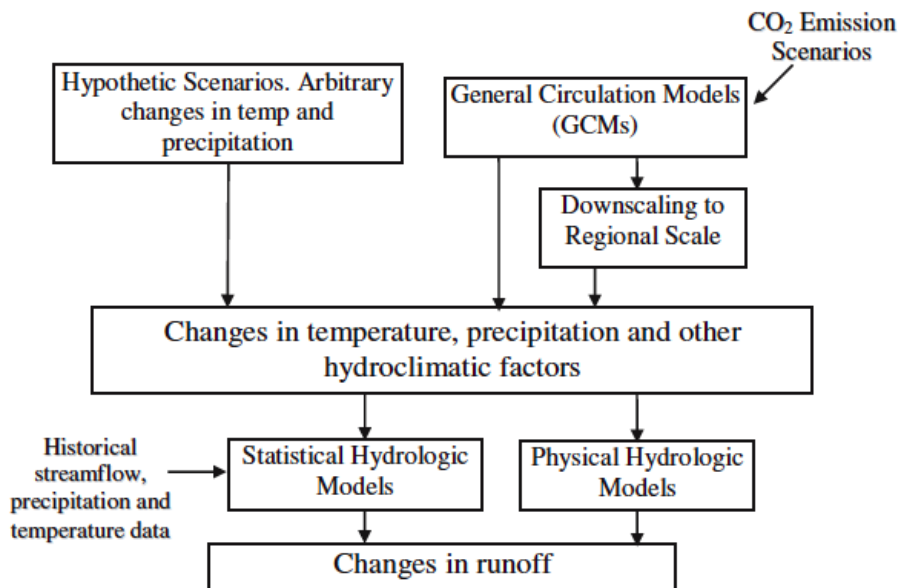


Figure 3.2. Schematic representing two approaches to determine changes in the hydrological cycle in accordance with climate change impacts.

3.2.1 Establishing changes in temperature and precipitation

Projected hypothetical scenarios are valued for representing a wide range of end-of-century temperature possibilities (+2°C to +5°C), while testing for both increases and decreases in precipitation projections (Vicuna and Dracup 2005). The wide range of plausible future climate shifts allows for a thorough assessment of alternative projections and basin sensitivity, but does not help determine the probability of climate scenarios. Therefore, hypothetical projections cannot aid in understanding the most probable impacts of climate change, rendering the approach unhelpful in evaluating future water resource management mitigation strategies. With climate change threatening water resources, GCMs have largely eclipsed the use of hydrological climate scenarios in climate research (Ficklin et al. 2009; Wang et al. 2011; Georgakakos et al. 2012; Pierce et al. 2013; Stewart et al. 2015; Ishida et al. 2017).

Unlike broad hypothetical temperature and precipitation scenarios, GCMs are computer-intensive coupled models allowing for simulations of atmosphere-land-ocean-ice interactions. Complex in nature, GCMs perform calculations over a given area across horizontal and vertical dimensions through a series of timesteps. Popular global models employed by recent climate change studies are the UK's Hadley Center (HadCM2 and HadCM3), the NCAR (CCM3 and PCM), and the Canadian Center for Climate Modeling and Analysis Canadian (CGM1). In order to successfully use GCM outputs, data must be downscaled to parallel the respective hydrological model's spatial and temporal resolutions so that outputs may be applied to surface variables at the basin scale.

Localized climate changes over complex orography impacts convective precipitation, requiring downscaling techniques to bridge the gap between coarse resolutions of GCMs and local sub-grid catchment scales. Thus downscaling efforts are especially pertinent in regions of varying topography such as snowmelt-fed basins and watersheds. Prevailing models of downscaling in climate modeling literature are the following: delta/ratio perturbation methods; stochastic/statistical downscaling; and dynamic downscaling (Wood et al. 1997). Although a simple perturbation method allows for higher resolution observations, current GCM studies more often apply either statistical or dynamic downscaling methods for increased confidence in climate change impact assessments. Statistical downscaling is a two-step process involving (1) the creation of statistical relationships between local climate variables (e.g. precipitation and surface air temperature) and large-scale predictors (e.g. sea level pressure), and (2) the application of such determined relationships to GCM outputs in order to establish future local climate

predictions (Vicuna and Dracup 2005). Curtailing inconsistencies in GCM output data aids in lessening general ambiguity in observed climate modeling trends.

3.2.2 Determining changes in natural runoff

To determine fluctuations in surface streamflow, historical temperature and precipitation data are used to project changes in natural runoff. This process can either be completed via statistically or physically based models. Statistically based methods employ either regression or observational analysis to determine the relationship between runoff and temperature/precipitation, but are unable to evaluate how climate forcings interact with the physical environment. Because of this shortcoming, most recent studies for the California mountainous region are physically based models. Physically based models incorporate the important physical processes and mechanisms necessary to deduce a hydrological basin's response to climate change. Although it is possible for researchers to build a personal model for the given study area, all literature included use already established models. Most common physical models include: the SUGS Precipitation-Runoff Modeling System (PRMS); the Soil and Water Assessment Tool (SWAT) (Ficklin et al. 2009; Stewart et al. 2009); the U.S. National Weather Service River Forecast System Sacramento Soil Moisture Accounting and Anderson Snow Models (SAC-SMA); the Water Evaluation and Planning System (WEAP) model; the Variable Infiltration Capacity (VIC) model; the Weather Research and Forecasting Model (WRF) (Pierce et al. 2013; Ishida et al. 2017); the Integrated Forecast and Reservoir Management (INFORM) (Georgakakos et al. 2012); and The Weather Research and Forecasting Model (WRF) (Ishida et al. 2017).

3.3 GCMS: PREDICTED TRENDS IN ENVIRONMENTAL INDICATORS

To estimate future burdens of climate change borne by California's water resources, researchers determine projected changes in climatic variables and evaluate the resulting divergence in streamflow from observed historical patterns. Recent studies exhibited a wide range of solutions to decrease uncertainty – experimenting with different GCMs' outputs and GHG emission scenarios (Miller et al. 2003; Hayhoe et al. 2004; Ficklin et al. 2009; Wang et al. 2011; Ishida et al. 2017), narrowing uncertainty variables to the local level (Dettinger 2005; Stewart et al. 2015), and running multiple different modeling programs to appraise statistically significant calculations across all run GCMs (Maurer and Duffy 2005; Wang et al. 2011; Pierce et al. 2013; Ishida et al. 2017).

3.3.1 Temperature and precipitation

The IPCC Fifth Assessment Report (IPCC 2013) describes warming projections as “vertically certain” and GCMs consistently forecast a temperature increase in California during both summer and winter seasons. Depending on the chosen emission scenario, summer temperatures are estimated to endure an increase between 3.87°F and 14.9°F by 2100. Likewise, winter temperatures are assessed to increase between 3.87°F and 7.2°F (Cavagnaro et al. 2006). Future simulations conducted by Scripps Institution of Oceanography calculate that by 2060–2069, mean temperatures will be 3.4°F to 4.9°F higher than their 1985–1994 counterparts (Cavagnaro et al. 2006).

Despite a general consensus in warming trends, there is broad variability in precipitation projections depending on the GCM formed. End of the century Northern California precipitation projections range from about –300 to +250 mm yr⁻¹ (He et al.

2013). Contradictory findings can be attributed to researchers considering differing GCM outputs, utilizing various GHG emission scenarios, and different modes of downscaling via dynamical methods to better simulate the complex Sierra Nevada orography (Kiparsky and Gleick 2003). Research conducted by Caldwell (2010) indicated that regional models often overpredict, while large-scale models tend to under predict future California precipitation forecasts. For example, Mauer (2007) infers of an increase in winter-time precipitation over Northern California and a smaller increase of wintertime precipitation across Southern California from a statistical downscaling of 11 GCMs, yet Ishida et al. (2017) found no significant trend among 4 GCMs in annual accumulated average precipitation over a large area of 8 California basins.

Additional studies have determined contradicting evidence within their respective studies, such as Cayan et al. (2008). As analyzed from one GCM simulation, Cayan et al. (2008) saw a 10–20% reduction in precipitation across California, yet described increased future extreme precipitation events over Northern California similar to Pierce et al. (2013). Pierce et al. (2013) determined mixed precipitation findings across 25 dynamically and statistically downscaled models; of the 25 model projections evaluated, 21 GCMs shown a decrease in precipitation by 2060s, with a mean reduction of 6-14 days yr¹ and a general precipitation decrease of about 5.7%. In the same study, 16 of the 25 GCMs determined a daily precipitation intensity increase of 5.3% annually.

3.2.2 Loss of snowpack

Results of recent downscaled studies propose that as temperatures increase nationally, more precipitation will occur earlier in the spring and fall as snow (Knowles et

al. 2006; Null et al. 2010; Hanak and Lund 2011). As discussed earlier, increasing temperatures will reduce Northern California snowpack in thickness and duration. However, apart from this general agreement, there is substantial ambivalence between GCM projections in both the spatial and temporal magnitude of snowpack deterioration. According to Scripps Institution of Oceanography modeling research, the Sierra Nevada snowpack will endure a 48–65 percent loss from the 1961–1990 average depending on warming scenario (DWR 2015). A bleaker picture is set by Meisen (2011), with projections of 70–90% snowpack reduction by the turn of the century if current rates of emissions persists. If the lowest emission scenario is actualized, Meisen (2011) calculates a still substantial decrease of at least 35–45% by 2100.

Reductions in snowpack are apt to increase flood peak flows and flood volume, complicating flood control methods dependent on maintaining historical precipitation trends (Hanak and Lund 2011). Reservoirs downstream from the Sierra Nevada will experience probable major flood risks due to a culmination of climate change effects: enhanced temperatures, possible precipitation decline, and inflated flood volumes. Research completed by Cayan et al. (2008) referenced earlier, describes further flood amplification by a projected increase in major storm intensity and frequency due to climate change.

3.4 GCMS: PREDICTED TRENDS IN RUNOFF AND NATURAL STREAMFLOW

Variation in California's streamflow patterns were first explored by Roos (1987, 1991), in a study focusing on the Sacramento basin. Roos' research concluded that

seasonal fractional runoff during the spring season (April–July) was decreasing during the 20th century. More recent studies no longer utilize seasonal fractional runoff as a parameter for change because this measure could indicate changes in the spring runoff, or winter runoff, or both. In order to prevent uncertainties, Dettinger (2005), Cayan et al. (2009), and He et al. (2013) introduce different methodologies to measure changes in streamflow patterns. Dettinger (2005) focuses on more common climate change projections than extreme projections using a resampling method, “projection distribution functions” (PDFs). Cayan et al. (2009) employed two downscaling methods from the 2009 California Assessment: constructed analogues downscaling daily large-scale data, and bias correction and spatial downscaling which downscales monthly data, with a random sampling technique to generate daily values. Whereas, He et al. (2013), utilized flow-weighted timing, or “center of mass” (CT) of streamflow, as a metric to determine runoff timing.

Based on the findings of Dettinger (2005) and Cayan et al. (2009), the cumulative effects of climate change on total runoff volumes is inconclusive, other than describing a shift to an earlier, shorter spring snowmelt. Similarly, He et al. (2013) concluded broad annual streamflow variation between -41 and $+16.2\%$ (based on a precipitation ratio change between 0.8 and 1.2). Although, He et al. (2013) was able to determine the runoff center of mass (CT) will shift by 15–46 days on average due to temperature rises, and vary by 1–4 days on average due to temperature increases. High variability of streamflow will lead to a deviation in CT from the dry season (April–September) to the wet season (October–March).

On the other hand, a more recent study completed by Stewart et al. (2015) evaluating the A2 IPCC scenario with CMIP3 GCM, found an increase in overall

occurrence of streamflow exceeding 150% of historic monthly averages for winter and increased fluctuations in extreme low flows (<50% of historic monthly averages) during summer months by 2099. Further variability in flow volume was recognized under the IPCC A1B scenario with CCSM3.0 GCM by Georgakakos et al. (2012), as results concluded an earlier shift in monthly average streamflow.

CHAPTER 4

BACKGROUND ON UTILIZED MODELING PROGRAM AND CLIMATE MODELING DATA

4.1 INTRODUCTION

This paper projects two GCMs, The First Institute of Oceanography-Earth System Model (FIO-ESM) and the Met Office Hadley Center (HasGEM2-ES), onto a simulated Upper Merced Basin hydrological SWAT map. GCM data are projected from 2040-2099, under two likely greenhouse gas emission scenarios (RCP6.0, and RCP8.5). The SWAT program is a prolific watershed model within the scientific community, and has been utilized to investigate climate change effects on water resources by hundreds of case studies (Rosenberg et al. 1999; Stonefelt et al. 2000; Fontaine et. al 2001; Schuol et al. 2008; Ficklin et al. 2010; Ficklin et al. 2013).

To better define unique topographical areas within the Upper Merced Basin, SWAT allows the watershed to be partitioned into various subwatersheds called hydrological response units (HRUs). HRUs are grouped by comparable geomorphic and hydrological properties (Flugel 1995; Ficklin et al. 2009). A specific HRU is classified using soil, slope, and land use data, which were acquisitioned from government websites. Utilizing a strategy employed by Ficklin et al. (2009) climate change sensitivity in the San Joaquin watershed research, only land, soil, and elevation properties constituting over 5% of the subbasin were used in this study's HRU definition. Water delineation within the units is split into five storage areas: canopy interception, snow, soil profile, shallow

aquifer, and deep aquifer. Flow generation is found by an aggregation of flow across all included HRUs (Arnold et al. 2012).

4.2 SOIL AND WATER ASSESSMENT TOOL (SWAT)

SWAT is a publically available hydrologic and water quality model developed by the United States Department of Agriculture-Agricultural Research Service (USDA-ARS) and is an extension of the ArcGIS program. The SWAT model is utilized by the U.S. Environmental Protection Agency (U.S. EPA) in their Better Assessment Science Integrating Point and Nonpoint Sources (BASINS) software interface, employed by over 250 peer-reviewed published articles across many scientific disciplines (Gassman 2007). Figure 4.1 shows a schematic of SWAT's water management pathways.

The purpose of the project is to predict the impact of climate change on streamflow and water balance within the basin. SWAT can be utilized to run simulations for hydrological cycle, agricultural pollutant transport, weather conditions, and plant growth. To split the watershed, SWAT divides the region into multiple HRUs (Neitsch 2005). HRU water balance is defined by five storage components: canopy interception, snow, soil profile, shallow aquifer, and deep aquifer. SWAT evaluated flow generation across all HRUs in a subwatershed and maps the route through channels and reservoirs to the outlet (Neitsch 2005).

SWAT is physically based. Instead of using regression equations to describe the relationship between input/output variables, SWAT uses weather, soil, topography, vegetation, and land management data to express water and sediment movement, crop growth, and nutrient cycling. The program is especially adapted for agricultural

watersheds, performing analyses such as Total Maximum Daily Load (TMDL) and Best Management Practices (BMPs) evaluations.

Surface runoff predictions are derived from a similar method as CREAMS runoff model (Ficklin et al. 2010). Total runoff volume is determined with a SCS curve number method, which encapsulates soil, land use, and management data (USDA-SCS 1984). Potential evaporation is estimated using the Penman-Monteith method. This method is especially well suited for climate change scenarios that account for variation in CO₂ levels. Soil erosion and sediment routing equations such as the Modified Universal Soil Loss Equation (MUSCLE) involving nutrient outputs, are calculated using the SWAT platform. Although this paper does not focus on nutrient loads and daily nutrient runoff losses, SWAT is used to evaluate levels based on concentration in the top soil layer, the MUSCLE equation, and a soil-to-land use type ratio (Arnold et al. 1998).

4.3 THEORETICAL BACKGROUND OF SWAT

The Soil and Water Assessment Tool (SWAT) is an established hydrological model designed to simulate water availability, sediment levels, and agricultural chemical transport of an entire watershed. The platform allows for the simulation of climate, hydrology, crop growth, and erosion parameters under current and future projected conditions of climate change. In order to build a physically based and “quasi-physically based” model, SWAT employs methods to establish a hydrologic water budget, hydraulic river routing, reservoir simulation, diversion simulation, and snow pack simulation (Ficklin 2010).

4.3.1 Water yield

The hydrologic inputs of SWAT are based on the water balance equation applied to flow of water through soil:

(1)

$$SW_t = SW_o + \sum_{i=1}^n (R_{day} - Q_{surf} - E_a - w_{seep} - Q_{gw})$$

The above water balance equation simulates the land phase of the hydrological cycle by evaluating the following naturally occurring processes: precipitation, surface runoff, evapotranspiration (ET), recharge, and soil water storage.

4.3.2 Surface runoff

The Soil Conservation Service (SCS) curve number procedure (USDA-SCS 1972) method is used for estimating surface runoff and infiltration volumes using daily rainfall data. For each hydrological response unit (HRU), SWAT simulates surface runoff volumes and peak runoff rates. The SCS curve number equation utilized to estimate surface runoff is:

(2)

$$Q_{surf} = \frac{(R_{day} - 0.2S)^2}{(R_{day} + 0.8S)}$$

where, Q_{surf} is the daily surface runoff or rainfall (mm), R_{day} is daily rainfall (mm), and S is the retention parameter (maximum potential difference between rainfall and runoff from the onset of the rainstorm) (mm).

SCS assigns three preliminary moisture conditions: I – dry (wilting point), II – average moisture, and III – wet (field capacity) (Shawul 2013). The lowest value the daily curve number can simulate for dry conditions is moisture condition I. Moisture conditions I and III are calculated using Eqs. (3) and (4), respectively (Shawul 2013).

4.3.3 Retention parameter

There are two methods for calculating the retention parameter within SWAT. The “traditional” method is to enable the retention parameter to fluctuate with soil profile water content (Saleh et al. 2009). A more responsive evaluation of the retention parameter is the second method, which allows the retention parameter to vary with plant evapotranspiration (ET). By calculating daily CN as a function of plant ET, the value reflects the surrounding climate instead of possible soil storage (Neitsch et al. 2005). The daily retention parameter as a function of plant ET can be computed with the following equation:

(3)

$$S = S_{prev} + E_o * \exp\left(\frac{-cncoef - S_{prev}}{S_{max}}\right) - R_{day} - Q_{surf}$$

where S is the retention parameter for a given day (mm), S_{prev} is the retention parameter for the previous day (mm), E_o is the potential evapotranspiration for the day (mm), $cncoef$ is the weighting coefficient used to calculate the retention coefficient, S_{max} is the maximum value the retention parameter can accumulate per day (mm), R_{day} is daily rainfall (mm), and Q_{surf} is surface runoff (mm).

4.3.4 Evapotranspiration

SWAT uses two methods to calculate potential evapotranspiration (ET) – Hargreaves (Hargreaves et al. 1985) and Penman-Monteith (Monteith 1965). The Hargreaves method needs only daily air temperature to evaluate ET. Penman-Monteith method applies solar radiation, air temperature, wind speed, and relative humidity as inputs. The equations for Hargreaves (Hargreaves et al. 1985) and Penman-Monteith (Monteith 1965) are below, respectively:

(4)

$$ET_o = 0.0023 (T_c + 17.8)R_a(T_d)^{1/2}$$

where, T is daily mean temperature ($^{\circ}\text{C}$), T_c is monthly mean temperature ($^{\circ}\text{C}$), T_d is the difference between mean minimum and mean maximum temperatures for the month ($^{\circ}\text{C}$), and R_a is extra-terrestrial solar radiation.

(5)

$$ET_o = \frac{0.408\Delta(R_n - G) + \gamma \frac{900}{\tau + 273} \mu_2 (e_s - e_a)}{\Delta + \gamma(1 + 0.34\mu_2)}$$

where, T is daily mean temperature ($^{\circ}\text{C}$), u_2 is mean wind speed ($m^{-2} d^{-1}$), R_n is net radiation ($\text{MJm}^{-2} d^{-1}$), G is soil heat flux density ($\text{MJm}^{-2} d^{-1}$), γ is the psychometric constant ($\text{kPa } ^{\circ}\text{C}^{-1}$), e_s is saturation vapor pressure (kPa) derived from mean air temperature ($^{\circ}\text{C}$) per day, and e_a is actual vapor pressure (kPa) derived from mean dew point temperature ($^{\circ}\text{C}$) per day.

4.3.5 Sediment yield

Soil erosion rate and sediment yield are estimated for each HRU using the Modified Universal Soil Loss Equation (MUSCLE). MUSCLE simulates rate of erosion and sediment transport using surface runoff volume and peak rate. The MUSCLE equation is as follows:

(6)

$$Sed = 11.8 (Q_{surf} * q_{peak} * area_{hru})^{0.56} * K_{USLE} * C_{USLE} * P_{USLE} * LS_{USLE}$$

where, Q_{surf} is surface runoff volume (mm/ha), q_{peak} is peak runoff rate (m^3/s), $area_{hru}$ is area of a given hydrologic response unit (HRU) (ha), K_{USLE} is the USLE soil erodibility factor, C_{USLE} is the USLE cropping and management factor, P_{USLE} is the USLE conservation support practices factors, and LS_{USLE} is the USLE slope length (m) and steepness factor.

4.4 SENSITIVITY ANALYSIS: LH-OAT

“Sensitivity is a measure of the effect of change in one factor regarding to change in another factor” (McCuen 1973). An analysis of sensitivity determines which parameters the model is most sensitive to, so that eventual model calibration is optimized. Utilizing the Latin-Hypercube (LH) One-factor-At-a-Time (OAT) random sampling procedure built into the SWAT interface, sensitive parameters were able to be identified (van Griensven, 2005). The concept of LH simulation is derived from the Monte Carlo simulation but utilizes a stratified sampling instead of a random sampling (Melesse et al. 2011, Mishra

2013). Parameter distribution is split into n ranges, each range with the possibility of happening equal to $1/n$.

Below is the formula for the Monte Carlo simulation:

(7)

$$Y = f(x_1, x_2, \dots, \dots, x_k)$$

x are independent variables.

The range of each variable is split into non-overlapping intervals and one value from each interval is chosen. From here, n values of x_1 is randomly paired to n values of x_2 . These pairs are randomly combined to n value of x_3 to form n triplets, which is then repeated to form n k-tuplets called the LH Sample (LHS). From here, the OAT scheme performs the sensitivity analysis via SWAT (Melesse et al. 2011). The most sensitive parameters were identified using this method.

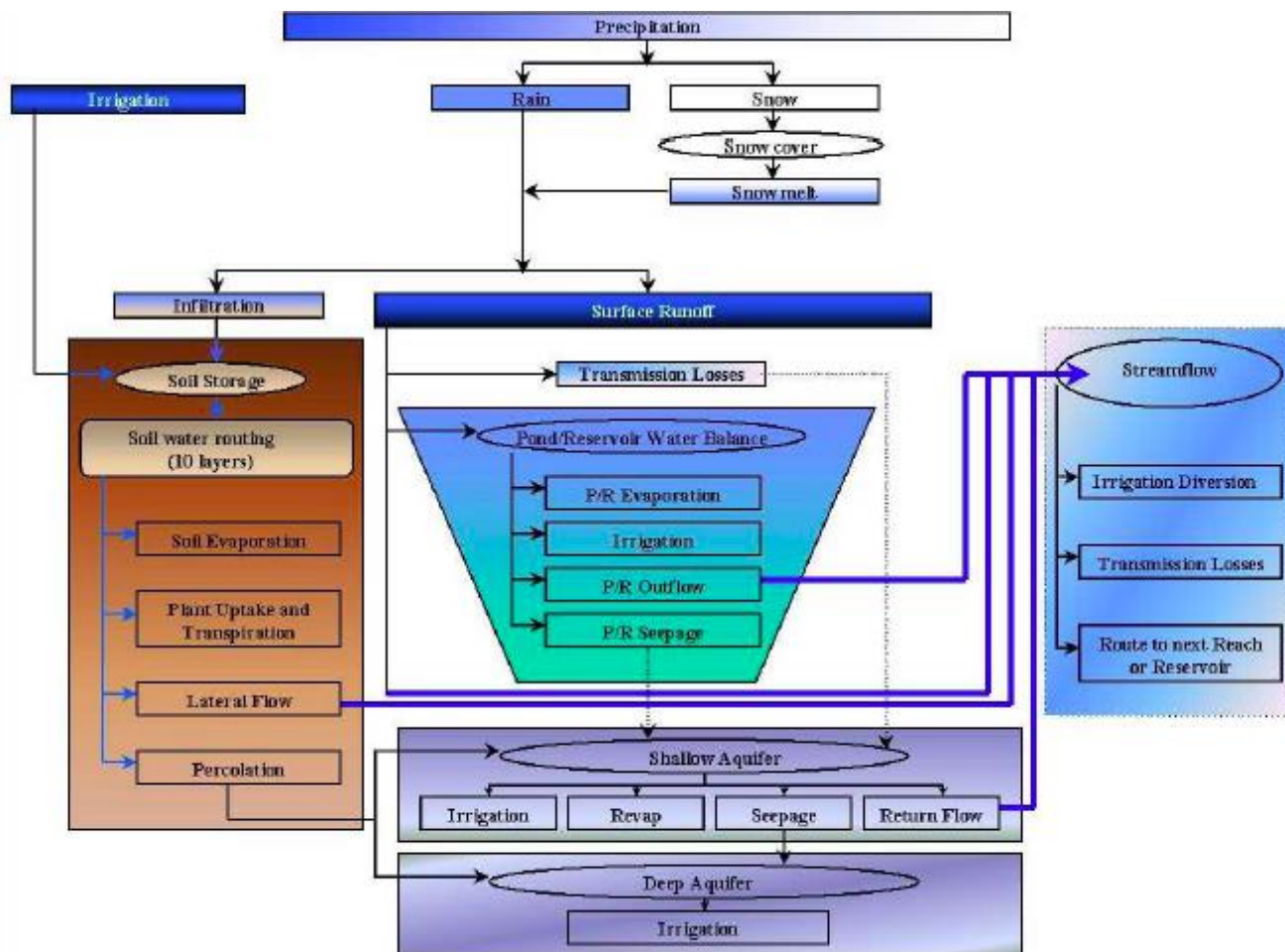


Figure 4.1. Schematic of water movement pathways in SWAT. Image pulled from “Soil and Water Assessment Tool Theoretical Documentation—Version 2005”, the work of the Soil and Water Research Laboratory completed by Neitch et al. (2005).

4.5 CALIBRATION AND VALIDATION METHODS: SWAT-CUP

The process of calibration is necessary and crucial to model application. Calibration is a procedure that seeks to evaluate and further refine model parameters as to compare observed and simulated values. Validation is an enlargement on calibration, the purpose of which is to make certain the newly calibrated simulation is aware of all outstanding variables, while assuring the model can predict further data accurately outside of the calibrated value set.

Calibration and validation are performed using the SWAT Calibration and Uncertainty Programs (SWAT-CUP). SWAT-CUP (Abbaspour et al. 2007) is a public domain program, which enables a SWAT project to be analyzed through SUFI2, PSO, GLUE, ParaSol, and MCMC procedures. Sequential Uncertainty Fitting Program 2 (SUF-2), a stochastic approach, was chosen to calibrate the model. SUFI-2 expresses uncertainty in parameters within a chosen range, allowing for the model result to account for most sources of uncertainty in climate driving variable. According to the SWAT-CUP program literature, model output variables are calculated at 2.5% and 97.5% levels of LAT-OAT output variable cumulative distribution (Abbaspour 2012). SWAT-CUP model results therefore provide 95% prediction uncertainty, referred to as 95PPU. To decipher between fit and calibration result, the “percentage of observed data enveloped” by the model (P-factor) and “the thickness of the 95PPU envelope (R-factor) are estimated. It is suggested P-factor have a value >70% for discharge, and R-factor exist around 1 (Abbaspour 2012).

bR^2 was chosen as the model’s objective function. An adjusted coefficient of determination R^2 , bR^2 is R^2 multiplied by the coefficient of the regression line b . This function can range between 0 and 1, where 1 is the goal value. Equation for bR^2 is below (Krause et al. 2005):

(8)

$$bR^2 = \begin{cases} |b|R^2 & \text{if } |b| \leq 1 \\ |b|^{-1}R^2 & \text{if } |b| > 1 \end{cases}$$

where, R^2 is the coefficient of determination and b is the slope of the regression line between the observed and simulated variables.

When b is the coefficient of the regression line, the coefficient of determination is computed as (Abbaspour et al. 2004):

(9)

$$R^2 = \frac{[\sum_i (Q_{m,i} - \bar{Q}_m)(Q_{s,i} - \bar{Q}_s)]^2}{\sum_i (Q_{m,i} - \bar{Q}_m)(Q_{s,i} - \bar{Q}_s)^2}$$

where, Q_m is the mean of observed discharges and Q_s is simulated discharge.

R^2 model results are considered “good” if the coefficient was larger than 0.5, and better if the coefficient is closer to 1 (Santhi et al. 2001; Moriasi et al. 2007; Abbaspour 2012).

From here, the Nash-Sutcliffe coefficient of efficiency (Nash and Sutcliffe 1976) and Percent Bias are applied. NSE is evaluated for “goodness of fit” as suggested by the American Society of Civil Engineers (ASCE, 1993). The NSE coefficient quantitatively describes the accuracy of model outputs, indicating closeness of observed data versus simulated data to an equal value (1:1) line. Model results were considered “good” if the coefficient was larger than 0.75, and “decent” if the coefficient was between 0.36 and 0.75 (Van Liew and Garbrecht, 2003; Larose et al. 2007; Luo et al. 2008). The equation for NSE is as follows (Moriasi et al. 2007):

(10)

$$NSE = 1 - \frac{\sum_{i=1}^N (Q_{obs,i} - Q_{sim,i})^2}{\sum_{i=1}^N (Q_{obs,i} - \bar{Q}_{obs})^2}$$

where, $Q_{obs,i}$ is the observed flow for the time step i , $Q_{mod,i}$ is the modelled flow for the timestep i , and N is the number of time steps.

Percent Bias (PBIAS) is used as a way of statistical analysis to evaluate errors within the deviation of data (Moriassi et al. 2007). Essentially, PBIAS measures the tendency of modelled data to be larger or smaller than the observed data. Optimal PBIAS value is 0.0, indicating accurate modelling. A positive PBIAS value shows an underestimation of bias, whereas a negative PBIAS value shows an overestimation of bias (Piniewski and Okruszko 2011). PBIAS is determined by the following equation (Moriassi et al. 2007):

(11)

$$PBIAS = \frac{\sum_{i=1}^N (Q_{obs,i} - Q_{sim,i}) \times 100}{\sum_{i=1}^N Q_{obs,i}}$$

where, $Q_{obs,i}$ is the observed flow for the time step i , $Q_{mod,i}$ is the modelled flow for the timestep i , and N is the number of time steps. PBIAS is expressed as a percentage.

To evaluate the performance of the chosen statistics, NSE and PBIAS scores can be compared to a standard. Moriassi et al. (2007) recommended ranges for monthly statistics, which will be used to understand model performance (Table 6.2). Summary statistics of relevant functions can be seen in Table 6.3, similarly adapted from Moriassi et al. (2007). The data was collected through a literature review of relevant studies under a daily and monthly time step. Overall daily NSE proved higher than monthly values, contradicting select individual studies; a possible cause for this discrepancy might be larger sample size (n on average with daily data (Fernandez et al. 2005; Van Liew et al. 2007)).

CHAPTER 5

METHODOLOGY

5.1 INTRODUCTION

SWAT requires a number of publically available data sets to build a model. These data inputs were used to delineate the watershed, create a hydrological response unit (HRU) overlay, and run a sensitivity analysis required for calibrating model parameters. Daily climate data (maximum/minimum temperature and precipitation), topography, land use, soil layers, stream gage information, and streamflow are integrated into the SWAT project. All map layers and data sets are projected using the Universal Transverse Mercator (UTM) zone 10. Figure 5.1 presents a framework of SWAT assessment for the study of climate change impacts on future streamflow (Dlamini et al. 2017).

The program does not have saved data, so all data used must be manually entered. Time series of observed data (e.g. rainfall, minimum/maximum temperature, solar radiation, wind speed, humidity) are inputs for water balance table output (Gurung et al. 2013). Under SWAT, the watershed is divided into subbasins, which are further split into Hydrologic Response Units (HRUs) (Neitsch 2015). HRUs are grouped by unique soil, land use, and slope characteristics so that areas with similar hydrology are coupled together. The initial project was run from 1/1/1979 to 12/13/2013 using a monthly time up and a three-year warm-up period (Figure 5.2).

For this project, ArcGIS (ESRI 10.4) with the extension ArcSWAT version 2012.10.19 (USDA-ARS 2012) was used. Latin-Hypercube one-factor-at-a-time (LH-

OAT) evaluated sensitivity analysis and calibration/validation as described above was performed through SWAT-CUP 5.1.6.2.

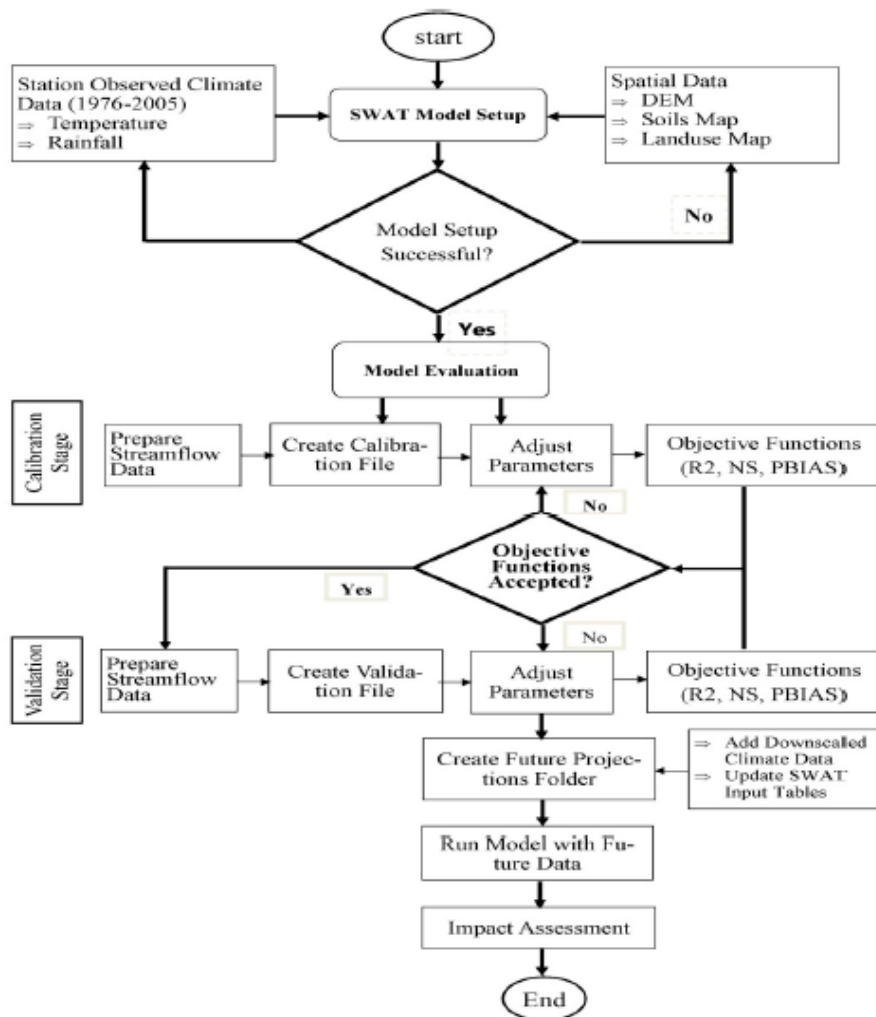


Figure 5.1. SWAT framework for climate change assessment on future streamflow. NS=Nash-Sutcliffe; PBIAS=Percent Bias (Dlamini et al. 2017).

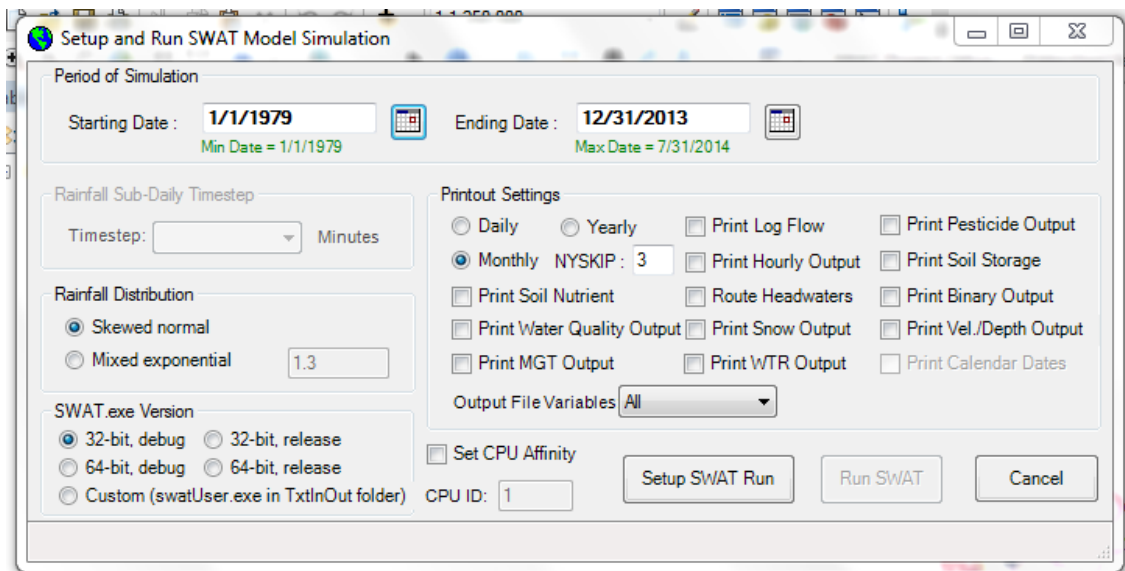


Figure 5.2. Upper Merced basin SWAT model run prompt box. Simulation was run from 01/01/1979 to 12/31/2013 at a monthly-time step. Model inputs are daily (USDA—ARS 2012).

5.2 SWAT MODELING

5.2.1 Watershed delineation

To fashion a simulation in the SWAT program, first the watershed must be delineated. The Digital Elevation Model (DEM) is utilized to build the watershed so that SWAT could simulate stream networks, runoff, and sub-watersheds within the basin (5.1.1a). Further, a shapefile of the Upper Merced Basin acts a “mask” for the watershed. The “mask” allows SWAT to focus solely on the Upper Merced Basin, enabling a faster simulation overall. Projected layers of data are inputted into the water delineation. The project DEM was downloaded from the USGS website, and then projected from North American Datum of 1983 (NAD 1983) to UTM₁₀.

After the DEM setup was complete within the Watershed Delineation box (Figure 5.5), flow direction and accumulation are derived from the DEM. The stream definition covered an area of 6430.4 Ha. From here, the stream network was defined using the DEM once again. Once a stream network had been established, the whole watershed outlet was

selected manually, and the watershed was then delineated. The last steps to watershed delineation are allowing SWAT to calculate watershed parameters and the number of subbasins within the model (Figure 5.3).

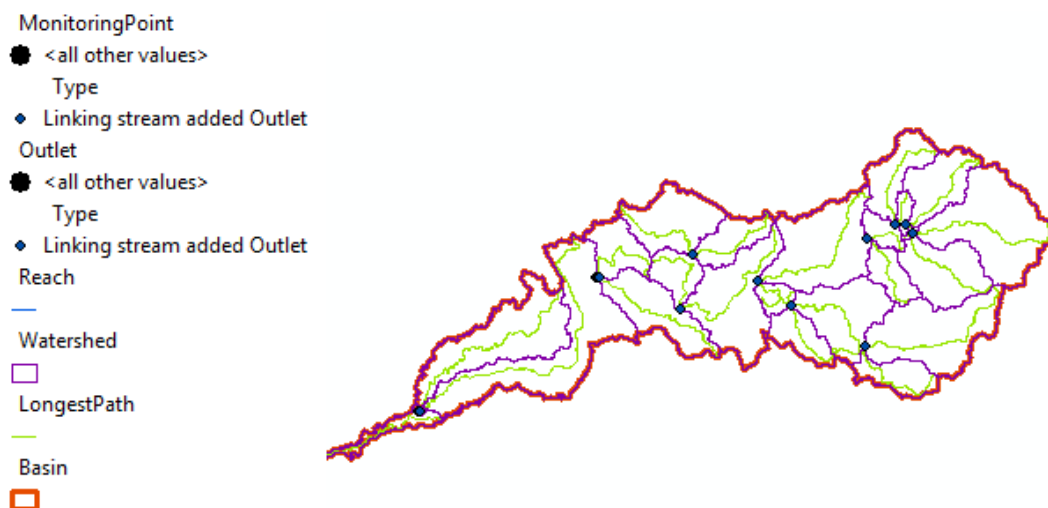


Figure 5.3. Upper Merced basin ArcHydro-GIS layer simulated through SWAT. A red line outline the watershed, with subbasins split by the purple line, recording gages dotted throughout the watershed, and the stream network defined in blue (USDA—ARS 2012).

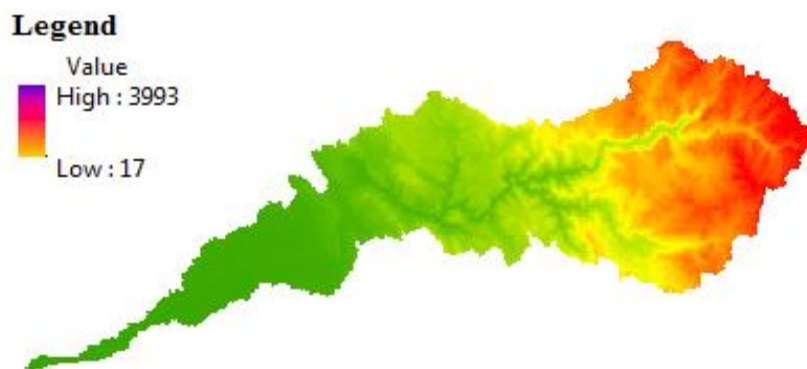


Figure 5.4. Upper Merced basin DEM layer projected in ArcMap through SWAT. Higher elevations are in red on the right, flowing into lower elevations represented in yellow/green (USDA—ARS 2012).

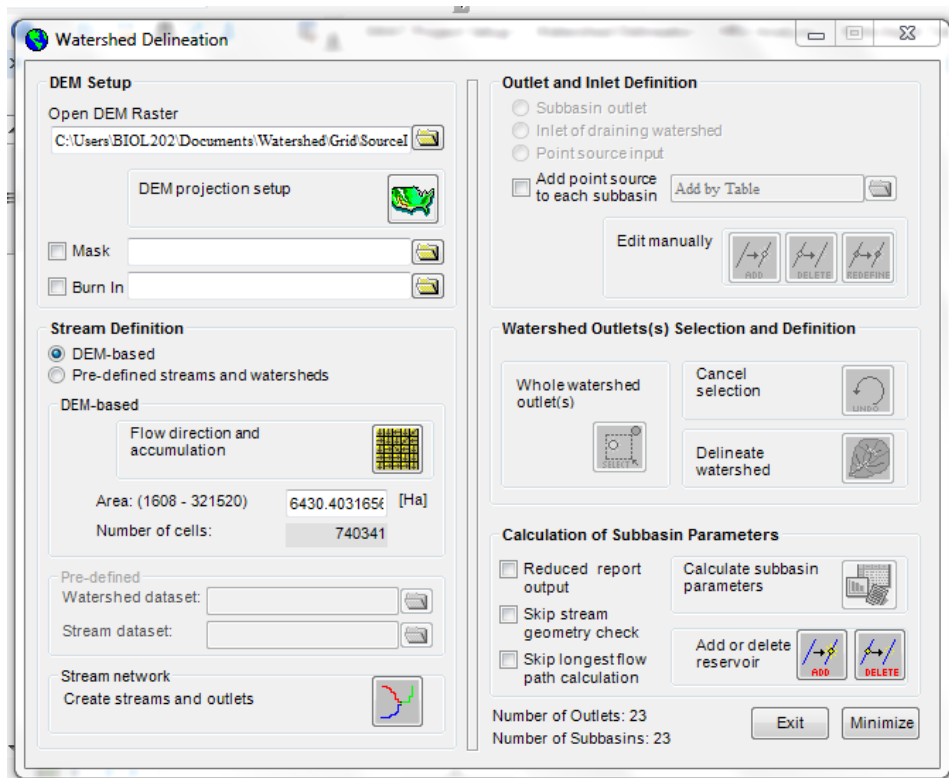


Figure 5.5. Upper Merced basin SWAT model run water delineation box. Stream definition, stream network, outlet/inlet definition, watershed delineation, and subbasins are derived from the DEM layer (USDA—ARS 2012).

5.2.2 HRU analysis

SWAT further defines the area into Hydrological Response Units (HRUs) based on slope, soil class, and land use (Figure 5.6). Multiple HRUs were assessed based on a percentage of 10%, 20% soil, and 10% slope class percentage as was recommended in the SWAT manual. A projected National Land Cover Data (NLCD) set and SWAT's built-in soil classification (STATSGO), further characterized the HRUs. Once slope, soil, and land use were successfully overlaid, the HRUs were created and SWAT provided a written HRU report to review.

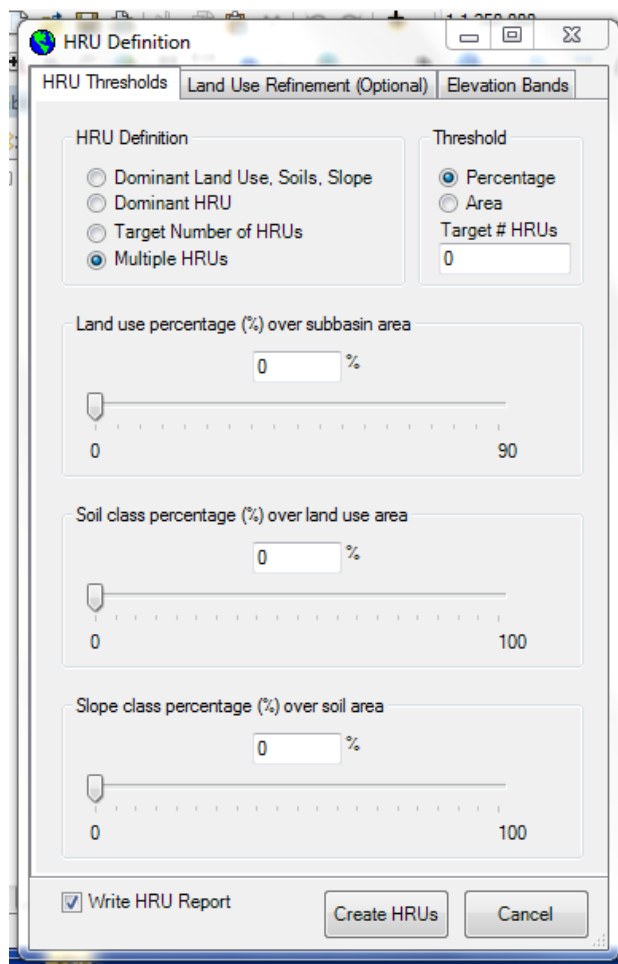


Figure 5.6. Upper Merced basin SWAT model run Hydrological Response Unit (HRU) definition box. HRUs are further defined by the model using slope, land use data sets, and elevation bands (USDA—ARS 2012).

5.3 SWAT DATA INPUTS

5.3.1 Land cover data

To map the watershed's surrounding land use, the most recent National Land Cover dataset (NLCD 2011) from U.S. Geological Survey (USGS) website was employed.

NLCD 2011 tracks land cover trends and changes over space and time from 2001 to 2011, while providing 5-year periodic updates of land cover and subsequent modifications.

Datum format and projection are NAD83 and Albers Conical Equal Area. The following

16 land cover classes considered are the following: open water, perennial ice/snow, developed-open space, developed-low intensity, developed-medium intensity, developed-

high intensity, barren land, deciduous forest, evergreen forest, mixed forest, shrub/scrub, grassland/herbaceous, pasture/hay, cultivated crops, woody wetlands, and herbaceous wetlands. Figure 5.7, shows the general distribution of land use across the watershed.

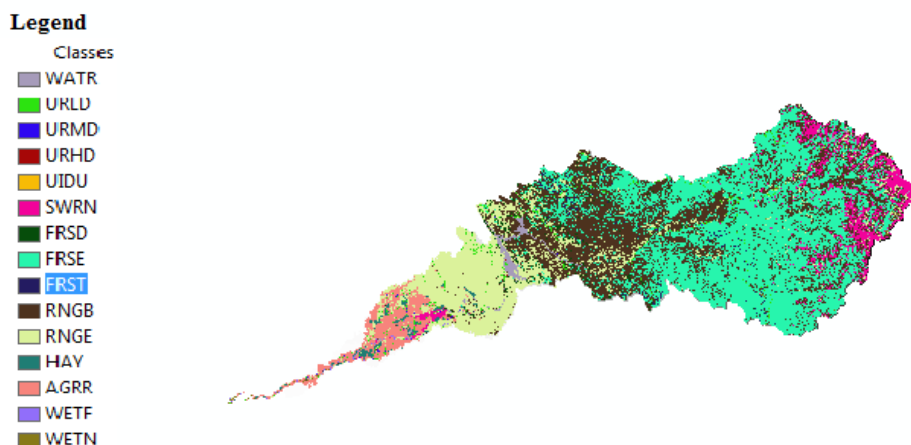


Figure 5.7. Upper Merced basin SWAT model Land Use layer projected through ArcMap. Key for land use classes on the left. NLCD set is projected in UTM_10 for the study area (USDA—ARS 2012).

5.3.2 Topography and soil data

Topographic information was accessed for the model from Digital Elevation Model (DEM) data. DEMs with an approximate 10m resolution (1/3 arc-second) were used to provide more reliable topographical information and streamflow paths for the watershed. The original horizontal datum for the obtained DEMs is North American Datum of 1983 (NAD83) and the vertical datum for elevation is North American Vertical Datum 1988 (NAVD88), with vertical units in meters.

Soils data were acquired through the Soil Survey Geographic database (SSURGO) soil layer in order to reduce the computational obligations of the model and ease of use (Ficklin et al. 2013; Obispo 2013). SSURGO spatial data includes a geo-referenced vector dataset, and the tabular data includes soil chemical/physical properties and soil

classifications. The model does not discern between surficial soils due to fluctuating denseness and complex arrangement (Figure 5.8). Soil attributes were associated with the soil layer using the map unit key (MUKEY).

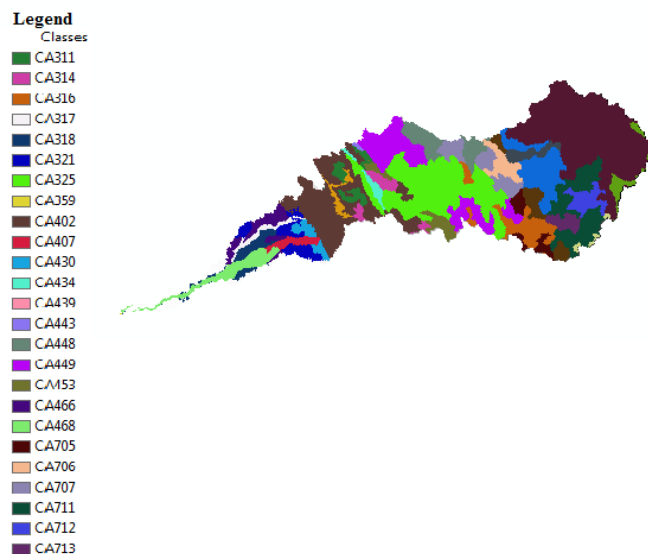


Figure 5.8. Upper Merced basin SWAT model soil layer projected through ArcMap. Key for soil classes on the left. STATSGO set is projected in UTM_10 for the study area (USDA—ARS 2012).

5.3.3 Climate data

Climate data points were inputted for daily precipitation and daily max/min temperature. Weather data observed were gathered from observed were derived from four weather stations monitored by the California Data Exchange Center (CDEC) and accessed on the CDEC website. Modes of climatic data collection varied at the gauge, but included Fenwall Thermistor/HUMICAP H-sensor (temperature/relative humidity), anemometer (wind speed), and tipping-bucket rain gauge (precipitation). According to the CIMIS website, the program derives reference evapotranspiration using the CIMIS Penman and Penman-Monteith equations and general climate data measured over “well-watered grass surfaces”, otherwise known as “reference surfaces” (CIMIS 2016). CIMIS estimates

additional parameters such as roughness coefficient and aerodynamic resistances from previously conducted research. All referenced sites are currently irrigated.

Temperature and precipitation information were formatted into simple .txt files, with a corresponding station location table communicating the file name and location for each gage. To fill short gaps in data, the average maximum and minimum temperatures/precipitations were copied from the previous and following days. Similarly, average maximum and minimum temperatures/precipitations from previous and following years were utilized for longer stretches of missing data. The text files were plugged into the SWAT model with the Weather Data Generator box, seen in Figure 5.9.

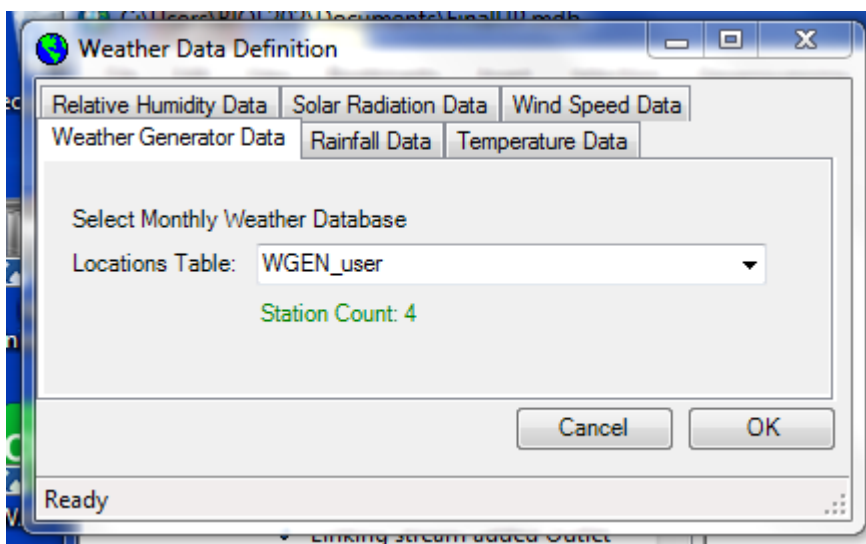


Figure 5.9. Upper Merced basin SWAT model Weather Data Definition prompt box. Observed .txt files for max/min temperature, precipitation, and reference table are uploaded using the data definition box (USDA—ARS 2012).

5.3.4 Snow data

SWAT uses a temperature-based approach to snow simulation. The program utilizes average daily temperature to classify precipitation as rain or snow (Neitsch et al. 2005).

SWAT splits the study area by elevation bands, enabling greater assessment of differences between snow cover and snow melt based on orographic temperature variation. Three

elevation bands were utilized for the Upper Merced Basin, enabling snow accumulated to be evaluated. The snow cover component of SWAT allows for a more complex model involving non-uniform snow cover in the form of shading, drifting, and topography/land cover variations (Neitsch et al. 2005).

5.4 SWAT-CUP CALIBRATION AND VALIDATION

SWAT-CUP's Sequential Uncertainty Fitting program (SUFI2) was chosen for program calibration due to relative ease of calibration. Saved simulation output ("TxtInOut") was loaded into the SWAT-CUP program. At the outset, the project was run in junction with SWAT 2012, 64-bit software, and the method of calibration chosen was SUFI-2. After the project setup through New Project Wizard, SWAT output files were linked so that variables from output.rch, output.hru, output.sub, output.res, and output.mgt could be calibrated. The starting simulation number (1) and ending simulation number (300) were added to the following SUFI2_swEdit.dbf file. SWAT was run with a five-year warm-up period, and so the automatically input File.cio was adapted. The number of years simulated (SBYR), beginning year of simulation (IYR), and number of years to skip due to the warm-up period (NYSKIP) were added to the file. Information on the Absolute_SWAT_Values.txt file was not altered in anyway. The file holds a helpful registry of generic program ranges for parameters, which served as initial parameters for the project.

Observed monthly streamflow data from USGS stream gauge at Pohono Bridge (USGS ID 112665001941) was used to calibrate and validate SWAT monthly simulated streamflow. Observed data from January 1984 – December 2005 (including a 5-year

warm-up period) was inputted to Observed.txt file during the calibration process, and streamflow data from January 2006 – December 2013 was inputted during the validation process. Although the Happy Isles Bridge (HAP) stream gauge also operates within the basin, Pohono Bridge (POH) is chosen for calibration and validation because of its downstream location and breadth of monitoring. Installed in 1916, POH is the furthest downstream gauge within the study area, and measures at an elevation of 1,177 m above sea level (United States Geological Survey 2015b). Streamflow is measured in cubic meters per second, consisting of water discharged from natural streams or surface water at the watershed outlet. POH streamflow data was formatted into a .txt file with a corresponding station location table communicating the file name and location for the gage.

After the calibrated parameters satisfied the objective function, the model was validated using the new best parameter ranges. SUFI-2 does not provide a way in which to perform validation. Instead, updated streamflow data between 01/01/2006 and 12/31/2013 were inputted. Observed.txt, SUFI2_extract_rch.def, and file.cio were updated to reflect the validation period. The program ran for a final complete simulation of 300 iterations, to mimic a calibration run.

5.4.1 Parameter fitting

Instead of a “trial and error” deterministic approach to parameter selection, stochastic calibration was chosen with the goal of bridging the gap between modeled flow and the process within a natural system. Curbing errors with targeted parameters, in order

to identify uncertainty within the calibrated model result is important to analyze simulation and observation results.

Prior to full calibration, the initial model structure and parameters are tested in SWAT-CUP. A dummy parameter was set:

```
r_ESCO.hru 0      0
```

Then Pre, Run, and Post processing was executed within SWAT-CUP. Looking at the 95PPU result of the initial model run, although the simulated and observed data points were not within the same 95PPU band, it was clear that the data followed similar peaks and cycles. Acknowledging the similarities in data points, further parameter selection was completed.

The process of parameterization is to localize or regionalize parameters within the watershed. SWAT splits the basin into hydrological response units (HRUs) seeking the smallest unit of spatial separation. HRUs are grouped due to likeness in elevation, soil, and landuse, as well as spatial parameters such as soil bulk density and hydraulic activity. Based on the initial global sensitivity analysis and a review of relevant literature, parameters were fitted with an identifier code, indicating the type of change which will be applied to the parameter. The code represents how change is to be applied to the parameter, showing either that the parameter will be replaced by a given value (v__), will be added to an existing parameter value (a__), or will be multiplied by 1+a given value (r__). Most parameters were replaced by the best parameter range (v__), but parameters with a smaller range (less than one unit in range difference) were multiplied by 1+a given value (r__) for greater specificity and relative change.

A *t*-test is performed through a global sensitivity analysis using the Latin hypercube equation. The results describe the sensitivity to the chosen objective function resulting from modification to a given parameter. As suggested from the official SWAT-Cup manual, parameters with a larger *t*-Stat value and a smaller *p*-Value, functioned as the most sensitive parameters. It is important to note that a Global Sensitivity analysis characterizes sensitivity based on “linear approximations” and therefore defines partial sensitivity.

Since the Upper Merced Basin sits at the foothills of a snowy mountain range, elevation parameters are calibrated first, as temperature and precipitation driven snow accumulation is assumed in SWAT using elevation bands. Before adding the tested sensitive parameters from the LH-OAT sensitivity analysis, Precipitation Lapse Rate (PLAPS) and Temperature Lapse Rate (TLAPS) were calibrated first (Figure 5.10). Once set, PLAPS and TLAPS were removed from the calibration. Following elevation fixing, seven snow parameters were calibrated and set to their best parameter ranges: SFTMP, SMTMP, SMFMX, TIMP, SMFMN, SNO50COV, and SNOCOVMX (Figure 5.11).

Sensitive groundwater, management, and HRU parameters were calibrated. Initial input calibration ranges are suggested by the SWAT-CUP program, and the final best calibrated input and ranges were calculated after multiple iterations of 300 simulations each. One cycle averaged about three hours. Calibration parameters for the basin are shown in Table 6.5. Parameter identifier, initial calibration range used are provided, with the best found calibration range. Eight simulations were completed to ensure a final narrow parameter range (Figure 5.12). Parameter selection was aided using a published SWAT model for Europe, authored by lead SWAT programmers (Abbaspour et al. 2015). Based

on initial model performance, relevant parameters were chosen in accordance with report guidelines. From the starting calibration, the Upper Merced model exhibited low simulated peak flows compared to observed peak flows, but otherwise, an overall overestimation of baseflow. In order to localize parameters so that simulated and observed peak flows fit more completely, Abbaspour et al. (2015) suggests fitting the following parameters: CN2.mgt, ESCO.hru, GWQMN.gw, GW_REVAP.gw, and REVAPMN.gw. At first, SWAT provided ranges were utilized for the above listed parameters, except for CN2. Users within the SWAT-user Google Group provided clarification on a realistic starting range for CN2, causing the initial range to be between -0.2 and 0.2.

After inputting suggested groundwater, groundwater, management, and HRU parameters, model *P*-factor and *R*-factor continued to be small, 0.30 and 0.35 respectively. Due to underestimated baseflow, additional groundwater parameters were calibrated (GWQMN, ALPHA_BF, REVAPMN, GW_REVAP, and RCHRG_DP). Three additional iterations were run, stopping calibration when satisfactory *P*-factor, *R*-factor, R^2 , and NSE statistics were found.

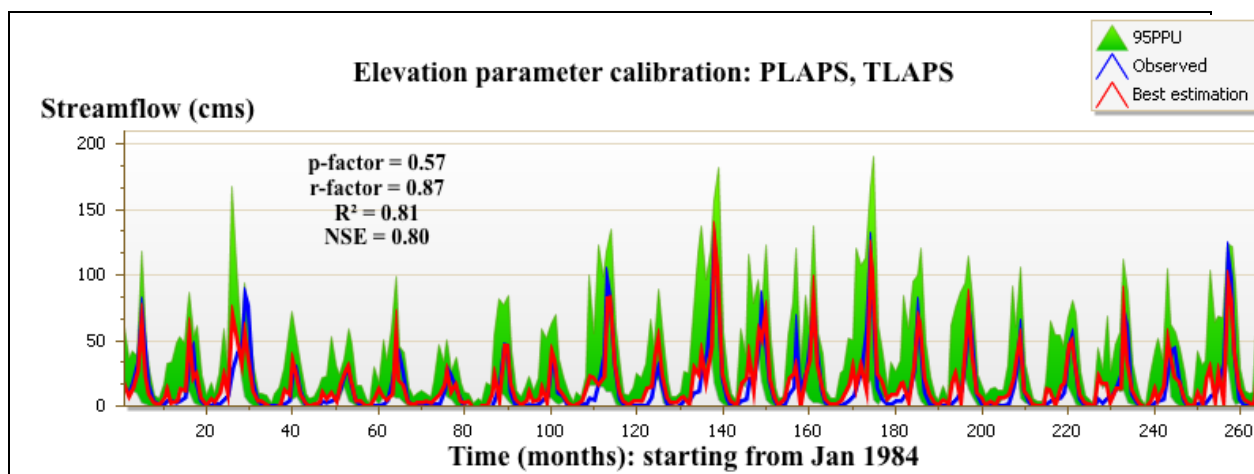


Figure 5.10. SWAT-CUP calibration compared observed daily streamflow data from USGS gage at Pohono Bridge (USGS ID 112665001941) to simulated streamflow in subbasin 5 from years 1984-2005. Initial calibration ran only TLAPS and PLAPS, elevation parameters. Calibration model statistics are representative of prediction uncertainty within the model, expressed as the 95PPU band. TLAPS and PLAPS were fixed after one calibration iteration only, so not to excessively condition elevation parameter ranges and narrow the 95PPU band. Simulated streamflow is shown in red, observed streamflow is shown in blue, and the bounds of the 95PPU band is shown in green.

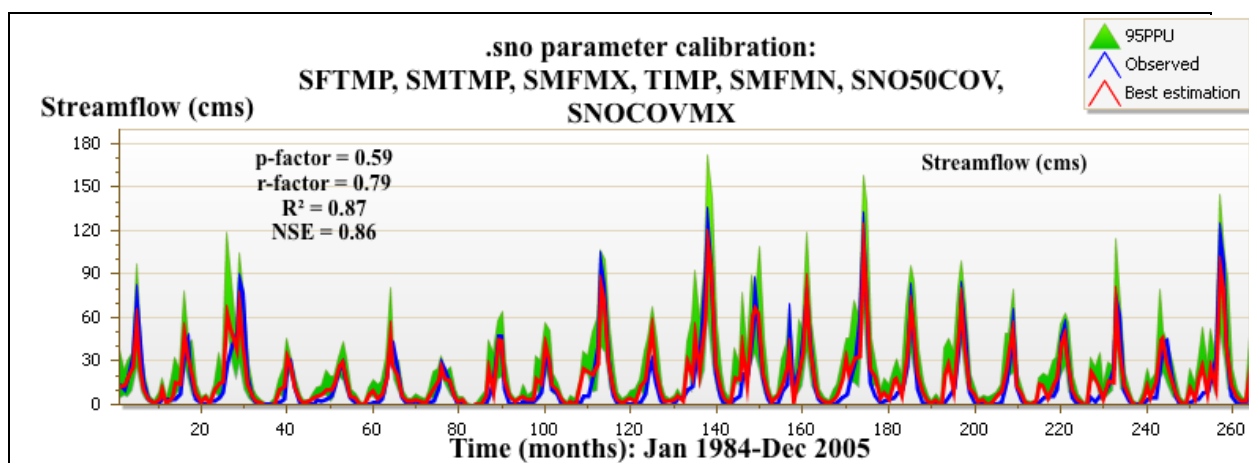
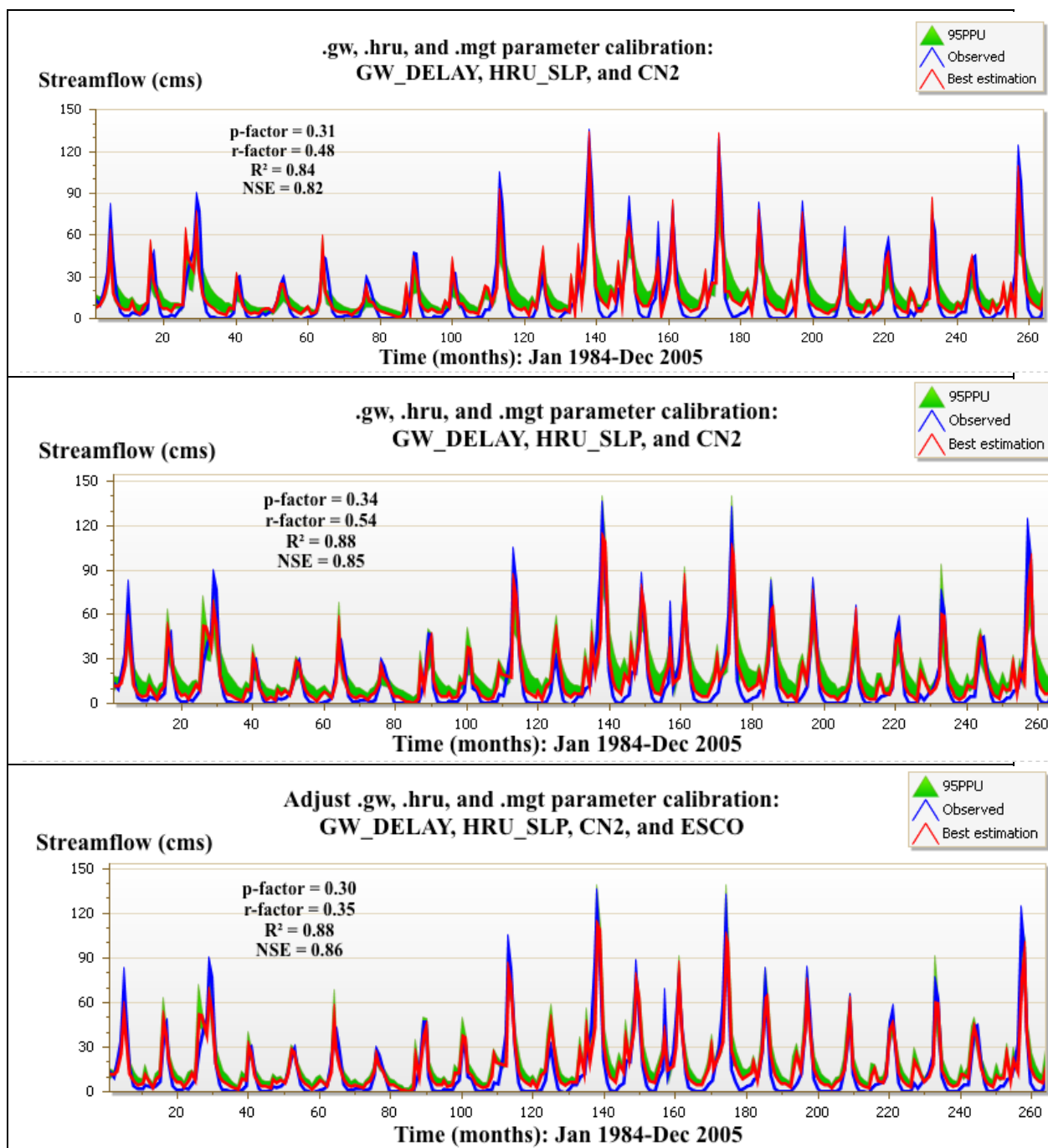


Figure 5.11. SWAT-CUP snow parameter calibration. Using observed daily streamflow data from USGS gage at Pohono Bridge (USGS ID 112665001941) to simulated streamflow from a manually added outlet in subbasin 5 from years 1984-2005. The following snow parameters were calibrated: SFTMP, SMTMP, SMFMX, TIMP, SMFMN, SNO50COV, and SNOCOVMX. In order to avoid a small 95PPU, snow parameters were calibrated and fixed after one iteration. Simulated streamflow is shown in red, observed streamflow is shown in blue, and the bounds of the 95PPU band is shown in green.



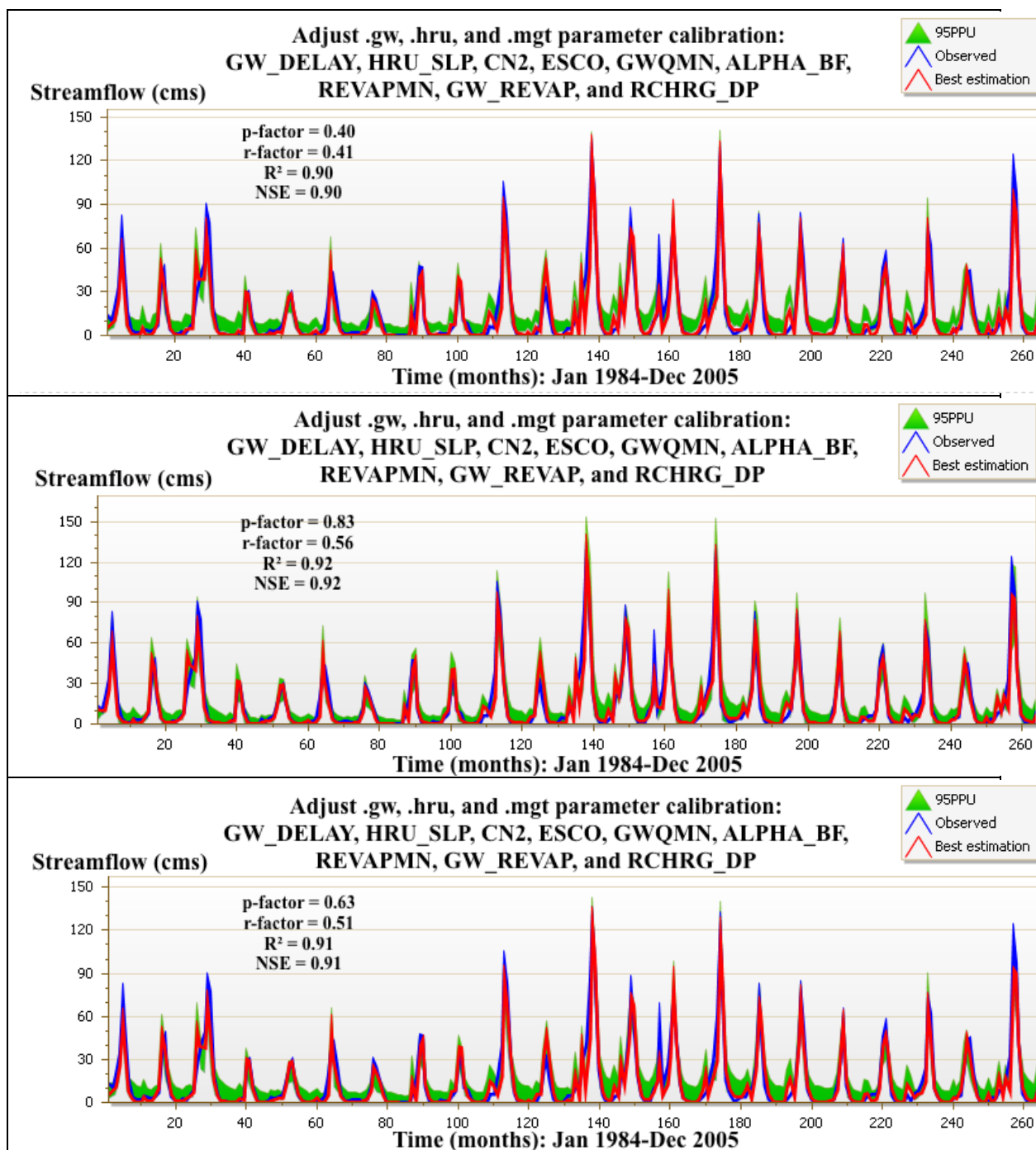


Figure 5.12. Progression of parameter modifications for the purpose of calibration, with the final calibration last. Parameter adjustments increased the 95PPU band, to better represent an envelope of good model solutions or outputs. Groundwater (.gw), HRU (.hru), and management (.mgt) parameters were calibrated and fixed to the original SWAT project. Figure 5.11 and Figure 5.12 present the full range of inputted daily climate data from 1984-2013. Simulated streamflow is shown in red, observed streamflow is shown in blue, and the bounds of the 95PPU band is shown in green.

5.4.2 Observation files

Three files inhabit the observation folder: observed_rch.txt, observed_hru.txt, and observed_sub.txt. For this project, only the observed_rch.txt was evaluated. Within this file, FLOW_OUT_5 (observed streamflow at POH in subbasin #5) was chosen as the calibration's one variable. USGS streamflow was easily copied and pasted from an Excel .csv file, once the inputs were arranged by variable name, month, year, and variable value. Historical data was split for calibration (1984-2005) and validation purposes (2006-2013) in a split-sample calibration/validation procedure. And so, observed_rch.txt runs from FLOW_OUT_1_1984 to FLOW_OUT_365_2005.

The No Observation file enabled uncertainties that do not have observed data available to be simulated such as soil moisture. The .def files are similar to the Extraction files and require inputs of simulation beginning and year-end data range, information about the time-step, and the total number of subbasins. The No Observation file does not include a warm-up period. Lastly, the 95ppu_No_Obs.def file is adjusted. Variable names are preloaded into the file. Number of data points was added; 264 (22 years x 12 months).

5.5 CLIMATE SCENARIO MODELING

Inputs from two GCMs were plugged into the model – The National Center for Atmospheric Research (CCSM4) and the Met Office Hadley Center (HasGEM2-ES). Simulated data began at year 2040 and ended at 2099. SWAT climate data input files were generated using the WEPP/SWAT Future Climate Input File Generator, produced by Joseph Trotochaud, a researcher at Purdue University. The Future Climate Generator provided an Excel macrobook, able to execute data manipulation and modify MarkSim

outputs for SWAT usage (Trotochaud et al. 2014). MarkSimGCM has been updated to include data from the IPCC's Fifth Assessment Report (CMIP5), which enables users to produce future climate data using varying GHG emissions in accordance with specific RCPs. Users can run a combination of low, moderate, and/or high emissions pathways, or simulate conditions under one climate change scenario.

For remaining climate data (solar radiation and relative humidity), SWAT's own WXGEN weather generator (Sharpley and Williams, 1990) was used. Minimum/maximum temperature, solar radiation, and relative humidity are generated based on the incidence of rain for the day. Generated relative humidity values are accommodated for either wet or dry circumstances based on the prevalence of wet or dry days in a given month.

Organization	Forcing Scenario	GCM	Resolution	
			Latitude	Longitude
Met Office Hadley Centre	RCP6.0; RCP8.5	HadGEM2-CC	1.88	1.25
National Center for Atmospheric Research		CCSM4	1.25	0.94

Table 5.1. General circulation models (GCMs) used in this study. Met Office Hadley Centre Model 2 -- Carbon Cycle (HadGEM2-CC); The National Center for Atmospheric Research (CCSM4)

CHAPTER 6

RESULTS

6.1 SENSITIVITY ANALYSIS

Sensitivity analysis was performed against the observational baseline period within the uncalibrated model to pinpoint the most sensitive parameters affecting discharge simulation. Table 6.1 ranks the streamflow parameters calibrated in decreasing order from most sensitive to least within the Upper Merced Basin prior to full calibration. Using the global sensitivity analysis, larger t-stats and smaller p-values are indicative of sensitive parameters. From the parameters evaluated for sensitivity, nine were chosen to include within the model (excluding elevation and snow parameters).

Parameter	Sensitivity Index Number	Mean Sensitivity Index	Unit
CN2	1	13.31281	---
HRU_SLP	2	3.616100307	m/m
RCHRG_DP	3	1.2010246	---
GWQMN	4	1.0945072	mm of water
GW_REVAP	5	0.998511037	---
ESCO	6	0.364438536	---
REVAPMN	7	0.248553893	mm of water
GW_DELA Y	8	0.005332875	days
ALPHA_BF	9	-0.057076116	1/days

Table 6.1. Upper Merced SWAT model sensitivity results obtained through Latin-Hypercube sampling. Elevation parameters TLAPS and PLAPS were unranked. Elevation parameters were calibrated first, optimizing for NSE and PBIAS, then fixed into the SWAT model. The process was repeated for snow parameters.

6.2 CALIBRATION AND VALIDATION

Model calibration is conditional. From the outset, a myriad of inputs can influence calibration. To name a few components affecting calibration are the SWAT hydrological model, observation files, chosen objective function, chosen parameters (Abbaspour, K.C. et al. 2015; Arnold et al. 2012; Stinsen et al. 2011; Yang et al. 2008). Therefore, each model is unique to the respective calibration, and the “goodness of fit” is at the discretion of the author. The purpose of calibration is to provide a model with “high-value information”, although the quantification of this goal is at the discretion of the analyst.

Throughout the calibration process, the *P*-factor and *R*-factor of each iteration was used to easily understand the goodness of fit. When modeling for an objective function, SWAT-CUP generate a *P*-factor and an *R*-factor to quantify uncertainties in the model calibration. Either expresses performance for whichever objective function is employed. The proportion of observations that fall within the 95% prediction uncertainty (95PPU) is indicated by the respective *P*-factor. If most observed data are within the 95PPU band, the model is calibrated correctly (Li et al. 2016). On the other hand, the *R*-factor is a measure of the width of 95% probability level. For discharge, ideally the *R*-factor would be <1.5, describing 100% of observations covered, and the *P*-factor would be >0.7 or 0.75, showing little uncertainty in model estimations (Abbaspour et al. 2004). The *R*-factor found during calibration for the basin was 0.92, while the *P*-factor was found to be 0.83. The model was calibrated so that the *P*-factor was optimized over the *R*-factor. Looking at the validation run statistics, the *P*-factor stayed high at 0.73, while the *R*-factor dropped to 0.47 as a larger *P*-factor is achieved at the expense of a high *R*-factor (Abbaspour et al. 2004). Yet, focusing on the *P*-factor allowed for more significant relationships between model

statistics.

Calibration/validation results were evaluated using two additional objective functions: NSE (Nash and Sutcliffe), PBIAS (percent bias), and RSR (RMSE observation standard deviation ratio). These functions can be utilized to optimize model and were evaluated based on a report published by Moriasi et al (2007) which presents general performance ratings for these statistics (Table 6.3). The program additionally calculates a *P*-factor and an *R*-factor, each quantifying model prediction uncertainty (Li et al. 2016).

Performance Rating	NSE	RSR	PBIAS (%)
Very Good	$0.75 < \text{NSE} \leq 1.00$	$0.00 \leq \text{RSR} \leq 0.50$	$\text{PBIAS} < \pm 10$
Good	$0.65 < \text{NSE} \leq 0.75$	$0.50 < \text{RSR} \leq 0.60$	$\pm 10 \leq \text{PBIAS} < \pm 15$
Satisfactory	$0.50 < \text{NSE} \leq 0.65$	$0.60 < \text{RSR} \leq 0.70$	$\pm 15 \leq \text{PBIAS} < \pm 25$
Unsatisfactory	$\text{NSE} \leq 0.50$	$\text{RSR} > 0.70$	$\text{PBIAS} \geq \pm 25$

Table 6.2. General performance ratings for NSE and PBIAS statistics under a monthly time step. PBIAS = percent bias, NSE = Nash-Sutcliffe efficiency. Adapted from Moriasi et al. (2007).

Statistic	Calibration				Validation			
	NSE		PBIAS		NSE		PBIAS	
	Daily	Monthly	Daily	Monthly	Daily	Monthly	Daily	Monthly
<i>n</i>	92	33	72	0	128	70	82	0
Minimum	-0.23	0.14	-91.7	NA	-1.81	-3.35	-155.6	NA
Maximum	0.95	0.91	26.5	NA	0.89	0.93	47.18	NA
Median	0.89	0.79	-1.3	NA	0.67	0.63	-1.9	NA

Table 6.3. General NSE and PBIAS ratings under daily and monthly timesteps. PBIAS = percent bias, NSE = Nash-Sutcliffe efficiency, *n* = sample size, and NA = not available. Adapted from Moriasi et al. (2007).

In the same study carried out by Moriasi et al. (2007), daily and monthly NSE and PBIAS values were compared. Seen above in Table 6.3, overall daily NSE proved higher than monthly values, contradicting select individual studies; a possible cause for this discrepancy might be larger sample size (*n* on average with daily data (Fernandez et al.

2005; Van Liew et al. 2007). NSE and PBIAS statistics tend to perform better during the calibration period over the validation period, further exemplified in Table 6.3.

Comparing statistics to Moriasi (2007), the calibration and validation both improved significantly from the initial model run. Based on NSE, RSR, and PBIAS optimal values (Moriasi 2007), calibrated NSE levels were in the “very good range” and validated NSE levels were in the “satisfactory” range (Table 6.4). For the calibrated run, PBIAS was in the “very good” range; for the validated run, PBIAS was in the “good” range. The initial model had a large RSR value (satisfactory), and decreased significantly by the final calibrated run (very good). The validated model had an increased RSR, at 0.60 (good). From these statistics, it can be implied that the NSE, RSR, and PBIAS values have a positive relationship.

Run	Statistics		
	RSR	PBIAS	NSE
Initial	0.68 (satisfactory)	-20.2 (unsatisfactory)	0.49 (unsatisfactory)
Calibration (1984-2005)	0.28 (very good)	2.4 (very good)	0.92 (very good)
Validation (2006-2013)	0.60 (good)	13.0 (good)	0.64 (satisfactory)

Table 6.4. Model statistics RSR, PBIAS, and NSE of streamflow during initial, calibration, and validation runs.

As seen in Figure 6.1 below, the observed and best estimation peaks begin to separate at January 2011, the 60th month in the validation simulation. Simulated streamflow is underestimated in the validation simulation, but is supremely underestimated (trailing by 51 cms) during Spring 2010. Snowmelt in subsequent years, 2012 and 2013, seemed to become more consolidated, peak higher than model simulations, and experience a brief one-month stabilization around 35 cms during 2012 and 2013 spring seasons. Although the simulation lacked

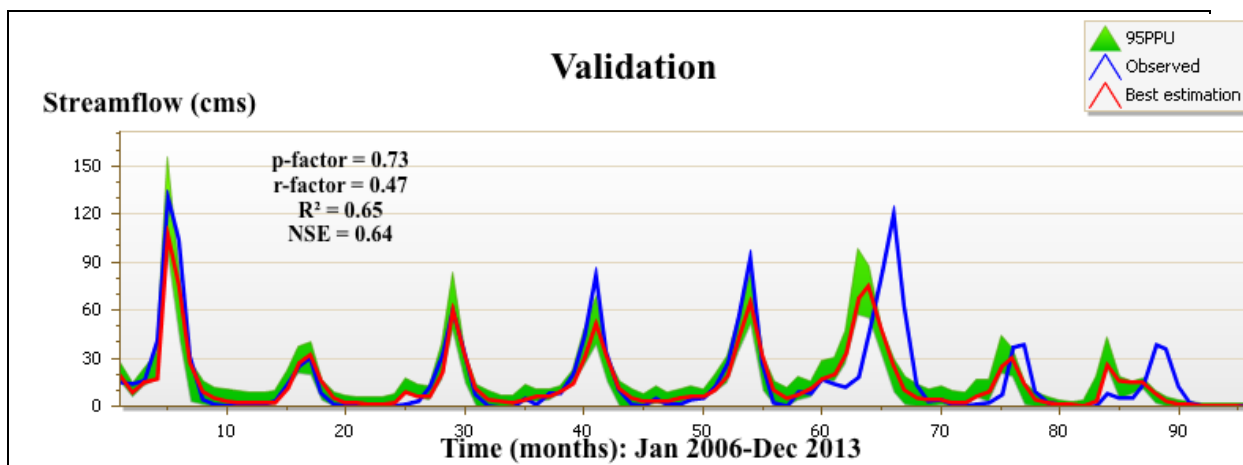


Figure 6.1. Validation for the Upper Merced Basin using final calibration set best parameter ranges and USGS observed daily streamflow measurements at Pohono Bridge (USGS ID 112665001941) from 2006-2013.

6.2.1 Final model parameter ranges

Following multiple iterations of chosen parameters, final parameter ranges were selected based on their respective p-factor, r-factor, R^2 , and NSE scores. As advised by the SWAT-CUP 2012 manual, the Upper Merced model was calibrated using the entire range of parameters, not simply the “best parameter set”. Further analysis represents the watershed more completely by fixing parameters to their adjusted ranges, as there is no one solution able to describe a waterbody in its totality. The purpose of inputting the full calibrated parameter range via SWAT-CUP opposed to manually editing parameters directly into the SWAT model, is preservation of the uncertainty index of each parameter. With wide latitude in data collection, uncertainties in SWAT inputs such as soil, landuse, climate data, and outlet selection, is great. As seen in Table 6.3, parameters were repeatedly iterated until ranges produced a calibrated model understanding of model ambiguity.

Parameters with a small range often pushed the lower and upper ends of their uncertainty limit, even when the updated parameter spectrum was pragmatically

unjustified. For example, average slope steepness (HRU_SLP), functions using a range between 0 to 0.6 m/m. Program calculations of a negative calibrated slope steepness factor is SWAT-CUP babble. Snow parameters (SNOW50COV, SNOCOVMX, SMFMX, TIMP) and groundwater parameters (RCHRG_DP, REVAPMN, ALPHA_BF, GW_DELAY, GWQMN) requiring a positive range, were logically assessed and altered accordingly. In these cases, the lower limit was bumped up to 0 and the upper limit was expanded in varying orders of magnitude specific to the tightness within a particular parameter's range.

Parameter	Identifier	Component	Input Calibration Range		Best Calibrated Parameter [Range - Max;Min]	Definition
			Min	Max		
PLAPS	v	Subbasin	-1000	1,000	-231.87 ; -178.32	Precipitation lapse rate (mm H2O/km)
TLAPS	v	Subbasin	-10	10	8.777313 ; 10.101123	Temperature lapse rate (°C/km)
SFTMP	v	Snow	-5	5	-5.027175 ; 1.66059	Snowfall temperature (°C)
SMTMP	v	Snow	-5	5	-2.410580 ; 2.777248	Snow melt base temperature (°C)
SMFMN	v	Snow	-5	5	-3.577077 ; 5.477077	Melt factor for snow on June 21 (mm of water/°C-day)
SNO50COV	v	Snow	0	1	0 ; 0.577893	Fraction of snow volume shown by SNOCOVMX that corresponds to 50% snow cover
SNOCOVMX	v	Snow	0	500	136.974487 ; 411.358856	Minimum snow water content that corresponds to 100% snow cover, SNO_{100} (mm of water)
SMFMX	v	Snow	0	20	2.322213 ; 7.444455	Melt factor for snow on June 21 (mm H2O/°C-day)
TIMP	v	Snow	0	1	0.258112 ; 0.755188	Snowpack temperature lag factor
CN2	r	Management	35	98	-0.335625 ; 0.042717	Initial SCS (Soil Conservation Service) runoff curve for return flow to occur
RCHRG_DP	v	Ground water	0	1	0 ; 0.320815	Deep aquifer percolation fraction
GW_REVAP	v	Ground water	0.02	0.2	0.073349 ; 0.175149	Groundwater "revap" coefficient
REVAPMN	v	Ground water	0	500	5.003967 ; 265.982483	Threshold depth of water in the shallow aquifer required for "revap" to occur (mm H2O)
ALPHA_BF	v	Ground water	0	1	0.25456 ; 0.797868	Baseflow alpha factor (1/days)
GW_DELAY	v	Ground water	0	500	93.595192 ; 144.302362	Groundwater delay time (days)
GWQMN	v	Ground water	0	5000	859.078918 ; 2583.996338	Threshold depth of water in the shallow aquifer required for return flow to occur (mm H2O)
ESCO	v	Hydrological Response Unit	0	1	0.837605 ; 1.742411	Soil evaporation compensation factor
HRU_SLP	v	Hydrological Response Unit	0	0.6	0 ; 0.139539	Average slope steepness (m/m)

Table 6.5. Parameters chosen for the SWAT-Cup project in order to calibrate and validate the corresponding SWAT model. Identifier code represents the following: v_ indicates the existing parameter value is to be replaced by a given value; a_ indicated a given value is to be added to the existing parameter value r_ indicates an existing parameter value is to be multiplied by (1 + given value). Parameter definitions are pulled from the most recent official SWAT Input/Output documentation (Arnold, et al. 2012).

6.2.2 Observed, uncalibrated, and calibrated streamflow comparison

Below, Figure 6.1, visualizes how uncalibrated SWAT outflow, calibrated SWAT outflow, and observed data plot against each other from January 1984 to December 1999. The entire historical data set is not included for readability. USGS observed data at Pohono Bridge from 1984 – 1999 was included in the calibration process only, not validation. From the initial model run, the uncalibrated streamflow output (seen in grey) is both underestimating and overestimating peak flows. In beginning simulation years (1984-1985), SWAT underestimates discharge by about 20 to 40 cms. On the other hand, initial model estimates drastically overestimate peak flow the following year, 1986, by nearly 70 cms. From January 1987 to near May 1992, SWAT underestimates peak flows but mirrors a similar maximum monthly pattern to the observed data set.

Model outflow was calculated from a manually inputted outlet in subbasin 5 within the greater Upper Merced Basin model in order to mirror the location of USGS streamflow gage at Pohono Bridge. Both Pohono Bridge and the added outlet in subbasin 5 experienced fluctuating streamflow from 1984 to 1999. During May 1987 to May 1992, monthly streamflow increased steadily from baseflow during spring months (March, April, May), peaking around 20 to 30 cms. On one occasion, May 1989, peak flow climbed to 60 cms, but dropped back down to 27 cms the following year. Starting in January of 1993, outflow becomes much greater, jumping from 60 cms in May 1994 to 110 cms in May 1993. May of 1996 and 1999 were more modest (80 cms) compared to surrounding years on either side. SWAT uncalibrated outflow increased at a similar rate, but experienced a lag in flow throughout the simulated time period.

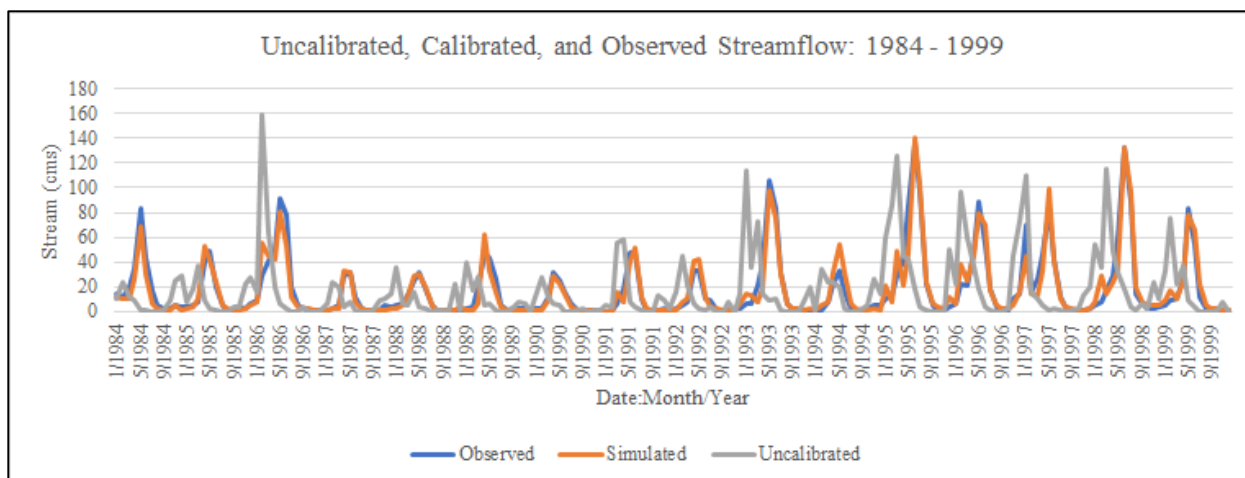


Figure 6.2. USGS observed flow at Pohono Bridge shown in blue, uncalibrated SWAT outflow in grey, and final calibrated SWAT outflow in orange. Selection of data ranging from January 2000 to December 2009. All streamflow is in cms.

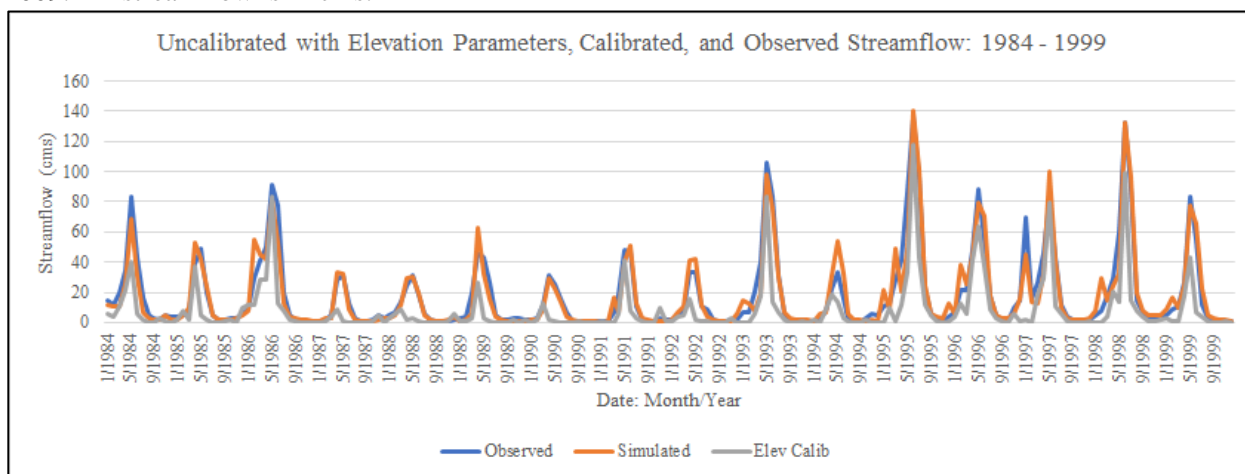


Figure 6.3. USGS observed flow at Pohono Bridge shown in blue, uncalibrated SWAT outflow with added elevation parameters in grey, and final calibrated SWAT outflow in orange. Selection of data ranging from January 2000 to December 2009. All streamflow is in cms.

To begin to fix a lagging simulated flow, elevation parameters were input to aid SWAT in understanding how precipitation falls within the elevated region. Figure 6.3 shows uncalibrated outflow but with added elevation parameters (PLAPS and TLAPS). Further sensitive parameters were added to increase overall model performance, the output of which is seen in orange, as final calibrated outflow. The addition of PLAPS and TLAPS allowed for SWAT to begin understanding how elevation bands change the effect of temperature and precipitation on water distribution within the Upper Merced basin hydrological cycle. Although

further groundwater parameters were applied in subsequent SWAT-CUP iterations, the initial inclusion of three elevation bands improved the accuracy of simulated streamflow in both time and streamflow projections from the outset of calibration.

6.3 HISTORICAL DATA PEAK STREAMFLOW

The annual variability of annual peak streamflow over the historical period is shown in Figure 6.4. Orange bars indicate peak streamflow occurred in May, blue bars for an April annual peak flow, and green bars for a June annual peak flow. Less significant peak flows tend to be clustered, such as years between 1987 and 1992 (31 and 33 cms) and 1999 to 2003 (60 to 80 cms). A steady increase in streamflow is seen beginning in 2007 (31 cms) and ending abruptly in 2011 (122 cms). The following two years, 2012 and 2013, both stay low at a peak of 39 cms.

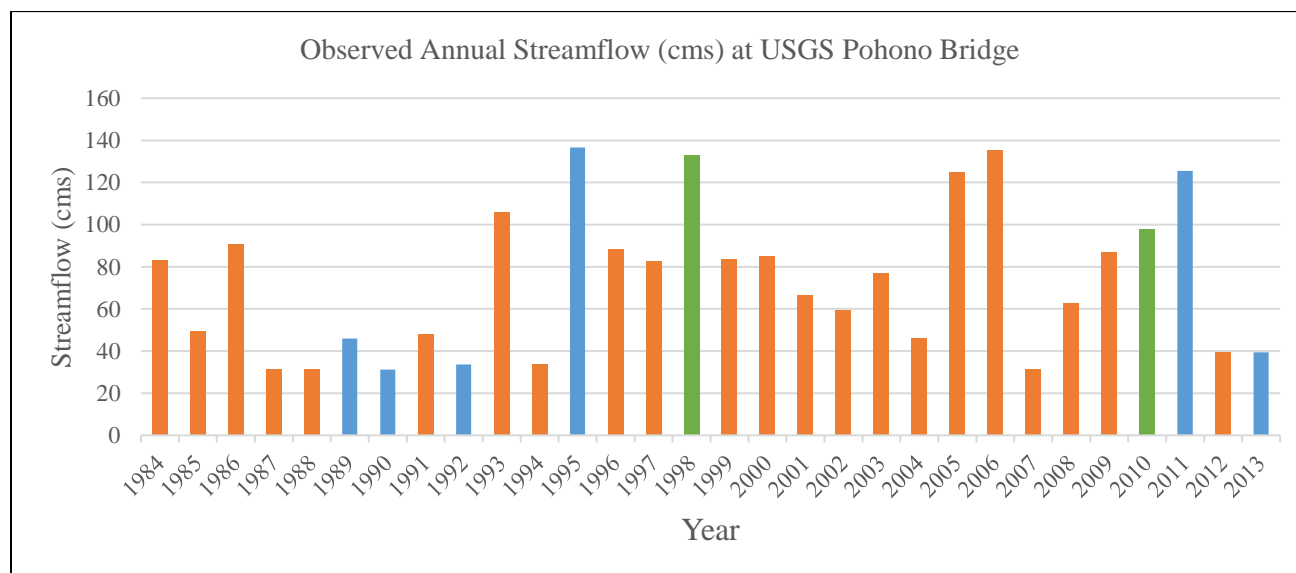
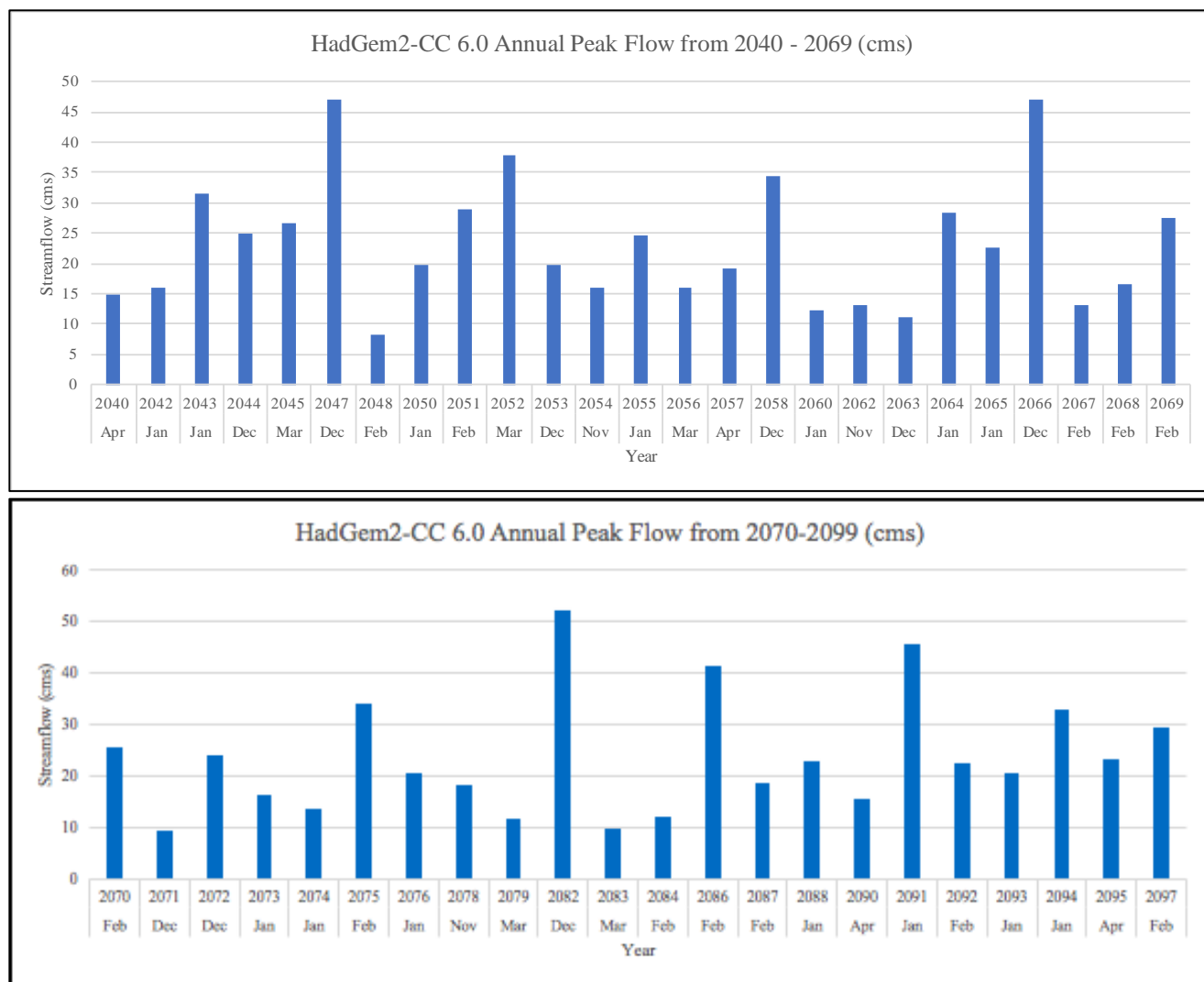


Figure 6.4. Observed annual streamflow measured at Pohono Bridge (USGS #11266500) during the years 1984 – 2013. Peak streamflow occurring in May is indicated by an orange bar (22 months, 73%), June annual peak streamflow is represented in green (2 months, ~7%), and April peak streamflow is in blue (20%). Total yearly flow ranged from 136.5 cms (June 1995) to 31.2 cms (May 2007).

May was overwhelmingly the most meaningful month for peak streamflow within the observed data set. Of the 39 years measured, 73% had the largest peak flow event occur in May, 20% in April, and 7% in June. Higher peak flow was exhibited during the following years: 1995 (136 cms), 1998 (133 cms), 2005 (124 cms), 2006 (135 cms), and 2011 (125 cms). On the other hand, 1987 (31 cms), 1988 (31 cms), 1989 (45 cms), 1990 (31 cms), 1991 (47 cms), 1992 (33 cms), 2007 (31 cms), 2012 (39 cms), and 2013 (39 cms), were particularly low peak flow years.

6.4 CLIMATE PROJECTION PEAK STREAMFLOW

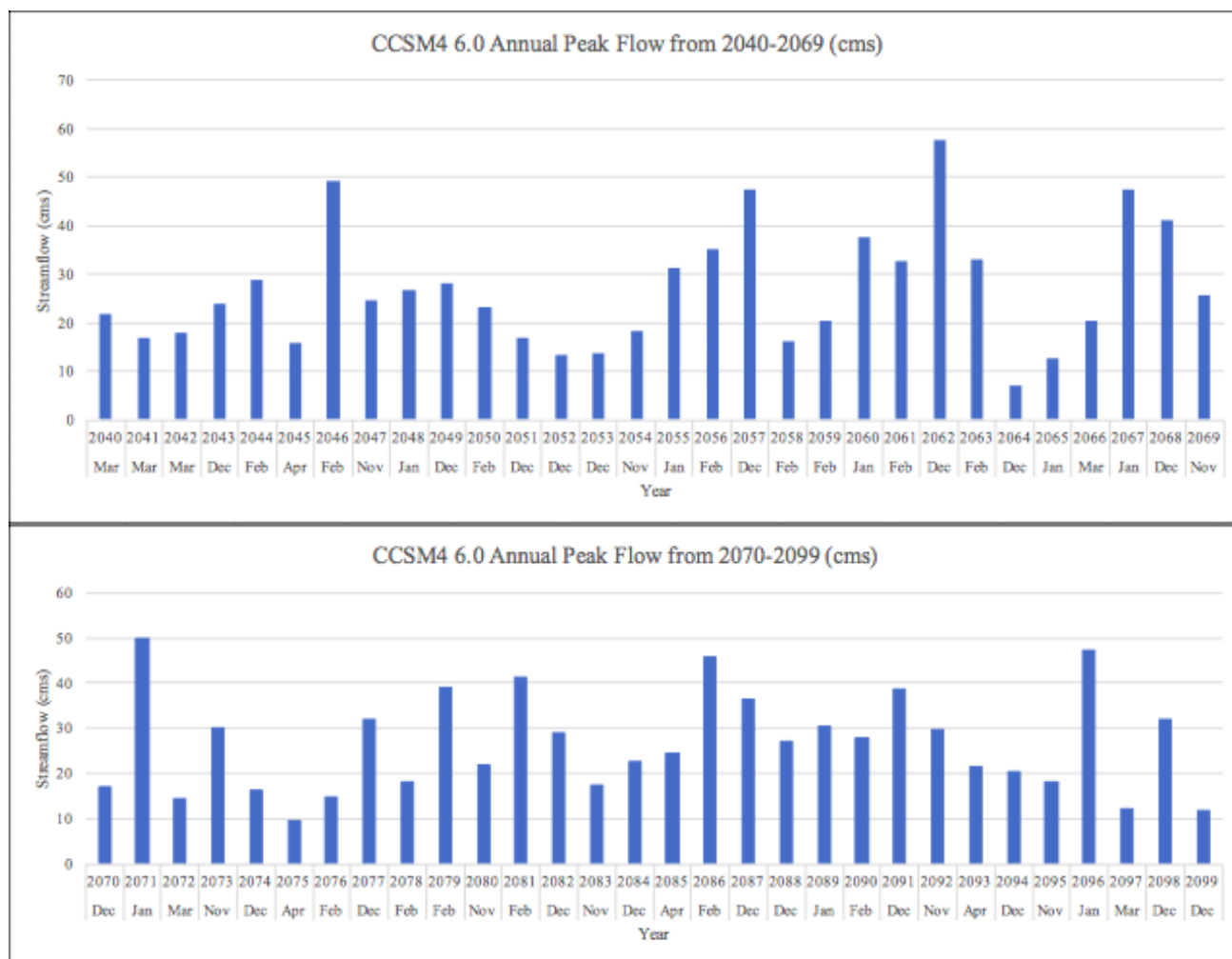
The following series of figures (Figure 6.5--6.12) show annual peak flow per year for HadGem2-CC and CCSM-4 climate scenarios under both forcing scenarios, RCP 6.0 and RCP 8.5. For readability, projected climate data are split so individual graphs refer to either 2040-2069 or 2070-2099. Under each data point (represented by a bar) the corresponding year and month of peak flow occurrence is written.



Figures 6.5 and 6.6. Projected annual peak flow under climate model HadGem2-CC and RCP scenario 6.0. Top figure illustrates projected data from 2040 – 2069, bottom figure shows future data from 2070-2099. Climate scenario data from MarkSim Weather Generator was inputted into a calibrated ArcSWAT model of the Upper Merced Basin. X-axis reads year of annual peak flow and the month in which peak flow occurred.

HadGem2-CC RCP6.0 data from 2040 – 2099 found peak flow occurring four times in April, 15 times in December, 14 times in November, 12 times in February, 16 times in January, 4 times in March, and 3 times in November. Peak flow varied wildly. The lowest peak flow projected is in February 2048 at 8.3 cms, second to December 2071 at 9.4 cms, and March 2083 at 9.7 cms. Highest streamflow predictions are for December 2089 at 55.11 cms, December 2082

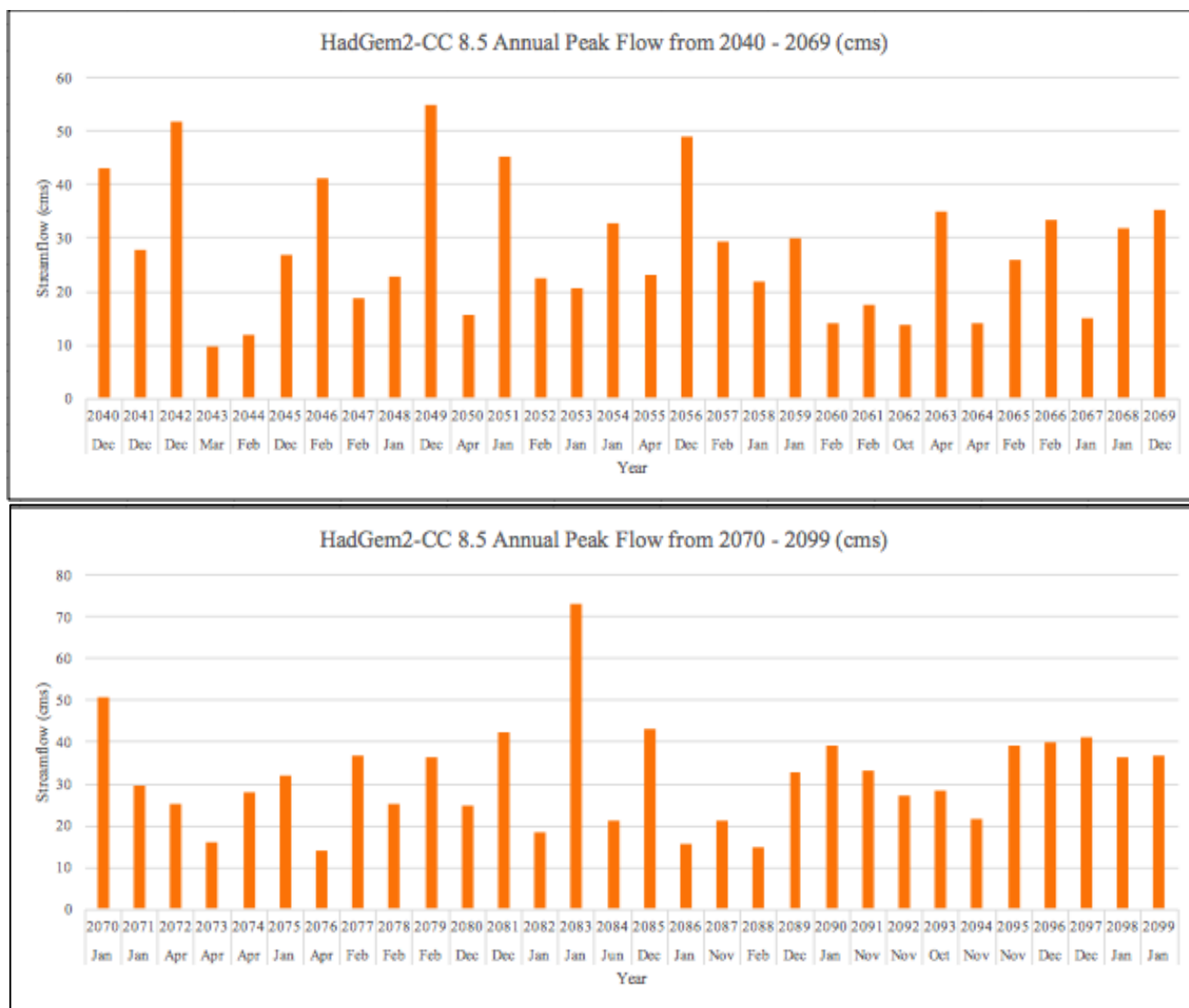
at 51.96 cms, and December 2096 at 49.13 cms. The majority of peak flow fell between 20 cms and 29 cms.



Figures 6.7 and 6.8. Projected annual peak flow under climate model CCSM4 and RCP scenario 6.0. Top figure illustrates projected data from 2040 – 2069, bottom figure shows future data from 2070-2099. Climate scenario data from MarkSim Weather Generator was inputted into a calibrated ArcSWAT model of the Upper Merced Basin. X-axis reads year of annual peak flow and the month in which peak flow occurred.

CCSM4 RCP6.0 data from 2040 – 2099 found peak flow occurring four times in April, 19 times in December, 7 times in November, 7 times in January, 13 times in February, and 5 times in March. The lowest peak flow projected is in December 2064 at 7.13 cms, second to April 2075 at 9.4 cms, and December 2099 at 11.84 cms. Highest streamflow predictions are for December 2062 at 57.6 cms, January 2071 at 49.77 cms, and December 2057 at 47.43 cms.

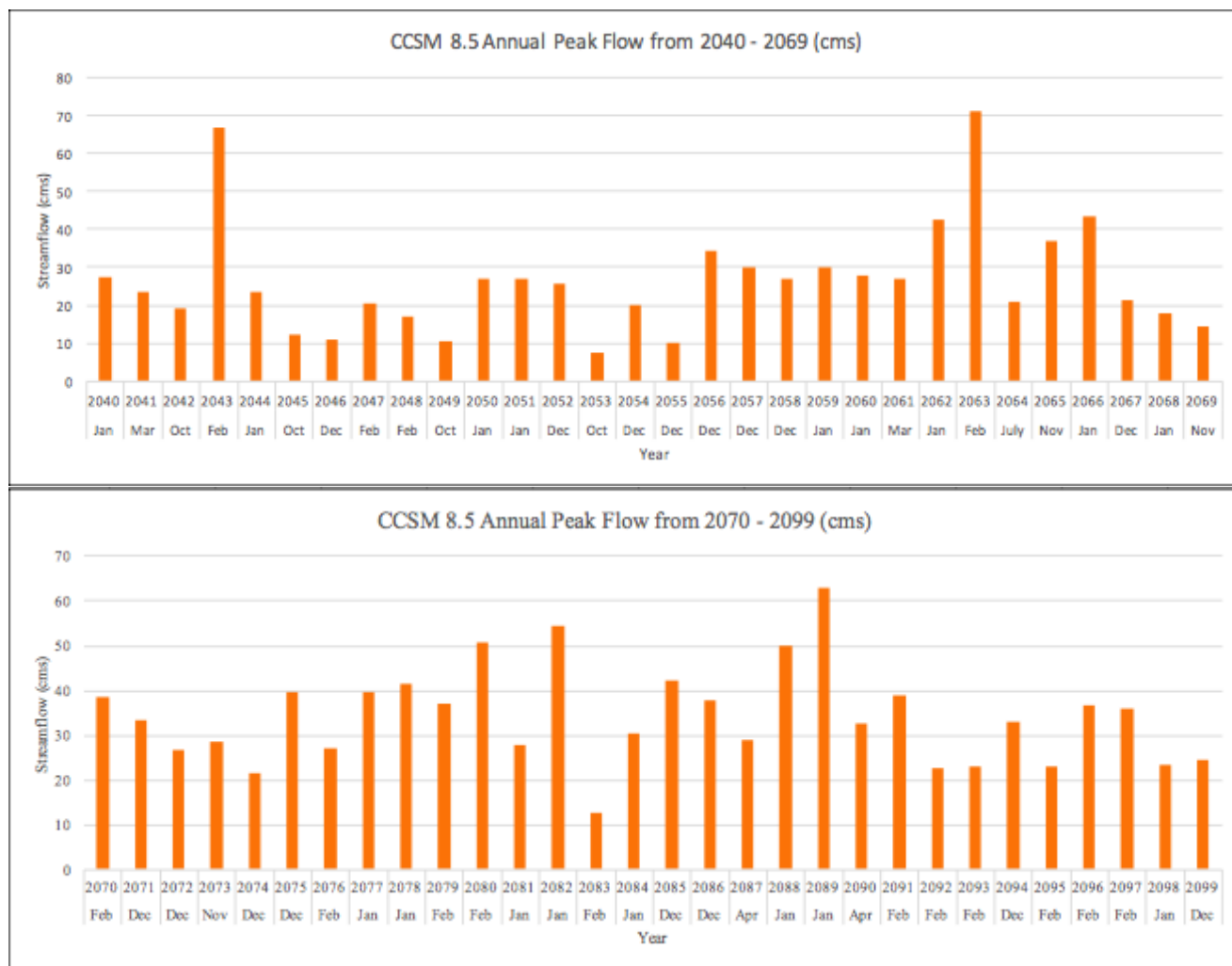
CCSM4 exhibited an overall higher streamflow than HadGem2-CC, with more annual peaks occurring between 20 cms and 30 cms across the data set.



Figures 6.9 and 6.10. Projected annual peak flow under climate model HadGem2-CC and RCP scenario 8.5. Top figure illustrates projected data from 2040 – 2069, bottom figure shows future data from 2070-2099. Climate scenario data from MarkSim Weather Generator was inputted into a calibrated ArcSWAT model of the Upper Merced Basin. X-axis reads year of annual peak flow and the month in which peak flow occurred.

HadGem2-CC RCP8.5 data from 2040 – 2099 found peak flow occurring 7 times in April, 12 times in December, 5 times in November, 12 times in February, 16 times in January, once in March, 3 times in November, twice in October, and once in June. The lowest peak flow

projected is in March 2043 at 9.7 cms, second to October 2062 at 13.62 cms, and April 2076 at 14.05 cms. Highest streamflow predictions are for January 2083 at 73 cms, December 2042 at 51.9 cms, and January 2070 at 50.76 cms. Unlike RCP 6.0, RCP 8.5 has June (2084) and October (2062 and 2093) projected as months of highest annual outflow.



Figures 6.11 and 6.12. Projected annual peak flow under climate model CCSM4 and RCP scenario 8.5. Top figure illustrates projected data from 2040 – 2069, bottom figure shows future data from 2070-2099. Climate scenario data from MarkSim Weather Generator was inputted into a calibrated ArcSWAT model of the Upper Merced Basin. X-axis reads year of annual peak flow and the month in which peak flow occurred.

CCSM4 RCP8.5 data from 2040 – 2099 found peak flow occurring twice in April, 15 times in December, 3 times in November, 14 times in February, 16 times in January, once in

July, twice in March, 3 times in November, and four times in October. The lowest peak flow projected is in October 2053 at 7.5 cms, second to December 2055 at 10.25 cms, and October 2049 at 10.6 cms. Highest streamflow predictions are for February 2063 at 71 cms, February 2043 at 67 cms, and January 2089 at 63.1 cms. Unlike RCP 6.0, RCP 8.5 has July (2064) and October (2042, 2045, 2049, and 2053) projected as months of highest annual outflow.

6.5 PROJECTED MONTHLY STREAMFLOW

Figures 6.13 through Figure 6.15 show the projected mean-monthly streamflow rates for the Upper Merced Basin over a selected data set of two years. Average monthly streamflow of HadGem2-CC 6.0 is shown in blue, HadGem2-CC 8.5 in orange, CCSM4 6.0 in grey, and CCSM4 8.5 in yellow.

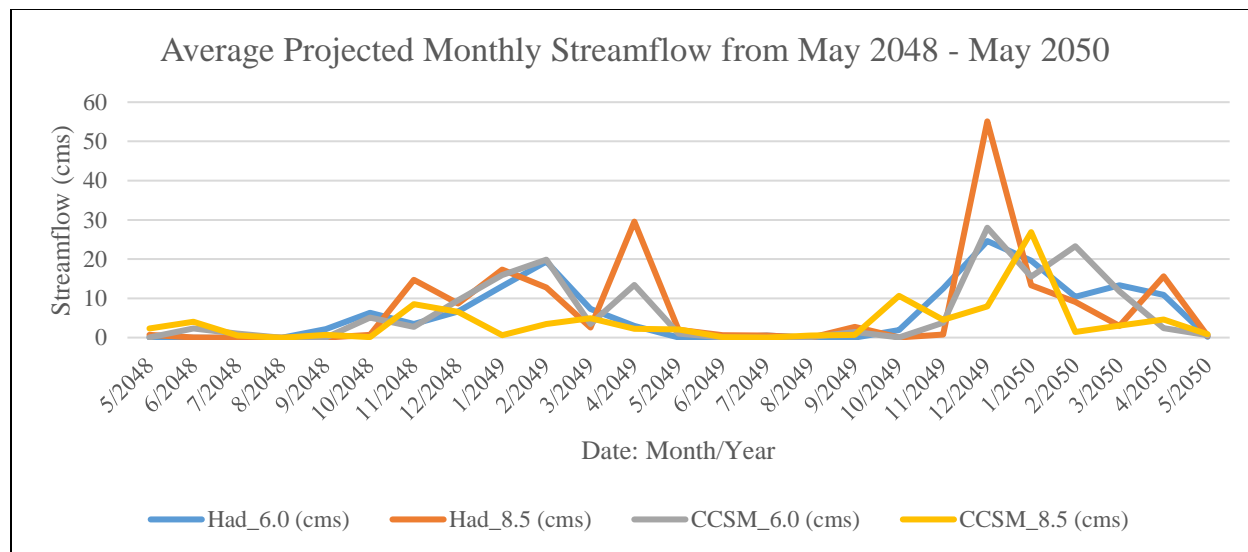


Figure 6.13. Projected mean-monthly streamflow rates for the Upper Merced Basin during a selected 2-yr period from May 2048 – May 2050. Forcing scenarios RCP6.0 and RCP8.5 are applied under two GCMs, HadGem2-CC and CCSM4. Climate modeling data in the form of projected precipitation, temperature, and solar radiation, were downloaded via MarkSim GCM Weather Generator and plugged into the Upper Merced Basin model built using the Soil and Water Assessment Tool (SWAT).

Figure 6.13 above shows average projected monthly streamflow from May 2048-May 2050 under the four chosen global climate scenarios. Looking at RCP6.0 first (blue and grey line), the two models hit peak streamflow first in February/March 2049 and then peak again near December 2049, followed by smaller peaks near March/April 2050. HadGem2-CC 8.5 stands out with the two highest peaks within the data set. In April 2049 HadGem2-CC 8.5 peaks at 30 cms, and then again between December 2049 and January 2050 at 55 cms. CCSM4 8.5 experiences a small peak near January 2049 of 8 cms, but later peaks more significantly in January/February 2050 at 29 cms.

From late May to September, all models project small summer streamflow. A flat streamflow is not unexpected, observed data from 1984-2013 exhibited dry conditions in summer months after available snowmelt has moved further downstream.

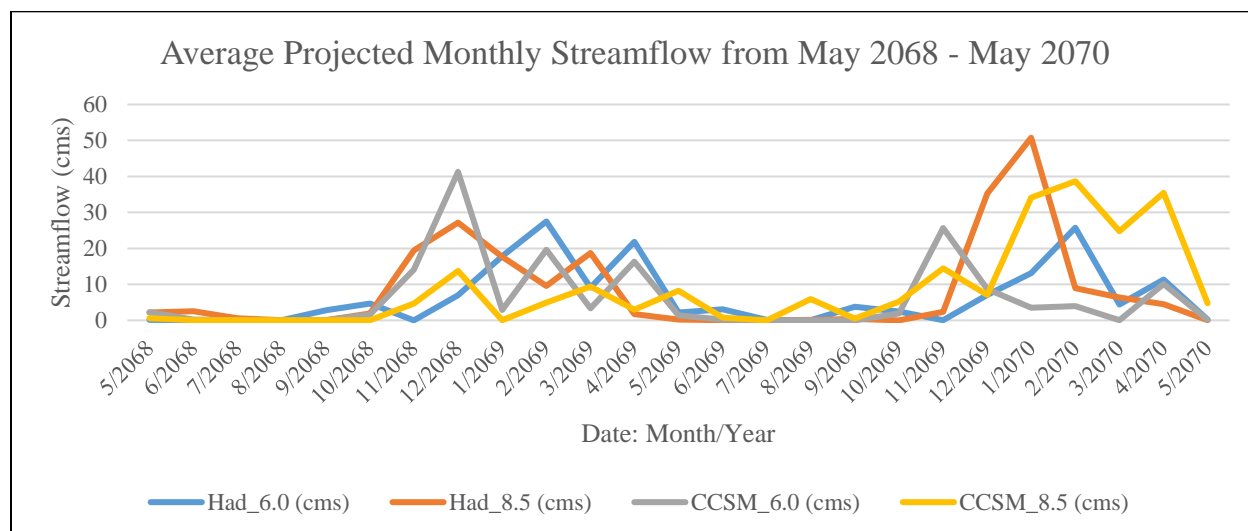


Figure 6.14. Projected mean-monthly streamflow rates for the Upper Merced Basin during a selected 2-yr period from May 2068 – May 2070. Forcing scenarios RCP6.0 and RCP8.5 are applied under two GCMs, HadGem2-CC and CCSM4. Climate modeling data in the form of projected precipitation, temperature, and solar radiation, were downloaded via MarkSim GCM Weather Generator and plugged into the Upper Merced Basin model built using the Soil and Water Assessment Tool (SWAT).

Average monthly streamflow from May 2068 – May 2070 shows the most amount of variability between model projections (Figure 6.14). Each model experiences numerous peaks

from November 2068 to May 2069, and October 2069 to May 2070. HadGem2-CC expressed the highest peak flow of the set, with 51 cms outflow in January 2070. There is a shorter and more fluctuating summer season from June 2069 to August/September 2069. CCSM4 8.5 and HadGem2-CC 6.0 experience outflows during the summer months, around 4 cms and 8 cms respectively.

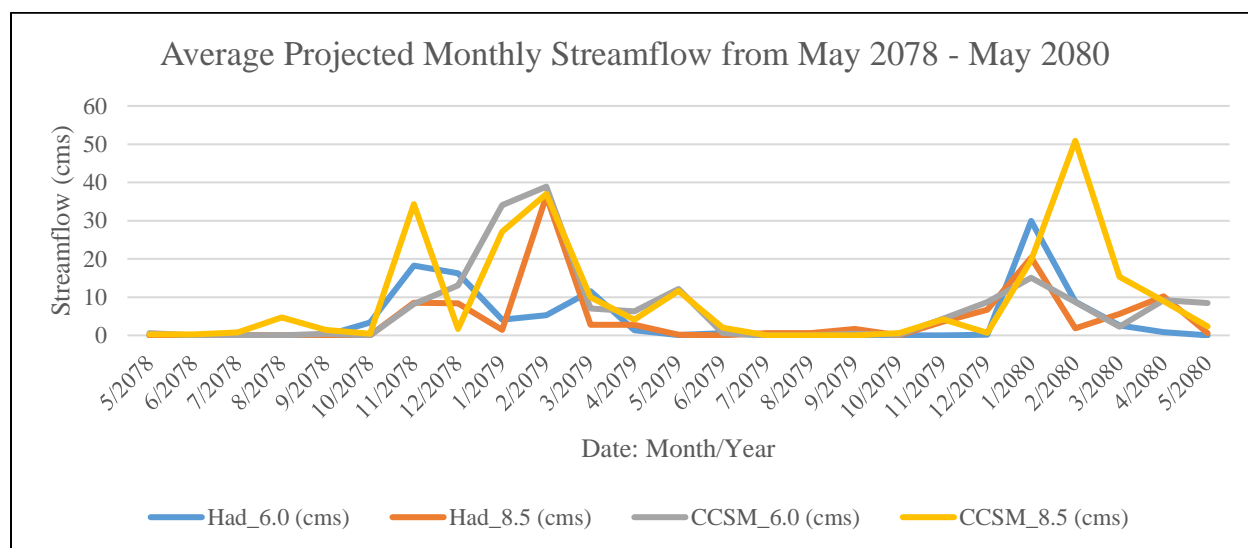


Figure 6.15. Projected mean-monthly streamflow rates for the Upper Merced Basin during a selected 2-yr period from May 2078 – May 2080. Forcing scenarios RCP6.0 and RCP8.5 are applied under two GCMs, HadGem2-CC and CCSM4. Climate modeling data in the form of projected precipitation, temperature, and solar radiation, were downloaded via MarkSim GCM Weather Generator and plugged into the Upper Merced Basin model built using the Soil and Water Assessment Tool (SWAT).

From May 2078 to May 2080 (Figure 6.15), the average projected monthly streamflow shows some noteworthy differences from May 2048-May 2050 streamflow (Figure 6.13). The RCP 6.0 scenarios are no longer peaking similarly; HadGem2-CC 6.0 slightly peaks in December 2078 (18 cms) and then again a few months later in March 2079 (10 cms). HadGem2-CC 6.0 peaks more significantly in January 2080 at 30 cms. CCSM4 6.0 peaks in February 2079 (40 cms), again near May 2079 (10 cms), and then in January 2080 (14 cms).

HadGem2-CC 8.5 peaks in February/March 2079 (36 cms) and then in January 2080 (17 cms). CCSM4 8.5 shows the highest streamflow overall, with initial two large outflows, January 2078 (32 cms) and March 2079 (38 cms), and then 51 cms in February 2080. All models experience low streamflow from June 2079 to October 2079.

CHAPTER 7

DISCUSSION

7.1 VALIDATION

An anomalously 2010/2011 winter season is visualized in the SWAT-CUP Upper Merced Basin validation (Figure 6.2). This uncharacteristically snowy winter led to enhanced snowmelt in the spring, seen by an underestimated simulated streamflow and a high simulated streamflow peak (Guan et al. 2013). During the 2010/2011 winter and spring, mean April 1 SWE (snow water equivalent) was 55% (0.44 m) above normal across 100 Sierra Nevada snow sensors. Unlike an expected nine atmospheric rivers (ARs) per season, the Sierra Nevada experienced 20 ARs during the 2010/2011 winter, 14 of which were in December 2010. This jump in AR occurrence has been linked to negative phases of the Arctic Oscillation (AO) and the Pacific-North American (PNA) teleconnection pattern. Increases in negative phases can bring about “cyclonic anomalies” and colder temperatures, a coupling which can provide a high frequency of ARs (Guan et al. 2013).

7.2 OBSERVED PEAK STREAMFLOW

USGS 1984-2013 Pohono Bridge data measured highest flow during April, May, June, and July. Figure 6.4 illustrates monthly patterns in annual peak streamflow by color, showing peak annual streamflow in May in orange, June in green, and April in blue. Generally, peak streamflow can be clearly seen within the data as occurring in one standalone month. Yet for smaller monthly peak flows, flow measurements may be split across two consecutive months,

causing two months of moderate streamflow. 1987 recordings for example, read April as peak streamflow with 29.4 cms. The following month, May, records 18.1 cms, the second highest peak flow. 1994, a similarly has a “low” annual peak flow recording in May (33.6 cms). Streamflow in April 1989 is reported as 22.3 cms, and 15.7 cms in June 1989. Figure 6.4 offers not only a visualization of Upper Merced annual peak flow occurrence, but coupled with an understanding of snow accumulation within the elevated subbasin, Figure 6.4 can help answer broader inquiries of snowmelt and precipitation fluctuations.

Low peak flows within a basin dependent on snowmelt can be indicative of either an overall decrease precipitation resulting from drought conditions or a reduction in snowpack due to increased temperatures and therefore a higher likelihood of rain over snow events. From the above figure, it is apparent that past climate patterns for the Upper Merced Region allowed for snow accumulation during winter months, enabling snowmelt into the Merced River. During the observed historical period, 73% of peak flow months occurred in May, 20% in April, and 7% in June. This classic snowmelt pattern operates as a reservoir for Southern California with a historically reliable supply of freshwater available in the spring.

7.3 FUTURE CLIMATE SCENARIOS

Climate change warnings point to a future with fluctuating seasonality with a shift from snow to rain as a result of warming temperatures. Deviation in normal snow patterns to precipitation falling as rain is likely to present runoff earlier in the season, with an overall lower runoff ratio (Hunsaker et al. 2012).

Furthermore, research suggests that annual minimum flows within select California basins will drop to zero if SWE is cut to about half its historical average (Godsey et al. 2013).

Evidenced by Figure 6.13 through 6.15, the average projected monthly streamflow during select years in the 2040, 2060s, and 2080s, respectively, streamflow does fall to zero. During the RCP6.0 scenarios, streamflow most significantly fell to zero during September. Looking exclusively at HadGEM2-CC 6.0, streamflow reduced to zero during September of 2041, 2043, 2044, 2049, 2053, 2054, 2060, 2061, 2065, 2073, 2074, 2078, 2079, 2084, and 2085. Streamflow did drop to zero in surrounding autumn months, but most often the GCM calculated a zero September flow. HadGEM2-CC 6.0 expressed zero outflow over a total of 31 months from 2040 to 2099. Similarly, CCSM4 6.0 reported empty flows in and around September, but zero outflows are more widely distributed from July through December; a total of 34 zero monthly outflows are projected for the CCSM4 6.0 scenario. Looking at RCP8.5 scenarios, HadGEM2-CC 8.5 projected the highest number of all scenarios, 41, zero outflow months. Most often the zero outflows were during August. CCSM4 8.5 expressed 31 months with zero outflows, starting in June and ending by November.

It has been calculated that for every 10% decrease in peak SWE, the annual minimum flow may decrease by 9-22%, while occurring 3-7 days earlier in the year (Godsey et al. 2013). Although USGS observed flow from 1979-2013 did not indicate any measured flowrates at Pohono Bridge as zero, September through December flows rates were low indicating snowpack accumulation along higher elevations. The lowest measured flow was in September 1994, with a total of 0.336 cms outflow from the measuring station. Of the 54 months in which historical discharge below 1 cms, all were recorded between September and January, besides four August readings (1987, 2007, 2013). These August dates correspond with the following significant California droughts: 1986-1992, 2007-2009, 2011-2017.

7.4 PROJECTED ANNUAL PEAK FLOWS

Future climate change scenarios show a blatant shift in seasonality. Compared to the USGS historical data set, earlier peak streamflow is expressed across both GCMs under either forcing scenario. The simulated hydrological modeling for the Upper Merced Basin suggests that there might be a significant temporal shift in streamflow peaks and water availability over the next century. Observed data from 1985 – 2013 show peak streamflow occurring in April, May, and June, only. GCM data computed demonstrate peak annual streamflow happening most often in December, January, and February, opposed to spring months similar to the observed historical streamflow data (Figures 6.5 – 6.12). This evidence suggests that future maximum streamflow may occur up to three months earlier than observed peak discharge.

A possible suggestion for earlier streamflow is increased rain. Future temperatures are expected to increase, and this can cause winter precipitation to be experienced as rain over snow. Without cold temperatures at high elevations, snow accumulation may not be possible during winter months. Rain falling will immediately be included in streamflow, as precipitation will not become snowpack and therefore, California's winter water reservoir may be free to runoff and/or evaporate as soon as the precipitation event happens.

7.5 LIMITATIONS

Watersheds fed entirely or predominantly by rainfall-runoff constitute the bulk of SWAT publications (Wang et al. 2016). Study basins attributing a percentage of flow to snowmelt are less widely researched within the SWAT community, as the program has experienced challenges while modeling low-flow during snowmelt events. Regular streamflow events in the Upper Merced Basin are contingent on the successful trickle-down of spring snowmelt from the Sierra

Nevada Mountains into the basin. Successful flow modeling is contingent on a realistic interplay between elevation, snowfall, snow accumulation, temperature, and snow melt (Fountain et al. 2002; Sanadhya, et al. 2014). To better aid SWAT in furcating snowfall, snow data from gages would be helpful. Unfortunately, the Upper Merced Basin is located below the mountainous snowpack region and cannot utilize data falling outside of the basin's physical boundaries. Instead, snowmelt and snowfall were projected using temperature and precipitation only.

Reviewing projected snow data, SWAT was at times unable to accurately represent snow cover. The program struggled with accumulating enough snow pack during the winter months for runoff into the spring months. Rain events were often conflated with snowfall. SWAT mistakenly logged snow as an intense rain, causing the model to overcompensate and estimate runoff for the same event twice. As discussed previously, GW_DELAY was characterized as a highly sensitive parameter using LH-OAT and due to errors in water release timing/lag time, GW_DELAY was modified to help correct inadequate snow cover results. SURLAG was additionally calibrated to fix flow modeling.

Land use and land cover stayed static throughout the forecasted models. SWAT simulations assume no land use change as the model is set using the National Land use Cover Dataset (NLCD). The most recent National Land use Cover Dataset (NLCD 2012) was applied to the basin and so future climate scenarios operated under fixed land use conditions through 2099. Insights from a 2009 SWAT study evaluating flow simulation and forecasting in the Upper Bernam Malaysian river basin suggest that land use within the study area has greatly changed from 1981 through 2007 (Alansi et al. 2009). Five land use change scenarios were tested and the subsequent research implies that during high flow months, land use change was responsible for increasing annual flow depth between 8% to 39%, while decreasing annual flow depth between

3% to 32% during low flow months. From shifts in land use alone, monthly irrigation was reduced by 50% below necessary demand during low flow months (Alansi et al. 2009). The Upper Bernam river basin experienced rapid exponential land use transformation over the studied time frame, as is similarly indicated by socioeconomic-climate scenario research for the San Joaquin River Basin (Reclamation 2014). According to a climate impact assessment report for the San Joaquin Basin published by the Department of the Interior Bureau of Reclamation, the Central Valley's 2005 base population will likely increase by 19 million at the close of the century. As population swells, urban areas will expand in tandem to support the growing community. This sprawl will encroach neighboring agricultural fields at a rate of 500,000 irrigated acres by 2050 and 1.7 million acres by 2100 (Reclamation 2014). Streamflow modeling without consideration of future land use adaptations may prevent accurate future representations of flow within the basin.

Downscaling was used to translate climate information from GCMs chosen to the SWAT program. Downscaling enables realistic climate projection outputs by localizing GCM data by matching GCM longitude and latitude to that of the study area. MarkSim GCM data were downloaded for the study, which is a third-order Markov rainfall model with autoregressive temperature and radiation estimation to downscale daily weather data. Although downscaling is necessary, this method predicts temporal and pattern of rainfall will continue to be identical into the future (Dlamini et al. 2017). As evidenced by this research, the Upper Merced Basin will experience fluctuating precipitation events, altering the pattern of rainfall.

7.5.1 SWAT and SWAT-CUP Video Tutorials

As previously discussed, online groups are necessary outlets for users of dynamic, multi-operational programs such as SWAT. Not only can the proposed model objective be distinctive, but so can the model components and model operation of SWAT research. With numerous iterations in model setup and analysis, SWAT users would benefit from an archive of instructional videos. As of late 2017, the SWAT site includes short instructional “workshop” videos produced by Purdue University in collaboration with Texas A&M, with funding by the Environmental Protection Agency (EPA). The clips are a curt 3-5 minutes long, without much distinction in watershed examples. From experience, users would find advantage in a larger collection of tutorial videos detailing solutions to technical and analytical confusions. To name a few outstanding spaces needing clarification, future SWAT training videos might cover: expanding on downloading and setting up an ArcSWAT project, building weather data input tables from raw government data, editing input files to include additional water sources and water infrastructure such as reservoirs and conveyances respectively, and in-depth tutorials on how to read SWAT output files in order to pull out points for analysis.

However brief available ArcSWAT videos may be, the online collection lacks any SWAT-CUP videos for the purpose of calibrating and validating. To call this an oversight, is restrained. The importance of the SWAT-CUP procedure cannot be overstated as projected data must be calibrated to observed data in order to properly interpret any SWAT simulation. At the start of SWAT-CUP analysis, four modes of calibration are available, yet justification in selecting one method over another, is not completely rationalized in the SWAT-CUP manual. At minimum, video guidance should begin in determining the best strategy for calibration, progress into technical lessons on formatting and inputting observed values, choosing performance

indicators best suited for the model, creating a 95ppu plot from the 95ppu text file, and writing calibrated parameters back into the original ArcSWAT project. SWAT Google Groups are inundated daily with discouraged users stalled in their research; without detailed videos illustrating program procedure, students forfeit analytical time for the purpose of working through mechanical errors.

Altogether, the absence of visual explanations in trouble-shooting SWAT does the program a disservice. For such a beautifully applicable and adaptive hydrological program, misunderstandings should not impede student SWAT studies. The imaginary of SWAT research is boundless, in that individuals can work to forecast uncertainties without cumbersome equipment or excessive funding. Previously unbent water systems are being reformed in unknown ways by global climate chaos, and excessive investigation is the only approach to discern the uncertainties ahead. In reviewing emergent SWAT research, recent publications illustrate SWAT's suitability in examining the intersection between hydrology, climate change, and policy: best management practices (BMPs) in agricultural scenarios under pesticide action plans in France (Vernier et al. 2017), the significance of climate change on reservoir management in Portugal (Carvalho-Santos et al. 2017), and predicting the impression of past, current, and future land use changes on water balance (Kundu et al. 2017), to name a few.

With intention of building an exhaustive set of instructional videos, material can be consolidated from a wide range of resources such as international SWAT development conferences and workshops, hydrological research consortiums, established independent water modelers, professors with SWAT capabilities, and other helpful experienced SWAT-users. By integrating a wide scope of multi-media educational resources on the SWAT website, program software will become more accessible and easily read by students in applicable fields of study,

assisting in future SWAT development as more modelers gravitate towards the program. Having said this, it is important to note additional SWAT executables and software not employed in the Upper Merced model such as QSWAT (QGIS interface for SWAT), SWAT-MODFLOW (integrated model blending SWAT land surface processes with spatially-explicit GW flow processes), VIZSWAT (visualization and analysis tool for SWAT model output), MWSWAT (open source interface to SWAT using GIS system MapWindow), SLEEP (Soil-Landscape Estimation and Evaluation Program), Baseflow Filter Program (estimates baseflow and GW recharge from streamflow records), Potential Heat Unit Program (estimates the number of heat units required to bring a plant to maturity), and AVSWAT (preprocessor, interface, and post processor for SWAT), are similarly not further explained with tutorial videos.

7.6 SUGGESTIONS

Accuracy of future streamflow is limited by the regional nature of the climate models chosen. Projected rainfall and temperature are built upon gridded hydro-meteorological data, therefore subjecting the study area to hydrological modeling developed for the greater region of Northern California. Model specificity could be compromised as climate scenario temperature and precipitation data are relevant to the region in its entirety; gridded data does little to represent variations in divergent basins such as the California Delta lowlands, the glacial Sierra Nevada mountains, or the snowmelt fed Upper Merced Basin. To help remedy the regional nature of general circulation models so that future estimations are more localized, further climate variables may be added alongside rainfall and temperature. Helpful climate variable for input may be wind speed, solar radiation, and relative humidity. Although these variables are

propagated using the built-in SWAT stochastic weather generator, intentionally inputting such data may reduce overall uncertainty (Kilsby et al. 2007; Dlamini et al. 2017).

In general, SWAT does not include water added to flow through percolation into the aquifer layer. This added level of complexity is difficult to model, and so it is removed from the SWAT water balance algorithm. Instead, the program ignores water moving into the deep aquifer, reducing the amount of flow that might be rerouted back into the system as return flow. From model sensitivity analysis, groundwater parameters (RCHRG_DP, REVAPMN, GW_DELAY, GWQMN) were flagged as significant despite the program being unable to accurately describe all components of base flow. To provide a more complete representation of the hydrological cycle, the Baseflow Filter Program is available online to separate baseflow within a natural system (Arnold, J.G. Allen, P.M. 1999). Results have found model results are significantly improved as the ratio of surface runoff to baseflow is estimated more completely. Future studies should utilize programs similar to SWAT's Baseflow Filter Program for the purpose of understanding model groundwater interactions and baseflow contributions.

7.7 SWAT-USER AND SWAT-CUP GROUPS

The SWAT program is a public domain model developed by USDA Agricultural Research Service (USDA-ARS) and Texas A&M AgriLife Research. The program site (swat.tamu.edu) houses most recent SWAT2012 input/output file documentation and a literature database publically available for review. Though the site is comprehensive in including official SWAT material alongside user-submitted papers, due to the exhaustive applicability of the program, SWAT Google Groups can be elemental in navigating the nuances of model setup. SWAT students post queries onto the discussion boards, which are answered by an alliance of

SWAT programmers, hydrological modelers, and other learned SWAT students. The SWAT-user Google Group operates for model construction questions, whereas the SWAT-CUP Google Group is a forum dedicated to the subsequent calibration and validation processes.

Without access to the SWAT-user and SWAT-CUP Google Groups during the building and assessment stages, model effectuality would have suffered.

SWAT Google Groups are seemingly endorsed by the SWAT cooperative, as the program site directs users to respective Google forums for further questions. Posts are answered by the greater SWAT community, but if there is a lack of group support in trouble shooting an inquiry, Dr. Karim Abbaspour or Dr. Raghavan Srinivasan, lead researchers associated with SWAT, will respond. Together, Dr. Abbaspour and Dr. Srinivasan provided me with their thoughtful expertise via Google Group communications and email correspondence. Without pause, guidance by the above researchers was the impetus of my model's success. Experiencing conflicts beginning in basin delineation and constructing temperature and precipitation files, to uncertainties in choosing final parameters for best practice, I benefited greatly from the patient, unwavering assistance of Dr. Abbaspour and Dr. Srinivasan.

7.8 CONCLUDING THOUGHTS

After close examination of both current observation and conducted climate scenario studies on Upper Merced Basin hydrology, there are a number of major trends which can be gleaned from GCM research. First, streamflow deriving from the Sierra Nevada region will most likely occur earlier than historical recordings of peak streamflow. Although earlier snowmelt can possibly be attributed to increased temperatures resulting in a higher occurrence of rainfall over

snowfall, studies have not concluded whether earlier timing of streamflow is a result of climate change or climate variability within the region (Vicuna and Dracup 2005).

As evidenced by the multitude of climate studies conducted for the state of California, different approaches to determining temperature, precipitation, and streamflow via GCMs, scenarios, and downscaling techniques have concluded a wide range of projections for climatological variables. Results mostly agree on an increase in air surface temperature, however, there is not a consensus on total volume of runoff or average annual timing of increased streamflow. Hopefully with increased advancements in downscaling techniques which enable greater “matching” of spatial and temporal resolutions, future research will be able to better define variation in natural runoff. Further advancements in GCM research may allow for more precise precipitation forecasting, which is necessary for most California basins as they operate largely in snowmelt-fed regions.

Works Cited

- Abbaspour, K. C, Johnson, C. A, van Genuchten, M. T. (2004). Estimating Uncertain Flow and Transport Parameters Using a Sequential Uncertainty Fitting Procedure. *Vadose Zone J.* 3(5), 1340–1352.
- Abbaspour, K. C., Rouholahnejad, E., Vaghefi, S., Srinivasan, R. Yang, H., Kløve, B. (2015). A continental-scale hydrology and water quality model for Europe: Calibration and uncertainty of a high-resolution large-scale SWAT model. *Journal of Hydrology* 524, 733- 752.
- Alansi, A. W., Amin, M. S. M., Abdul Halim, G., Shafri, H. Z. M., Aimrun, W. (2009). Validation of SWAT model for stream flow simulation and forecasting in Upper Bernum humid tropical river basin, Malaysia. *Hydrology and Earth System Sciences* 6:7581-7609.
- Anderson, J., F. Chung, M. Anderson, L. Brekke, D. Easton, M. Ejeta, R. Peterson, and R. Snyder. (2008). Progress on incorporating climate change into management of California’s water resources. *Climate Change* 87(1): S91-S108.
- Aguado, E., Cayan, D.R., Riddle, L.G., Roos, M. (1992). Climatic fluctuations and the timing of West Coast streamflow. *Journal of Climate* 5, 1468–1483.

- Arnold, J. G., Allen, P. M. (1999). Automated methods for estimating baseflow and groundwater recharge from streamflow records. *Ground Water* 33(6): 1010-1018.
- Arnold, J. G., Moriasi, D. N., Gassman, P. W., Abbaspour, K. C., White, M. J., Srinivasan, R., Santhi, C., Harmel, R. D., Griensven, A. van, Van Liew, M. W., Kannan, N., Jha, M. K. (2012). SWAT: Model Use, Calibration, and Validation. *American Society of Agricultural and Biological Engineers* 55(4): 1491-1508.
- Barnett, T. P., D. W. Pierce, H. G. Hidalgo, C. Bonfils, B. D. Santer, T. Das, G. Bala, A. W. Wood, T. Nozawa, A. A. Mirin, D. R. Cayan, and M. D. Dettinger. (2008). Human-induced changes in the hydrology of the western United States. *Science* 319, 1080-1083.
- Bertoldi, G. L., Johnston, R. H., Evanson, K. D. (1991). Groundwater in the Central Valley, California – A summary report: US Geological Survey Professional Paper 1401-A.
- Bolger, B. L. (2009). “Simulating the Predevelopment Hydrologic Condition of the San Joaquin Valley, California.” PhD (doctor of Philosophy) thesis, University of Waterloo.
- Byrd, K. B., Flint, L. E., Alvarez, P., Casey, C. F., Sleeter, B. M., Soulard, C. E., Flint, A. L., Sohl, T. L. (2015). Integrated Climate and Land Use Change Scenarios for California Rangeland Ecosystem Services: Wildlife Habitat, Soil Carbon, and Water Supply. *Landscape Ecology* 30, 729-750.

- California Environmental Resources Evaluation System (CERES). "The San Joaquin Valley Bioregion -- An Overview." California Natural Resources Agency. 2005. Web. <http://ceres.ca.gov/geo_area/bioregions/San_Joaquin_Valley/index.html>.
- Carvalho-Santos, C., Monteiro, A. T., Azevedo, J. C., Honrado, J. P., Nunes, J. P. (2017). Climate change impacts on water resources and reservoir management: Uncertainty and adaptation for a mountain catchment in Northwest Portugal. *Water Resource Management* 31:3355-3370.
- Cavagnaro, T. R., Jackson, L. E., Six, J., Ferris, H., Goyal, S., Asami, D., Scow, K. M. (2006). Arbuscular mycorrhizas, microbial communities, nutrient availability, and soil aggregates in organic tomato production. *Plant Soil* 282, 209-225.
- Cayan, D. R., Maurer, E. P., Dettinger, M.C., Tyree, M., Hayhoe, K. (2008). Climate change scenarios for the California region. *Climate Change* 87(1), S21-S42.
- Cayan, D., M. Tyree, M. Dettinger, H. Hidalgo, T. Das, E. Maurer, P. Bromirski, N. Graham, and R. Flick. (2009). Climate change scenarios and sea level rise estimates for the California 2009 Climate Change Scenarios Assessment. Research Paper, CEC- 500-2009- 014- F.
- Central Valley Regional Water Quality Control Board (CVRWQCB). Basin Planning

Program. Rep. State Water Control Board, 5 Aug. 2005. Web.

<http://www.waterboards.ca.gov/centralvalley/water_issues/basin_plans/plannig_overview.pdf>.

Chang, H., Bonnette, M. R. (2016). Climate change and water-related ecosystem services: impacts of drought in California, USA. *Ecosystem Health and Sustainability* 2(12).

Cowan, T. California's San Joaquin Valley: A Region in Transition. Washington D.C., USA. UNT Digital Library.

CRS Report R43200, *Energy-Water Nexus: The Water Sector's Energy Use*, Carter, N., Copeland, C. (2017).

Dettinger M.D., Cayan D.R. (1995). Large-scale atmospheric forcing of recent trends toward early snowmelt runoff in California. *Journal of Climate* 8(3), 606–623.

Dettinger MD. 2005. From climate change spaghetti to climate-change distributions for 21st Century California. San Francisco Estuary and Watershed Science. Vol. 3, Issue 1, Article 4. <http://repositories.cdlib.org/jmie/sfews/vol3/iss1/art4>

Dlamini, N. S., Kamal, M. R., Bin Mohd Soom, M. A., Faisal bin Mohd, M. S., Fikri Bin Abdullah, A., Hin, L. S. (2017). Modeling potential impacts of climate change on

streamflow using projections of the 5th assessment report for the Bernam River Basin, Malaysia. *Water* 9(226).

Dwyer, C. (2017, April, 2017). Gov. Jerry Brown Lifts Drought Emergency For Most of California. *NPR*. Retrieved from < <http://www.npr.org/sections/thetwo-way/2017/04/07/523031241/gov-jerry-brown-lifts-drought-emergency-for-most-of-California>>

Escriva-Bou, A., McCann, H., Hanak, E., Lund, J., Gray, B. (2016). *Accounting for California's Water*. 28 pp. Public Policy Institute of California, San Francisco, CA.

Fernandez, G.P., Chescheir, G.M., Skaggs, R.W., Amatya, D.M. (2005). Development and testing of watershed-scale models for poorly drained soils. *Trans. ASAE* 48(2), 639-652.

Ficklin, D. L., Luo, Y., Leudeling, E., Zhang, M. (2009). Climate change sensitivity assessment of a highly agricultural watershed using SWAT. *Journal of Hydrology* 374: 16-29.

Ficklin, D. L., Yuzhou Luo, Luedeling, E., Gatzke, S. E., Zhang, M. (2010). Sensitivity of Agricultural Runoff Loads to Rising Levels of CO₂ and Climate Change in the San Joaquin Valley Watershed of California. *Environmental Pollution* 158(1), 223-34.

- Ficklin, D. (2010). "Modeling the Impacts of Climate Change on Hydrology and Agricultural Pollutant Runoff in California's Central Valley." PhD (doctor of Philosophy) thesis, University of California Davis
- Fountain, A. G., Hoffman, M., Jackson, K., Basagic, H., Nylén, T., Percy, D. (2007). Digital outlines and topography of the glaciers of the American West. U.S. Geological Survey open-File Report-1340, 23pgs.
- Freeman, G.J. (2002). Looking for recent climatic trends and patterns in California's Central Sierra. In Proceedings 19th Annual Pacific Climate (PACCLIM) Workshop, Pacific Grove, CA pp 35–48.
- Flugel, W. (1995). Delineating Hydrologic Response Units by Geographical Information-system Analyses for Regional Hydrological Modeling using PRMS/MMS in the Drainage-basin of the River BROL, Germany. *Hydrologic Processes* 9, 423-435.
- Gassman, P. W., M. R. Reyes, C. H. Green, and J. G. Arnold. "The Soil and Water Assessment Tool: Historical Development, Applications, and Future Research Directions." *American Society of Agricultural and Biological Engineers* 50.4 (2007): 1211-250. Print.
- Georgakakos, K. P., Graham, N. E., Cheng, F.-Y., Spencer, C., Shamir, E., Georgakakos, A. P., Yao, H., Kistenmacher, M. (2012). Value of adaptive water resources management in

northern California under climatic variability and change: dynamic hydroclimatology. *Journal of Hydrology* 412-412: 47-65.

Godsey, S., Kirchner, J., Tague, C. (2013). Effects of changes in winter snowpack on summer low flows: Case studies in the Sierra Nevada, California, USA. *Hydrological Processes* 28:5048-5064.

Gronberg, J.M., Dubrovsky, N.M., Kratzer, C.K., Domagalski, J.L., Brown, L.R., and Burow, K.R., 1998, Environmental setting of the San Joaquin-Tulare Basins, California: U.S. Geological Survey Water-Resources Investigations Report 97-4205, 45 p.

Guan, B., Molotch, N. P., Waliser, D. E., Fetzer, E. J., Neiman, P. J. (2013). The 2010/2011 snow season in California's Sierra Nevada: Role of atmospheric rivers and modes of large-scale variability. *Water Resources Research* 49:6731-6743.

Hanak, E., K. Lund, A. Dinar, B. Gray, R. Howitt, J. Mount, P. Moyle, and B. Thompson. (2011). *Managing California's Water: From Conflict to Reconciliation*. Public Policy Institute of California.

Hanak, E., Lund, J., Arnold, B., Escriva-Bou, A., Gray, B., Green, S., Harter, T., Howitt, R., MacEwan, D., Medellín-Azuara, J., Moyle, P., Seavy, N. (2017). *Water Stress and a Changing San Joaquin Valley*. 48 pp. Public Policy Institute of California, San Francisco, CA.

Hanak, E., Stryjewski, E. (2002). California's Water Market, By the Numbers: Update 2012. San Francisco, CA: Public Policy Institute of California.

Hayhoe, K., Cayan, D., Field, C. B., Frumhoff, P. C. (2004). Emissions pathways, climate change, and impacts on California. *National Academy of Science USA 101*(34): 12422-12427.

He, Z., Wang, Z., Suen, C. J., Ma, X. (2013). Hydrologic sensitivity of the Upper San Joaquin River Watershed in California to climate change scenarios. *Hydrology Research 44*, 723-736.

Herberger, M., Cooley, H., Herrera, P., Gleick, P., Moore, E. (2009). The impacts of sea-level rise on the California coast. Sacramento: California Climate Change Center.

Howitt, R. E., Medellin-Azuara, J., MacEwan, D. (2008). Calculating California Cropping Patterns in 2050. *CA Water Plan Update 2013 4*: 1-32.

Hunsaker, C. T., Whitaker, T. W., Bales, R. C. (2012). Snowmelt runoff and water yield along elevation and temperature gradients in California's southern Sierra Nevada. *Journal of American Water Resources Association 48*:667-678.

IPCC, 2013: Climate Change 2013: The Physical Science Basis. Contribution of Working Group I to the Fifth Assessment Report of the Intergovernmental Panel on Climate Change [Stocker, T.F., D. Qin, G.-K. Plattner, M. Tignor, S.K. Allen, J. Boschung, A. Nauels, Y. Xia, V. Bex and P.M. Midgley (eds.)]. Cambridge University Press, Cambridge, United Kingdom and New York, NY, USA, 1535 pp, doi:10.1017/CBO9781107415324.

IPCC, 2014: Climate Change 2014: Synthesis Report. Contribution of Working Groups I, II, and III to the Fifth Assessment Report of the Intergovernmental Panel on Climate Change [Core Writing Team, R.K. Pachauri and L.A. Meyer (eds.)]. IPCC, Geneva, Switzerland, 151 pp.

Ishida, K., Gorguner, M., Ercan, A., Trinh, T., Kavvas, M. L. (2017). Trend analysis of watershed-scale precipitation over Northern California by means of dynamically-downscaled CMIP5 future climate projections. *Science of the Total Environment* 592: 12-24.

Jackson, L., Van R.H., Wheeler, S.M., Hollander, A.D., Perlman, J., O'Geen, T., Mehta, V.K., Clark, V., Williams, J., Thrupp, A. (2012). University of California, Davis Vulnerability and Adaptation to Climate Change in California Agriculture. California Energy Commission.

Kilsby, C.; Jones, P.; Burton, A.; Ford, A.; Fowler, H.; Harpham, C.; Wilby, R. A daily weather generator for use in climate change studies. *Environmental Modeling Software* **2007**, *22*,

1705–1719.

Kiparsky, M., Gleick, P. (2003). Climate Change and California Water Resources: A Survey and Summary of the Literature. Pacific Institute for Studies in Development, Environment, and Security.

Knowles, N., Cayan, D. R. (2002). Potential effects of global warming on the Sacramento/San Joaquin watershed and the San Francisco estuary. *Geophysical Research Letters* 29(18): 1891.

Knowles, N., Dettinger, M. D., Cayan, D. R. (2006). Trends in Snowfall versus rainfall in the Western United States. *Journal of Climate* 19, 4545-4559.

Krause, P., Boyle, D. P., Bäse, F. (2005). Comparison of different efficiency criteria for hydrological model assessment. *Journal of Advanced Geoscience* 5, 89-97.

Kundu, S., Khare, D., Mondal, A. (2017). Past, present and future land use change and their impact on water balance. *Journal of Environmental Management* 197:582-596.

Lee, J., De Gruyze, S., Six, J. (2011). Effect of climate change on field crop production in California's Central Valley. *Climatic Change* 109: S335-S353.

Li, Y., Thompson, J. R., Li, H. (2016). Impacts of spatial climatic representation on hydrological model calibration and prediction uncertainty: A mountainous catchment of three Gorges Reservoir region, China. *Water* 8(73).

Lobell, D.B., Torney, A., Field, C.B. (2011). Climate Extremes in California Agriculture. *Climatic Change* 109, 355-363.

Luedeling, E. (2012). Climate Change Impacts on Winter Chill for Temperate Fruit and Nut Production: A Review. *Scientia Horticulturae*, 144(0), 218-229.

Luers, A. L., Mastrandrea, M. D. (2012). Climate change in California: scenarios and approaches for adaptation. *Climate Change* 111(1): 5-16.

Luers, Amy Lynd, et. al. *Our Changing Climate: Assessing the Risks to California: A Summary Report from the California Climate Change Center*. 2006.
http://meteora.ucsd.edu/cap/pdffiles/CA_climate_Scenarios.pdf

Lund, J. R., E. Hanak, W. E. Fleenor, J. F. Mount, R. Howitt, B. Bennett, and P. B. Moyle. 2010. *Comparing Futures for the Sacramento San Joaquin Delta*. Berkeley: University of California Press and Public Policy Institute of California.

- Luo, Y., Zhang, X., Liu, X., Ficklin, D., Zhang, M. (2008). Dynamic Modeling of Organophosphate Pesticide Load in Surface Water in the Northern San Joaquin Valley Watershed of California. *Environmental Pollution* 156, 1171-1181.
- Maurer, E.P., A.W. Wood, J.C. Adam, D.P. Lettenmaier. 2002. A long-term hydrologically based dataset of land surface fluxes and states for the conterminous United States. *J. of Climate*, 15(22): 3237-3251.
- Maurer, E.P.. (2007). Uncertainty in hydrologic impacts of climate change in the Sierra Nevada, California under two emissions scenarios, *Climatic Change* (82): 3-4, 309-325.
- Maurer, E. P., Brekke, L. D., Pruitt, T. (2010). Contrasting Lumped and Distributed Hydrology Models for Estimating Climate Change Impacts on California Watersheds. *Journal of the American Water Resources Association* 46(5), 1024-1035.
- McCuen, R. (1973). The Role of Sensitivity Analysis in Hydrologic Modeling. *Journal of Hydrological Engineering* 18(1), 37-53
- Mehta, V. K., Haden, V. R., Joyce, B. A., Purkey, D. R., Jackson, L. E. (2013). Irrigation Demand and Supply, Given Projection of Climate and Land-Use in Yolo County, California. *Agricultural Water Management* 117, 70-82.
- Meisen, P. (2011). Impacts of climate change on California's water supply. *Global Energy*

Network Institute (GENI).

Melesse, A. M., Abtew, W., Setegn, S. G., Dessalegne, T. (2011). *Nile River Basin: Hydrology, Climate, and Water Use*. Springer Press. Print.

Miller, N. L., Bashford, K.E., Strem, E. (2003). Potential impacts of climate change on California hydrology. *Journal of the American Water Resources Association* 39(4): 771-784.

Miller, Norman L., Jiming Jin, Katharine Hayhoe, and Maximilian Auffhammer. (2007). *Climate Change, Extreme Heat, and Energy Demand in California*. California Energy Commission, PIER Energy Related Environmental Research Program. CEC_500_2007_023.

Miller, N., et al. 2008. An Analysis of Droughts in the California Central Valley Surface-Groundwater Conveyance System. Proceedings of the California Central Valley Groundwater Modeling Workshop. Lawrence Berkeley National Laboratory, Berkeley, California.

Mote, P. W., Hamlet, A. F., Clark, M. P., and Lettenmaier, D. P. (2005). Declining mountain snowpack in western North America. *Bulletin of the American Meteorological Society* 86, 39-49.

- Mishra, S. K. (2013). "Modeling Water Quantity and Quality in an Agricultural Watershed in the Midwestern US Using SWAT: assessing implication due to an expansion in "biofuel" production and climate change." PhD (doctor of Philosophy) thesis, University of Iowa.
- Moriasi, D.N., Arnold, J.G., van Liew, M.W., Bingner, R.L., Harmel, R.D., Veith, T.L. (2007). Model evaluation guidelines for systematic quantification of accuracy in watershed simulations. *Trans. Am. Soc. Agric. Eng.*, 50, 885–900.
- Nash, J.E., Sutcliffe, J.V. (1976). River flow forecasting through conceptual models: part I. A discussion of principles. *Journal of Hydrology* 10, 282–290.
- National Agricultural Statistics Service (NASS). (2009). 2009 Consensus of Agriculture. Online at <http://www.agcensus.usda.gov/>
- Neitsch, S.L., J.G. Arnold, J.R. Kiniry, J.R. Williams. Soil and Water Assessment Tool Theoretical Documentation. 2005a. MS. Texas A&M University, Temple. Soil and Water Assessment Tool. Blackland Research Center, Web. <<http://swatmodel.tamu.edu/software/arcswat/>>.
- NOAA National Centers for Environmental Information. (2015). State of the Climate: National Overview for October 2015. Retrieved from <http://www.ncdc.noaa.gov/sotc/national/201510>.

- Null, S. E., Viers, J.H., Mount, J.F. (2010). Hydrologic response and watershed sensitivity to climate warming in California's Sierra Nevada. *PLoS ONE* 5(4).
- Null, S. E., Viers, J. H. (2012). *Water and Energy Sector Vulnerability to Climate Warming in the Sierra Nevada: Water Year Classification in Non-Stationary Climates*. California Energy Commission. Publication number: CEC-500-2012-015.
- Obispo, S. L. (2013). "Hydrologic Modeling of the San Joaquin Valley Watershed for Purposes of Nitrate Analysis." PhD (doctor of Philosophy) thesis, California Polytechnic State University.
- Opperman, J.J. (2012). A conceptual model for the floodplains in the Sacramento-San Joaquin Delta. *San Francisco Estuary and Watershed Science* 10(3).
- Piniewski, M., Okruszko, T. (2011). Multi-site calibration and validation of the hydrological component of SWAT in a large lowland catchment. In: *Modelling of Hydrological Processes in the Narew Catchment*. Geoplanet: Earth, and Planetary Sciences. 15-41.
- Phillips, S.P., Green, C.T., Burow, K.R., Shelton, J.L., Rewis, D.L.. (2007). Simulation of multiscale ground-water flow in part of the northeastern San Joaquin Valley, California: U.S. Geological Survey Scientific Investigations Report 2007-5009, 43 p

- Quinn, N.W.T., Tulloch, A. (2002). San Joaquin River Diversion Data Assimilation, Drainage Estimation and Installation of Diversion Monitoring Stations. CALFED Bay-Delta Program.
- Quinn, N.W.T., Jacobs, K., Chen, C.W., Stringfellow, W.T. (2005). Elements of a decision support system for real-time management of dissolved oxygen in the San Joaquin River Deep Water Ship Channel. *Environmental Modelling & Software* 20(12), 1495-1504.
- Reclamation, 2014. *West-Wide Climate Risk Assessment: Sacramento and San Joaquin Basin Climate Impact Assessment*, U.S. Department of the Interior Bureau of Reclamation, September 2014. Retrieved on August 28, 2014 from :
<<https://www.usbr.gov/watersmart/wcra/docs/ssjbia/ssjbia.pdf>>.
- Regonda, S.K., Rajagopalan, B., Clark, M., Pitlick, J. (2005). Seasonal cycle shifts in hydroclimatology over the Western United States. *Journal of Climate* 18(2), 372–384.
- Ritter, N.P., Uptain, C.E., Kelly, P.A.(2005). The potential for using locally-collected seed in San Joaquin Valley restoration. *Society for Ecological Restoration*, Bass Lake, CA.
- Roos, M. (1991). A trend of decreasing snowmelt runoff in northern California. In: Proceedings 59th Western Snow Conference, Juneau, AK, pp 29–36.
- Saleh, D.K., Domagalski, J.L., Kratzer, C.R., and Knifong, D.L., 2007, Organic carbon

trends, loads, and yields to the Sacramento–San Joaquin delta, California, water years 1980–2000, second edition: U.S. Geological Survey Water-Resources Investigations Report 03–4070, 77. p

Sanadya, P., Gironás, J., Mazdak, A. (2014). Global sensitivity analysis of hydrologic processes in major snow-dominated mountainous river basins in Colorado. *Hydrological Processes* 28(9): 304-3418.

Semenov, M.A., Barrow, E.M. (1997). Use of a stochastic weather generator in the development of climate change scenarios. *Climatic Change* 35(4), 397-414.

Semenov, M.A., Brooks, R.J., Barrow, E.M., Richardson, C.W. (1998). Comparison of WGEN and LARS-WG stochastic weather generators for diverse climates. *Climate Research* 10, 95-107.

Sharpley, A.N, Williams, J.R. (1990). Erosion/Productivity Impact Calculator, 1. Model Documentation. USDA-ARS Technical Bulletin 1768.

Sneed, M. (2001) Hydraulic and mechanical properties affecting groundwater flow and aquifer-system compaction, San Joaquin Valley, California: US Geological Survey Open-File Report 01-35.

Soil Survey Staff, Natural Resources Conservation Service, United States Department of Agriculture. Web Soil Survey. Available online at <https://websoilsurvey.nrcs.usda.gov/>. Accessed [01/10/2017].

Stewart, I.T., Cayan, D.R., Dettinger, M.D. (2005). Changes toward earlier streamflow timing across Western North America. *Journal of Climate* 18(8), 1136–1155.

Stewart, I. T., Ficklin, D. L., Carrillo, C. A., McIntosh, R. (2015). 21st century increases in the likelihood of extreme hydrologic conditions for the mountainous basins of the Southwestern United States. *Journal of Hydrology* 529: 340-353

Stillwater Sciences (2008). The Merced River Alliance Project Final Report. Volume II: Biological monitoring and assessment report. Prepared by Stillwater Sciences, Berkeley, California.

Stinsen, S., Sonnennborg, T. O., Hojberg, A. L., Troldber, L., Refsgaard, J. C. (2011). Evaluation of climate input biases and water balance issues using a coupled surface-subsurface model. *Valdosa Zone Journal* 10(1): 37-53.

Swain, D.L., Horton, D.E., Singh, D., Diffenbaugh, N.S. (2016). Trends in atmospheric patterns conducive to seasonal precipitation and temperature extremes in California. *Science Advances* 2, 1-13.

Trotochaud, J., Flanagan, D.C., Engel, B.A., (2014). A Simple Technique for Obtaining Future Climate Data Inputs for Natural Resource Models. (Working).

Umbach, Kenneth W. (2002) San Joaquin Valley: Selected Statistics on Population, Economy, and Environment. Sacramento: California Research Bureau, California State Library, 2002; www.library.ca.gov/crb/02/10/02-010.pdf.

USGS, 2011. National Land Cover Database (NLCD) 2011, U.S. Geological Survey, Earth Resources Observation Systems.

USGS, 2016. National Water Information System: Web Interface, United States Geographical Survey.

van Griensven, A., Meixner, T., Grunwald, S., Bishop, T., Diluzio, M., Srinivasan. (2006). A Global Sensitivity Analysis Tool for the Parameters of Multi-Variable Catchment Models. *Journal of Hydrology* 324, 10-23.

VanRheenen, N. T., A. W. Wood, R. N. Palmer, and D. P. Lettenmaier. 2004. Potential implications of PCM climate change scenarios for Sacramento-San Joaquin River Basin hydrology and water resources. *Clim. Change*, 62: 257-281.

Van Liew, M. W., T. L. Veith, D. D. Bosch, and J. G. Arnold. 2007. Suitability of SWAT for the conservation effects assessment project: A comparison on USDA-ARS experimental

watersheds. *J. Hydrologic Eng.* 12(2): 173-189.

Vernier, F., Leccia-Phelpin, O., Lescot, J. M., Minette, S., Miralles, A., Barberis, D., Scordia, C., Kuentz-Simonet, V., Tonneau, J. P. (2017). Integrated modeling of agricultural scenarios (IMAS) to support pesticide action plans: the case of the Coulonge drinking water catchment area (SW France). *Environmental Science and Pollution Research* 24(8):6923-6950.

Vicuña, S. Dracup, J. (2005). The evolution of climate change impact studies on hydrology and water resources in California. *Climatic Change* 82: 327-350.

Vicuña, S. 2006. Predictions of climate change impacts on California water resources using CALSIM II: a technical note. Prepared for California Climate Change Center. CEC-500-2005-200-SF.

Vicuña, S., E. P. Maurer, et al. 2007. The Sensitivity of California Water Resources to Climate Change Scenarios. *JAWRA*, 43(2): 482-498.

Wagner, R. W., Stacey, M., Brown, L. R., Dettinger, M. (2010). Statistical models of temperature in the Sacramento-San Joaquin Delta under climate-change scenarios and ecological implications. *Estuaries and Coasts*

- Wang, Y., Jianmin, B., Wangm S. Tang, J., Ding, F. (2016). Evaluating SWAT snowmelt parameter and simulating spring snowmelt nonpoint source pollution in the source area of the Liao River. *Political Journal of Environmental Studies* 25(5): 2177-2185.
- Wang, X., Melesse, A. M. (2006). Effects of STATSGO and SSURGO as inputs on SWAT model's snowmelt simulation. *Journal of the American Water Resources Association* 42(5):1217-1236.
- Wood, A, Lettenmaier, D., Palmer, R. (1997). Assessing climate change implications for water resources planning. *Climatic Change* 37:203-228.
- Yang, J., Abbaspour, K. C., Reichert, P., Yang, H. (2008). Comparing uncertainty analysis techniques for a Swat application to Chaohe Basin in China. *Journal of Hydrology* 358: 1-23.

Education	Towson University, Towson, MD 2014-2017 Masters of Science in Environmental Science: <i>Water Management Track</i>
	<ul style="list-style-type: none"> • <i>Thesis: Assessing the Ramification of Climate Change for the Purpose of Modeling Streamflow Within the Upper Merced Basin in California: 1984-2099</i>
Related Experience	Goucher College, Towson, MD 2010-2014 Bachelor of Science in Environmental Science
	<ul style="list-style-type: none"> • <i>Independent Study: Researching the urban heat island effect of Baltimore and examining the most cost efficient and sustainable solutions to the increase in temperature through a Petri dish experiment.</i>
Related Experience	Department of Environmental Science at Towson University, Towson, MD 2015-2017 <i>Graduate Assistant</i>
	<ul style="list-style-type: none"> • Aided in grading exams for environmental science department. • Served as a proctor during exams for undergraduate students.
	International Society for Ecological Modeling Global Conference, Towson, MD Spring 2015 <i>Volunteer Coordinator</i>
	<ul style="list-style-type: none"> • Coordinated community outreach to locate and schedule 35 volunteers for the conference. • Developed training and orientation meetings for volunteer program.
	Baltimore County Office of the Public Defender, Towson, MD Spring 2014 <i>Intern</i>
	<ul style="list-style-type: none"> • Assisted attorneys with interviewing clients and preparing legal research. • Consolidated online documentation for programs, schools, and facilities to assist juvenile clients.
	Department of Political Science at Goucher College, Towson, MD 2012-2014 <i>Goucher Poll State Surveyor</i>
	<ul style="list-style-type: none"> • Conducted political research through cold calls to Maryland residents. • Gathered data on current legislative topics in the state of Maryland.
	Boswyck Farms, Brooklyn, NY Summer 2013 <i>Hydroponics Intern</i>
	<ul style="list-style-type: none"> • Worked with Chief Hydroponics Specialist while developing an independent aquaponics project. • Contributed to the Certification Course Booklet through research and writing.
Goucher College, Towson, MD 2012-2014 <i>GRANOLA Trip Organizer and Leader</i>	
<ul style="list-style-type: none"> • Organized a ten-day volunteer trip to New Orleans, Louisiana for 21 people. • Collaborated and scheduled with community-based programs focused on sustainable educational and wildlife infrastructure. 	
Roosevelt Institute at Goucher College, Towson, MD 2011-2014 <i>Secretary</i>	
<ul style="list-style-type: none"> • Worked to cultivate new ideas and alternative long-term solutions to governmental policies. • Participate in weekly "think tank" meetings to discuss innovative approaches to government for young citizens. 	

Board of Trustees Committee at Goucher College, Towson, MD 2012-2014
Student Representative

- Provided current-student perspective to facilitate a greater alumnae/i audience.
- Collaborate with former students and the Office of Development and Alumnae/i Affairs to ensure a more dynamic alum support system for the college.

Office of Development and Alumnae/i Affairs at Goucher College, Towson, MD Summer 2012
East Coast Vagabond

- Traveled along the East Coast connecting with Goucher alumnae/i and incoming students.
- Utilized blogging, video creation, and social media to build connections.

The Quindecim of Goucher College, Towson, MD 2010-2013
Contributing Writer

- Contributed one story per edition for the Global Section.
- Submit blog pieces for online newspaper issue.

Writings

"White Policy Paper on the Effects of Hydraulic Fracturing Implementation in Maryland" 2014

- Wrote sections "Positive Economic Impacts of Hydraulic Fracturing: Natural Gas as a Bridge Fuel" and "Regulatory Framework". Researched state and federal regulations, state owned natural resources, risks to state natural resources, and issues when protecting state parks. Additionally, provided an overview to the pathways of contamination resulting from fracking via air, water, soil, and technological inefficiencies and risk.

"Ecological Footprint of Baltimore City in 2008" 2013

- Contributed to the publication by helping calculate the ecological footprint for Baltimore's good and services usage. Through obtaining local consumption data such as the average mileage of car travel for the transport of goods, number of consumed gallons of heating oil, and expenditures on different types of foods, I aided in deducing the overall carbon footprint for Baltimore.

"Boswyck Farms Certification Course Booklet" 2012-2013

- Contributed and helped edit a 45-page textbook which accompanies the Boswyck Farms hydroponic Certification course. The textbook provides an overview of hydroponics, an outline of crops, a description of planting seed, an outline of hydroponic system operation, details of harvesting, an explanation of proper data collection, solutions to common hydroponic problems, and a list of resources.

"The Heat Island Effect (UHI) of Baltimore, MD" 2013-2014

- Completed a 25-page independent project research paper that included a in-depth discussion of the heat island effect in Baltimore and an experiment on Goucher College's campus. The written discussion explains the phenomenon and its effect on air/water quality, the effect on public health, and the overall cost analysis associated with the heat island effect. The experiment examined two possible solutions for the mitigation of UHI's effects - white wash pavement and water evaporation.

Skills

SWAT, MS Word, MS Excel, MS Powerpoint, MS Access, Prezi

